Shape Evolution Mechanism and Characterization of Two-Dimensional MoS_2 and NbS_2

By

Ibrahim H Bozkurt

A Dissertation submitted to the

School of Graduate Studies – New Brunswick

Rutgers, The State University of New Jersey

In partial fulfillment of the requirements

For the degree of

Doctor of Philosophy

Graduate Program in Materials Science and Engineering

Written under the direction of

Professor Manish Chhowalla

And approved by

_____

_____

_____

_____

New Brunswick, New Jersey

October 2018

ABSTRACT OF THE DISSERTATION

Shape Evolution and Characterization of Two-Dimensional MoS_2 and NbS_2

By

Ibrahim H Bozkurt

Dissertation Director

Prof. Manish Chhowalla

Two dimensional (2D) semiconducting transition metal dichalcogenides (TMDs) have attracted much attention due to their unique physical and chemical properties. Increased interest in the research of 2D layered materials began in 2004 when graphene, a monolayer of graphite, was discovered. TMDs are a class of layered materials which consist of over 40 members ranging from semiconductors to insulator to metals. There are three polytypes crystal structure of TMDs (1T, 2H, and 3R), which represent trigonal, hexagonal and rhombohedral, respectively. TMDs can be synthesized by one of two different approaches, top-down and bottom-up. Top-down includes mechanical and chemical exfoliation, while bottom-up includes physical and chemical vapor deposition. Synthesizing these atomically thin materials enables a new set of properties due to the quantum confinement effects.

MoS_2 and NbS_2 are two significant members of the TMD family and are the main topic of work in this thesis. These two materials were successfully synthesized with chemical vapor deposition (CVD) by controlling their growth parameters, each of which has a great influence on nucleation and the growth mechanism. Their shape evolution mechanism provides important insight into their nucleation and growth mechanism. The

MoS_2 part of this work was dedicated to understand this mechanism and how to apply it to other TMDs. To do that, MoS_2 was synthesized on different substrates to explore the optimum surface chemistry between the substrate atoms and reactants. On the other hand, Niobium disulfide (NbS_2) has received less attention compared to other TMDS due to its unexplored properties. Therefore, analyzing growth parameters and the potential applications of NbS_2 was also another aim of this thesis.

In the NbS_2 part of this thesis, two different approaches were pursued growing NbS_2 flakes. The first approach used sulfur and Nb_2O_5 powders as the precursors. The second approach used an alkali promoter, Nb_2O_5, and sulfur. The alkali-assisted approach yielded high-quality growth of few-layered NbS_2 with thicknesses ranging from 2 – 10 nm and lateral dimensions in the hundreds of micrometers. Our Raman and transmission electron microscopy analyses suggested that the as-grown material is a mixture of 2H and 3R phases. It was found that there was a substantial amount of incorporated potassium ions from the growth process in the NbS_2 samples, which leads to doping and metallic behavior. In the absence of alkali growth promoters, the lateral dimensions of the crystals are smaller, but they displayed metallic behavior. The electrical and HER properties of NbS_2 exhibited a promising result for future studies. The realization of thin and metallic TMDs is crucial for studying potential integration into electronics and catalysis.

ACKNOWLEDGMENTS

During my long grad school journey, I have come across many people whose support and guidance was extremely important for me to make my dreams become true. The first one is undoubtedly my advisor Manish Chhowalla who always encouraged me to become a better researcher with his outstanding guidance and motivated me when unexpected results and incidents happened in every aspect of my life. To me, he is not only a supervisor but also a good life coach that can take you to brightness from the darkness. I feel lucky to be a part of his group member and hope that we will still be in touch in the future even if he is moving to Cambridge University for his new prestigious position. It is hard to explain how important family is in someone's life with a few sentences, however, I will try to do my best. My wife, meaning of my life, was another person who supported me when I was weak and lost during this journey. My son Joseph Berat who always cheered me up with his lovely smiles and put my mood up while I sometimes had a difficult day. There is one more special person that I am glad to have him in my life is Brett McGowan. He has shown me many times that blood does not always make a family. Love, trust, and respect can bind people together stronger than any bloodline. I thank him here one more time for being in my life as a big brother.

I would like to also acknowledge my committee members for their time, support and guidance during my long path. Professor Ahmed Safari, Lisa Klein, Thomas Tsakalakos and Eric Garfunkel will remain very special for the rest of my life. I am honored to have these prestigious scientists in my committee.

Feeling financially secure during a grad school is very important for someone in order to be able to focus only on research. I would like to send my sincere thanks and regards to the Rutgers School of Engineering for funding my education expenses.

The last but not least, I would like to thank each of my group members for their collaboration and support. Dr. Damien Voiry, Jieun Yang, Muharrem Acerce, Raj Kapera, Sol Torrel, Abdurrahman Mahmood and my colleagues Raymond Fallon, Yan Wang, Berra Beyoglu. My special thanks go to Fang Zhao for allowing me to use her facilities at Princeton University.

DEDICATIONS

In dedication to my beloved family for their infinite love and support. My genuine gratefulness and warmest regard go to my mentors and friends for their continued guidance.

TABLE OF CONTENTS

LIST OF TABLES

LIST OF FIGURES

LIST OF SYMBOLS

C	Capacitance
e	Elementary charge
Δ	Thickness differences
h	Reduced Planck's constant
I_{DS}	Drain-source current
I–V	Current-voltage
□	Dielectric constant
L	Length
m^*	Effective electron mass
T	Temperature
μ	Carrier mobility
V_{DS}	Drain-source voltage
V_{GS}	Gate-source voltage
V_{TG}	Top gate-source voltage
w	Width

LIST OF ABBREVIATIONS

2D	Two dimensional
3D	Three dimensional
AC	Alternating current
AFM	Atomic force microscopy
ALD	Atomic layer deposition
CIGS	Copper indium gallium selenide
CVD	Chemical vapor deposition
DC	Direct current
DFT	Density functional theory
DSSC	Dye-sensitized solar cells
EBE	Electron beam evaporation
FET	Field effect transistor
FTO	Fluorine doped tin oxide
HEMT	High electron mobility transistor
HER	Hydrogen evolution reaction
HRTEM	High resolution transmission electron microscopy
IR	Infra-red
LED	Light emitting diode
LIB	Lithium ion battery
MBE	Molecular beam epitaxy
MoX2	Molybdenum dichalcogenides
MT&DCs	Molybdenum trioxide and dichalcogenides

MT&DS	Molybdenum trioxide and disulphide
OPV	Organic photovoltaics
PEC	Photoelectrochemical
PL	Photoluminescence
PLD	Pulsed laser deposition
SEM	Scanning electron microscopy
SPM	Scanning probe microscopy
TMDC	Transition metal dichalcogenide
TEM	Transmission electron microscopy
XRD	X-ray diffraction
XPS	X-ray photoemission spectroscopy
VDW	Vander der waals

CHAPTER 1

1. Introduction

1.1 Motivation

Two dimensional (2D) materials, such as hexagonal boron-nitride, graphene, molybdenum disulfide, have captivated the attention of many researchers due to their unusual physical phenomena and unique optical properties[1]. The research on 2D materials has enormously increased since 2004, when Novoselov and Geim began to work on graphene, the monolayer counterpart of graphite and led to explore on 2D materials properties[2]. These researchers from Manchester, UK simply used a scotch tape to exfoliate graphite to a single layer of graphene. Hence, graphene was the first material that sparked a dramatic interest in layered materials. The discovery of single-layer graphene via mechanical exfoliation led them to win the Nobel Prize in 2010. Graphene is a desirable material in terms of its unique features such as high carrier mobility, thermal electrical and thermal conductor [3-6]. The fact that graphene lacks a bandgap and thus is not favorable for especially electronic applications. In order to overcome the graphene-zero bandgap issue, the alternative TMDCs have been gained a lot of attention. Metal chalcogenides, boron nitride, oxides, hydroxides, and oxychlorides are the examples of non-graphene layered compounds[7].

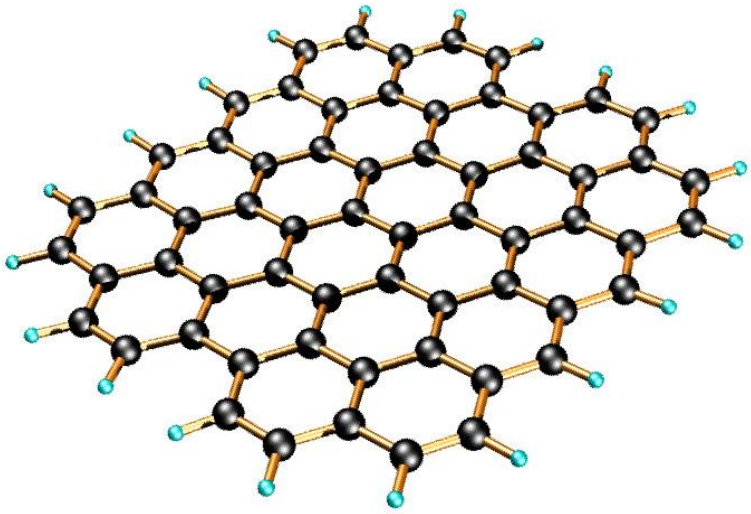

Figure 1 Single structure of graphene sheet[8]

Significant effort has been devoted to TMDCs due to their unique features. TMDCs are among the most studied layered materials where their monolayer form can be successfully synthesized. The researchers have widely studied TMDCs for decades both in academia and industry and the attention on these materials has enormously increased since 2004 when the graphene was discovered. Even though their properties have been explored and used in different applications, their role as near atomically thin materials is quite new. The range of their applications is not limited only for metallic or semiconductor scope. They also exhibit excellent charge density and superconductivity behaviors that enable the researchers to study a wide range of applications[2, 9, 10].

Although graphene and MoS_2 are the best-known family of 2D materials, the properties of other 2D materials have also been studied and explored recently. There are approximately 40 TMDC`s materials with different types of combination of chalcogen atoms and they can easily be classified according to the coordination and oxidation state of the metal atoms. The TMDCs, transition metal oxides, and perovskite-based oxides are

some examples of this family[2]. They exhibit interesting optical, electronic, mechanical, chemical and thermal properties on their atomically thin and bulk layers. Once TMDCs are exfoliated, they perform the large range of phenomena that are distinct from graphene. TMDCs have a large number of group members and are represented by a chemical formula of MX_2 where M consists of a hexagonal layer of transition metal atoms from group and X is sandwiched between two layers of chalcogen atoms. The examples of the transition metals are from group IV (Ti, Hf, Zr), group V (V, Ta, Ta) or group VI (Mo, W). On the other hand, S, Se or Te are the examples of a chalcogen atom for creating an MX_2 structure[11, 12].MoS_2, MoSe, NbS_2, and WS_2 can be given as the examples of this family. TMDCs exhibit different electronic properties based on the X-M-X formula and show the range from metallic to semiconducting as well as the same range of applications both in the industry and in academia [2, 13, 14].

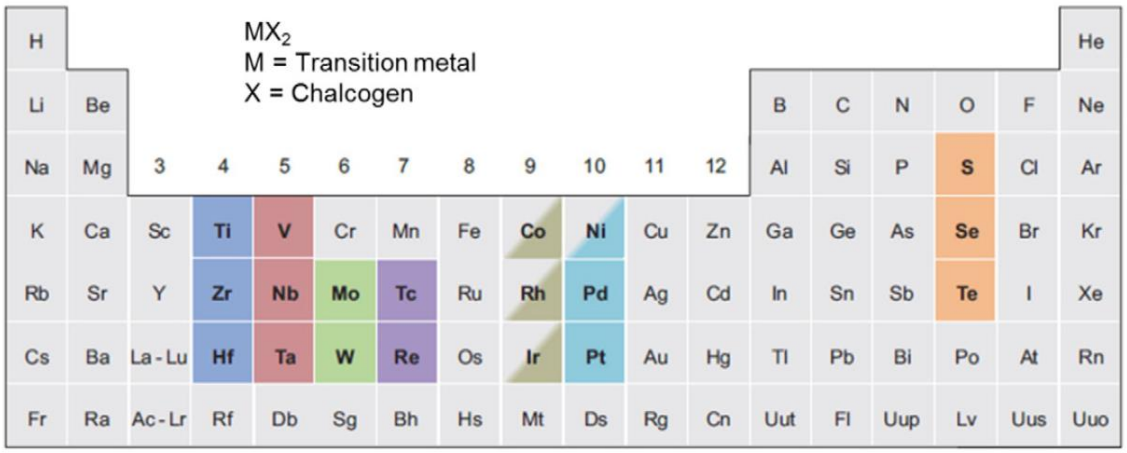

Figure 2 Transition metals and three chalcogen elements highlighted in the periodic table. M: Transition metal, X: Chalcogen [15]

TMDCs possess either a hexagonal or rhombohedral structure and metal atoms in the structure have octahedral or trigonal prismatic coordination. Adjacent layers are weekly bonded by Vander Waals forces while the same layer of the atoms is held by a covalent bond. Having a weak interlayer bond between layers enables to exfoliate of the bulk form to atomically thin layers [15]. Thus, the exfoliation of the single layers is feasible for many different TMDCs. Discovering the layer-dependent properties of TMDCs has revealed many unique phenomena for researchers. Graphene and MoS_2, which are one of most studied 2D family members, exhibit greatly different properties from their bulk form once they are synthesized as an atomically single layer. The electronic structure of the materials is tuned for several semiconducting of TMDCs with changing the layers. That's why the band gap value differs. For MoS_2, there is a transition from indirect band gap in the bulk form to a direct band in the monolayer. The band gap of bulk MoS_2 is 1.3 eV while the monolayer forms 1.8 eV[16]. The change of the band structure also enables to have photoluminescence from monolayer MoS_2, which is crucial for many optoelectronic applications[16-18].

.

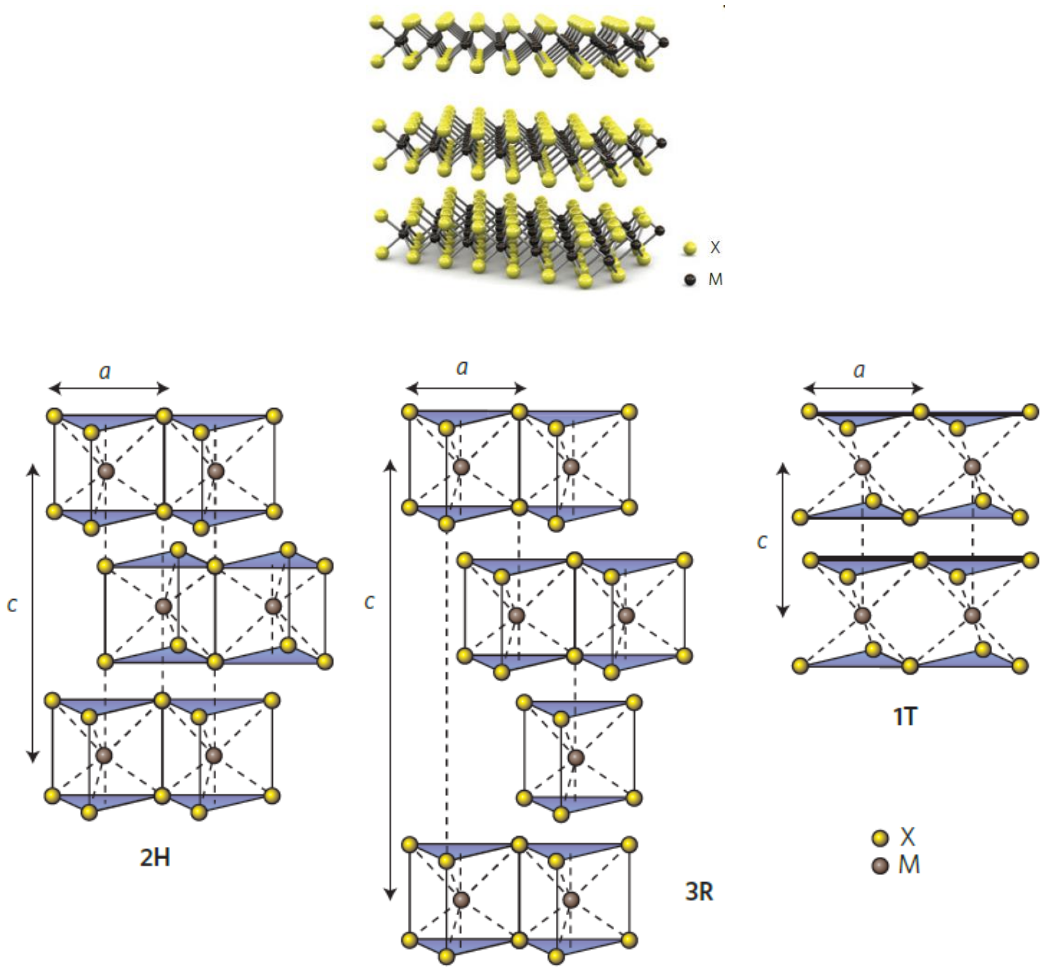

Figure 3 Illustrations of a typical MX2 structure and all polytopes 2H, 3R and 1T [2]

Bandgap (eV)		Mo	W	Ti	Zr	Hf	V	Nb	Ta	Ni	Pd	Pt
S	monolayer	1.8-2.1	1.8-2.1	~0.65	~1.2	~1.3	~1.1	metal	metal	~0.6	~1.2	~1.9
	Bulk	1.0-1.3	1.3-1.4	~0.3	~1.6	~1.6	metal	metal	metal	~0.3	~1.1	~1.8
Se	monolayer	1.4-1.7	1.5-1.7	~0.51	~0.7	~0.7	metal	metal	metal	~0.12	~1.1	~1.5
	Bulk	1.1-1.4	1.2-1.5	metal	~0.8	~0.6	metal	metal	metal	metal	~1.3	~1.4
Te	monolayer	1.1-1.3	~1.03	~0.1	~0.4	~0.3	metal	metal	metal	metal	~0.3	~0.8
	Bulk	1.0-1.2	metal	metal	metal	metal	metal	metal	metal	metal	~0.2	~0.8

Table 1 The common two-dimensional transition metal dichalcogenides and their bandgap values with different thickness[19]

1.2 Objectives of the work

The large family members of TMDCs have been studied in both academia and industry to explore their features and use them for different purpose of applications. MoS_2 and NbS_2 are well known of this family members and are the main study of this thesis. To synthesize these materials, there are two main methods which are top-down and bottom-up. Chemical Vapor Deposition (CVD) is one of the most studied bottom-up methods and has been used for this work to synthesize high-quality crystalline of MoS_2 and NbS_2 flakes and films. The work can be easily categorized into two sections, reproducibility and shape evolution of MoS_2 by using different substrates and synthesizing and characterization of NbS_2 with and without alkali-assisted. One of the main challenges of the first section is reproducibility. There have been many CVD MoS_2 studies that have proved that MoS_2 can be easily synthesized with the different conditions[9, 20-22] and still enormous effort has been continuously devoted to CVD grown MoS_2 in order to optimize the conditions. Therefore, it is important to know that exploring the shape evolution of TMDCs and understanding its mechanism will help researchers to understand and reveal their unique properties. Once TMDCs are synthesized atomically thin, the crystallographic structures are either trigonal prismatic or hexagonal and final shape evolution of these crystals has been straightforwardly shown in this thesis work.

Choosing convenient substrate for TMDCs is also crucial to have either large area thin films or flakes. In general, Silicon dioxide (SiO_2) is preferred by many researchers in terms of their features and accessibility[23, 24]. In order to investigate substrate-dependencies and atomic matching between MoS_2 and substrate atoms, MoS_2 was synthesized on different substrates such as silicon dioxide, sapphire, gold, quartz, and

glassy carbon. Demonstrating the study of shape evolution and substrate- dependency will be crucial to understanding the properties at the nanoscale to provide a new insight into the fundamental growing mechanism of MoS_2.

Synthesizing high quality, thin film niobium disulfide (NbS_2) is another scope of this work. Traditionally, to form of MX_2 is to use metal oxide precursor, in the case of MoS_2, (MoO_3) with sulfurization or selenization during the reaction. However, it is not very feasible for NbS_2 to grow due to the fact that the metal oxide of Nb has a very high melting point (Nb_2O_5-1512 ^{0}C). Thus, alternative methods have been sought to find the optimum precursors and halide group to have a large film of NbS_2. The alkali assisted of halide group has been used for decades in chemistry to enable a mass transport[25-27]. In this work, the halide group (KCl, KBr, NaCl, KI) has been also used to create a new eutectic point for the reaction temperature and have a maximum vapor pressure of the precursors. Hydrogen evolution reaction and conductivity measurement of NbS_2 thin films have been demonstrated as the result part to elaborate the film performance and activity. Since there haven't been many studied on alkali-assisted CVD NbS_2, this work hopefully will give a roadmap for the future development of NbS_2 and other TMDC compounds.

1.3 Organization of the thesis

This thesis covers two main members of TMDCs which are MoS_2 and NbS_2 whose properties and applications have been demonstrated in the different chapters. The thesis consists of 6 chapters and each of this chapter is significantly important to understand the fundamental mechanism of TMDCs and their potential applications. Each chapter is meticulously well divided to provide important information. Chapter 1 includes the introduction and motivation of TMDC family. Best known members of the TMDCs have

been explicitly explained in this chapter as well. The advanced literature review of the layered materials and two main examples of them establish the Chapter 2. In this chapter, detailed information of these two members has been provided including the structure, synthesizing methods and applications area of MoS_2 and NbS_2. This chapter also meticulously discusses potential applications of NbS_2 whose properties has not been well studied to apply them for further electronic and optoelectronic systems. Chapter 3 covers the characterizations of TMDC. Once the materials are synthesized, their properties are probed and characterized through the utilization tools such as Raman spectroscopy, electron spectroscopy, atomic force microscopy, and others in order to do further investigations. Each of this characterization method has been shown with their basis working principals. The experimental studies and results are the topics of chapter 4. CVD technique straightforwardly is explained for each material. Moreover, growing parameters and conditions are also listed in these chapters. Chapter 5 establishes the HER result of NbS_2 after the transferring the flakes from the silicon dioxide substrate to glassy carbon or gold. Chapter 5 also covers the conductivity measurements of alkali-assisted and without alkali-assisted NbS_2 flakes at room temperature measurement. Lastly, Chapter 6 completes the thesis with potential future works.

CHAPTER 2

2. Layered Materials

2.1 MoS_2

MoS_2 is a member of layered materials and there are two different bands in its structure, covalent and weak Van der Walls. While the weak Van der Walls interaction takes place between the molecules of MoS_2, the atoms within each layer (Mo-S) are

covalently bonded in a MoS_2 molecule with its vertically stacked structure. MoS_2, molybdenite, is a naturally occurring compound found in copper deposits and it has three different polymorphs that are 2H, 1T, and 3R. Since the 3R structure is uncommon, there have been extensive studies only on 2H and1T phase and 3R is not pertinent to present study. [28, 29]

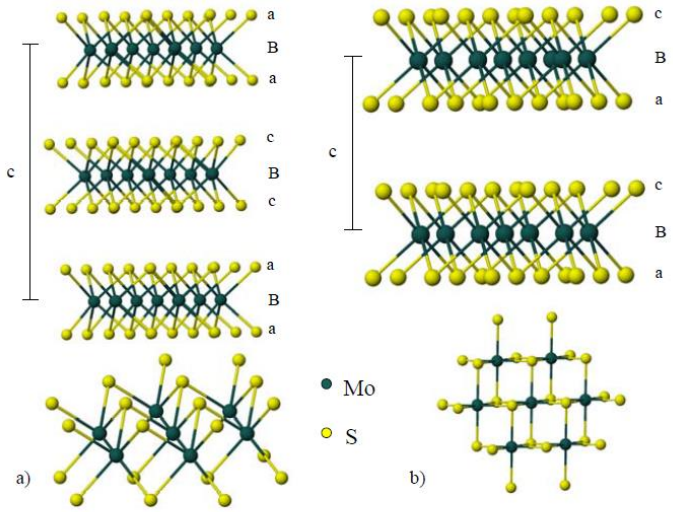

Figure 4 MoS_2 Structure, Ball-and-stick drawing of (a) 2H-MoS_2 and (b) 1T-MoS_2. The color scheme is as follows: Molybdenum, green; sulfur, yellow

2H-MoS_2 structure has P63/*mmc* crystal symmetry where $a = b = 3.15$ Å; $c = 12.27$ Å and its unit cell consist of two complete MoS_2 layers with an aBa ••• cBc repeat pattern in the *c* direction that is already held together by the force which is known as weak van der Waals.[30] There is a closed packed structure with molybdenum coordinated to six sulfur atoms with trigonal prismatic geometry for 2H-MoS_2. The 2H polymorph shows semiconductor behavior and it can be modulated by doping foreign compounds in the material`s interlayer spaces. On the other hand, for 1T-MoS_2, the Mo – S coordination is metastable and there is a change from trigonal prismatic to octahedral through

simultaneous glide motion by the molybdenum and sulfur planes. The geometry change causes the unit cell to one aBc layer. [31] Since there is no band gap for the 1T-MoS_2 polymorph, it exhibits metallic behavior and the effect of this behavior there is a structural transition with decreasing the crystal symmetry from *P*63/*mmc* to *P*3. [31]

	2H-MoS_2	**1T-MoS_2**
MoS6 Coordination	**Trigonal Prismatic**	**Octahedral**
Crystal Symmetry	**P 63/mmc**	**P 3**
Magnetism	**Diamagnetic**	**Paramagnetic**
Mo oxidation	**Mo(IV), d2**	**Mo(IV), d2**
Conductivity	**semiconductor**	**metallic**

Table 2 Characteristics of MoS_2 Polymorphs.

Due to MoS_2 `s exceptional mechanical strength properties, it is favorable to make this material desirable for use in use in flexible electronics and optoelectronic devices. MoS_2 nanosheets have 0.33±0.07 TPa Young modulus value which makes it strong enough to undergo elastic deformations of tens of nanometers without breaking due to having a low pre-strain and high strength.[32] Having these mechanical properties enable researchers to make flexible and high mobility FETs devices[33]. Like other TMDCs,

MoS_2 s band gap value is thickness dependent which increases from bulk to single layer. Theoretically, bulk MoS_2 has an indirect bandgap semiconductor whose bandgap energy is 1.2 eV while a single layer of MoS_2 shows 1.8 eV.[34] As MoS_2 goes to atomically thin layer, its bandgap value and its gap properties change. With decreasing the thickness, atomically thin layer MoS_2 can be observed with increasing band gap value since it exhibits dimensional confinement effects as the material becomes 2D.[24, 34, 35] This value change causes 0.6eV increase on bandgap value due to a crossover to a direct gap material in monolayers of MoS_2 [34, 36].

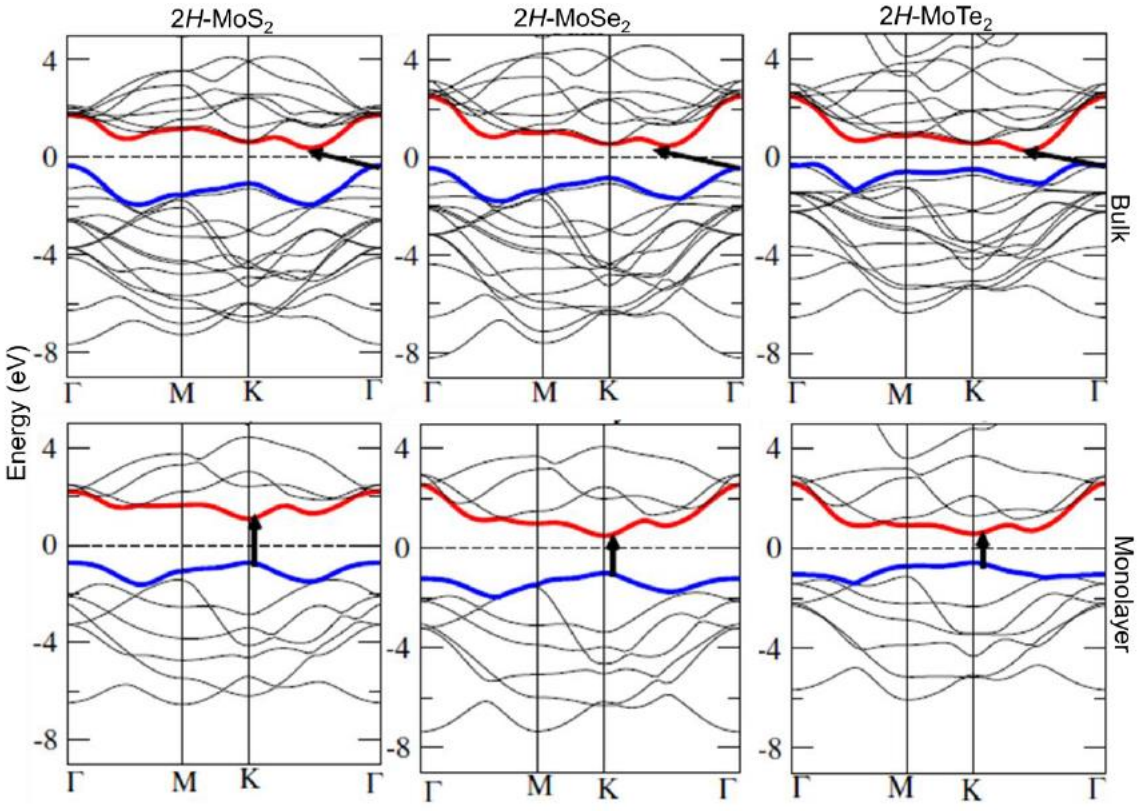

Figure 5 Band structures of bulk and monolayer MoX2 compounds obtained using DFT calculations[36]

To understand better of this confinement effect, the Brillouin zone mechanism of MoS_2 can be studied. Brillouin zone has certain points, which are represented in Figure 5, Γ-, K- M-and these points exhibit high symmetry in the zone. Due to the fact that the K-point in the Brillouin zone is more localized within the layer and there is a little bit increase in energy with decreasing layer thickness, the monolayer of MoS_2 shows bright photoluminescence [37]. Many studies on the calculation of the electronic structure of both bulk and monolayers of MoX2 have dedicated to a better understanding of these compounds including MoS_2. These calculations show that the density states around the Fermi level are essentially significant due to the molybdenum *d* states. Moreover, with these calculations, it can be observed that there is a strong hybridization between molybdenum *d* states and chalcogen *p* states below the Femi level. The calculations also present that there is a transition of the band structure from indirect to direct bandgap that takes place as decreasing the slab thickness from bulk to monolayer, which occurs due to changes in hybridization. It is clearly proved that thickness differences between bulk and monolayer of MoX2 reflect on their photoluminescence behavior that has been well studied to demonstrate the transition from indirect to direct band gap [11, 36, 38].

2.1.1 Synthesize methods of MoS_2 and other TMDCs

There are two main approaches to synthesize layered 2D materials, which are either top-down (mechanical or chemical exfoliations) or bottom-up (Chemical or physical vapor deposition) methods. In this section of the thesis, the example of each mechanism will be briefly explained and illustrated. It is worth mentioning that each method provides a different thickness of films or flakes and their properties. Knowing this will be significantly important to use them for further characterization and applications. Even though chemical

vapor deposition method is the main work of this thesis, besides that, some of the other methods including, chemical exfoliation, mechanical exfoliation, laser thinning and solid-state reaction method will be briefly discussed in this section.

2.1.1.1 Chemical / Liquid-phase exfoliation

Chemical phase exfoliation, known as also liquid phase exfoliation, is the method that intercalation chemistry takes an important role to exfoliate layers of 2D materials by interacting between the layers to separate.[31]. As mentioned earlier, there is a strong ionic or polar covalent between M – X bonds while weak van der Waals forces are held between the layers. Having this weak interlayer forces enable the layers to be exfoliated during any intercalation reaction. The host-guest material interaction causes some changes in physical properties which means that additional or removal of an electron to the empty or partially filled band possesses the material new feature and interaction. Many studies have been dedicated to exploring this property changes to insight the surface chemistry after an intercalation occurs to the layers. Host materials give rise to changes many material characteristic properties. Conductivity changes including; metallic to the insulator, a semiconductor to metallic, insulator to the semiconductor, paramagnetic to diamagnetic, or diamagnetic to paramagnetic are the example of these property changes [31, 39, 40]. The fact that MX2 compounds exhibit many different forms, known as polymorphs and these forms can undergo further structural changes upon intercalation. The intercalates size and orientation within the host indicate the interlayer expansion[41].

Molybdenite has a low electron affinity which means that it cannot be directly intercalated with large guest molecules. Therefore, MoS_2 can only react with a guest that has low ionization potential, in other words, it requires to have a donated electron that can

occupy electronic levels above the bandgap[42]. 2H-MoS_2 reacts with *n*-butyl lithium to achieve a stoichiometric product $LiMoS_2$ according to Eq. 1. [43, 44]

$$MoS_2 + n\text{-}BuLi \rightarrow LiMoS_2 + ½\ C4H10 + ½\ C4H8$$

$LiMoS_2$ adopts the 1T-MoS_2 structure with P3 crystal symmetry where $a = b = 3.360$ Å and $c = 6.311$ Å. [45]

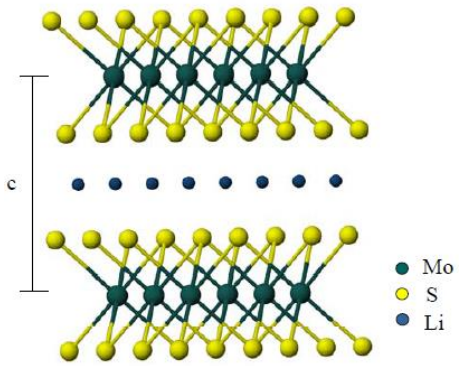

Figure 6 Ball-and-stick drawing of $LiMoS_2$ structure perpendicular to the c axis. The coloring scheme is as follows: molybdenum, green; sulfur, yellow; lithium, purple.

Due to the aqueous solution that a single layer of MoS_2 is suspended in, the majority of lithium ions are removed as lithium hydroxide. It has been well documented that approximately 10 % of the lithium remains intercalated in the MoS_2 layers.

$$LiMoS_2 + H2O \rightarrow LiOH(aq) + ½H2(g) + Li0.1MoS_2\ (exfoliated)$$

The production entails the time and some crucial points during the synthesis. It is important that the proposed reaction mechanism for dispersed MoS_2 particles occurs when

the lithium is able to disperse the structure of MoS_2. The reaction process can be represented below in Figure 7:

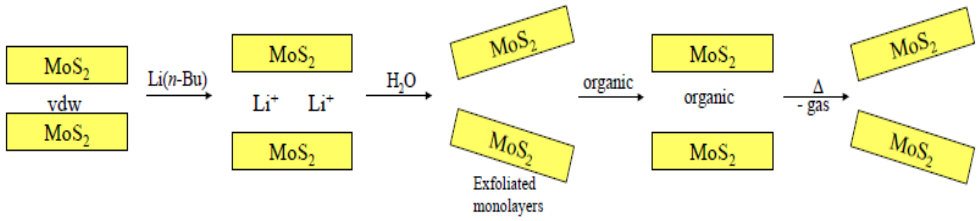

Figure 7 Proposed Reaction Mechanism for Dispersed MoS_2 particles [32]

During the process, it is important to mention that there is no need to use non- toxic gases that are environmentally friendly already.

Liquid phase intercalation/exfoliation method has been used since the early 1970`s both in industry and research [46]. There have been a number of studies recently proposed that especially on liquid-phase exfoliation of bulk MoS_2 powders in an appropriate organic solvent with aid of ultra-sonication as a viable route is achievable. This method enables to have facile fabrication of bulk films and composites of the exfoliated material.[47] The main purpose of intercalation engineering is to introduce the guest species in-between the gaps of the host layered materials and then separating them using various ways[48].

By using this method, the yield of thin sheets of MoS_2 thicknesses can vary of between 3 and 12 nm. Note that the thickness of monolayer sheet is corresponding to 5- 20 nm; however, monolayers might not be observed and it has been previously shown by Morrison and co-workers[47]. This study exhibits that Li-intercalated MoS_2 ($LixMoS_2$) can be exfoliated into monolayers via forced hydration, yielding a stable colloidal

suspension[49]. By using a different substrate that could be quartz and Si/SiO2 wafers micro exfoliation method can be used to obtain ultrathin MoS_2 layers [48].

2.1.1.2 Mechanical Exfoliation

Mechanical Exfoliation is another top-down method of synthesizing 2D materials to obtain them atomically thin layer. This method has been used widely since 2004 when two researchers from Manchester University discovered the graphene by using carbon scotch tape to exfoliate graphite. Ranging from a monolayer to a few layers or bulk can be obtained via this method. Working principle of this method is that a mechanical force is required to separate the layers by using an adhesive tape to exfoliate the bulk materials to a single layer. Even though the method has some critical steps to make an atomically thin layer of the sheet, there is some disadvantage for this method. The uncontrollable thickness and flakes size can be obtained. Another limitation of the method is that a large area scale cannot be implemented. Transferring the flakes on the substrate for further characterization has been a big challenge as well as the second transferring process to another substrate.

Depending on the thicknesses of the sheet, optical and electrical properties substantially show different features. For practical applications, a scalable and controlled deposition technique is required. Hence, mechanical exfoliation cannot be considered to be the most effective technique in establishing proof-of-concept studies. One of the most important advantages of using this method is that high quality intrinsic 2D materials can be synthesized as well as high quality of the sheet. [50]. Since the single precursors are used for mechanical exfoliation technique, not only it produces high quality intrinsic 2D materials, but also it can be considered to be the most effective technique in terms of establishing proof-of-concept studies.

2.1.1.3 Laser thinning

This method has been reported by Steele et al and it is a novel method to make monolayers 2D materials. [46]. Heat is a crucial point in terms of triggering the process that depends on the sublimation of 2D material. Due to the weak the van der Waals gap, in dissipating the laser-induced heat, therefore, sublimating only top layers in a multilayered flake is possible. If the fabrication of the large-scale production of electronic devices based on 2D materials is taken into the consideration, this technique can be potentially favorable. Even though the method has not been common in academia and industry since it is a new method, it is a significant way to synthesize monolayer 2D including MoS_2. However, the accessibility of the tools considering the laser and experimental set up is a big disadvantage for this method.

2.1.1.4 Solid State reaction

Searching for an alternative and decent way to fabricate 2D materials has been a big dedication for the researcher. Like laser thinning, solid state reaction is another novel method to fabricate 2D materials. Many research groups have been studied this method, however, the approach of by Bonneau *et al* enlightened and explored many unknown facts about solid state reaction. The production of layered MoS_2 and MoSe2 through rapid solid-state reactions between molybdenum chlorides and alkali metal chalcogenides has been successfully studied. The reaction has some steps and these steps are significant to generate crystals instantaneously and the layered materials to be simply separated by washing the final product. The method has not been used directly for forming exfoliated layers yet[51]. Prior to CVD detailed explanation which will be in the next section, all the techniques can be illustrated below in Figure 8.

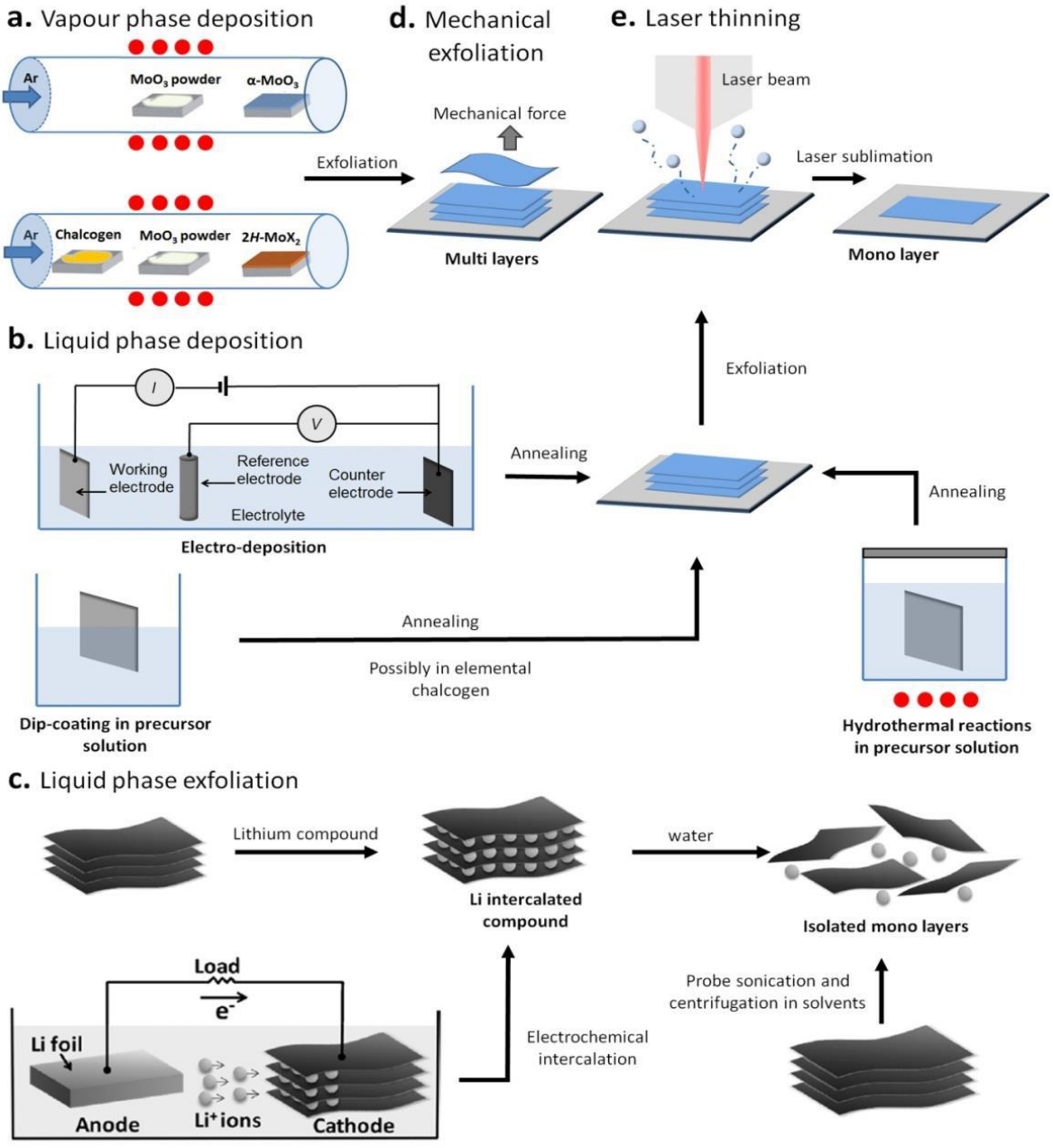

Figure 8 Illustration of the different methods to synthesize 2D materials. [52]

2.1.1.5 Chemical Vapor Deposition (CVD)

2.1.1.5.1 CVD systems

One of the most pillar methods of synthesizing high-quality large nanosheet is chemical vapor deposition. Many studies have been devoted to this method to improve the experimental set-up of CVD and its final products[53, 54]. The chemical vapor deposition process is very similar in some respects to physical vapor deposition that is known as PVD. The purpose of these two methods is to deposit a solid material from a gaseous phase onto the substrate for further characterization and applications. There are several types of CVD mechanisms that are listed below:

- ✓ Atmospheric Pressure Chemical Vapor Deposition (APCVD)
- ✓ Low-Pressure Chemical Vapor Deposition (LPCVD)
- ✓ Metal-Organic Chemical Vapor Deposition (MOCVD)
- ✓ Plasma Assisted Chemical Vapor Deposition (PACVD) or Plasma Enhance
- ✓ Chemical Vapor Deposition (PECVD)
- ✓ Laser Chemical Vapor Deposition (LCVD)
- ✓ Photochemical Vapor Deposition (PCVD)
- ✓ Chemical Vapor Infiltration (CVI)
- ✓ Chemical Beam Epitaxy (CBE)

Basic CVD process can be easily explained as follows: The solid form of precursors is placed in the reaction chamber which is generally a quartz tube and then the gases molecules from the precursors are formed and diluted in carrier gases at high temperature. The carrier gases entail to be inert not to have any reactions with precursors, for instance,

argon or nitrogen and can be delivered into the reaction chamber about at the ambient temperatures. Once the gases come into contact with a heated substrate, they react or decompose forming a solid state phase that is deposited onto the substrate. Substrate temperature and its position in the reaction chamber is very important for a successful CVD growth. All of the parameters that can effect on the nucleation and growth will be explicitly explained in the next chapter.

In order to build the CVD system, there are some crucial components which are listed below:

- ✓ Gas delivery system – For a supply of precursors to the reactor chamber
- ✓ Reactor chamber – A reaction chamber where deposition occurs
- ✓ Substrate loading mechanism – A system for introducing and removing substrates, mandrels etc.
- ✓ Energy source – Provide the energy/heat that is required to get the precursors to react/decompose.
- ✓ Vacuum system – A system for removal of all other gaseous species other than those required for the reaction/deposition
- ✓ Exhaust system – System for removing of unreacted volatiles from the reaction chamber.
- ✓ Exhaust treatment systems – In some instances, exhaust gases may not be suitable for release into the atmosphere and may require treatment or conversion to safe/harmless compounds.

- ✓ Process control equipment – Gauges, controls etc. to monitor process parameters such as pressure, temperature and time. Alarms and safety devices would also be included in this category.[3]

During a CVD reaction, choosing the precursors is a vital step since it requires them to be volatile to allow the deposition process occurred. The reaction temperature and time totally depend on the precursors, for instance, oxide precursors require a higher temperature to start to vaporize and longer time to consume all reactants from the precursors. There are many materials that can be synthesized by CVD method with a correct experimental set-up. The examples of these materials can be elements metals, alloys carbides nitrides borides and oxides intermetallic compounds[55].

2.1.1.5.2 CVD growth parameters

Each member of TMDCs has been widely studied via chemical vapor deposition. MoS_2 is the most potential for producing large scalable, uniform and single or multilayers of film or flakes[56]. Synthesizing of the films or crystals successfully is achieved once the precursors are vapored in an environmentally isolated chamber. Diffusion of the precursors is the main process for nucleation and growth in terms of having a large and uniform crystal of any TMDC compound. In order to clarify the reaction, it is important to analyze each variable parameter.

There is a certain temperature for synthesizing monolayer materials. In the case of MoS_2, it is more crucial to indicate the optimizing temperature for a single layer. The crystal formation occurs with the nucleation and growth once the reaction equilibrium temperature is completed on the surface of the substrate. Another key point is to take into

the consideration of the precursors melting points in terms of determining the activity of the synthesis reaction. In addition, choosing correct inert gas and its flow rate is significant in order to provide the reactants to the substrate surface as well as creating an oxygen-free environment that allows unreacted species to leave the furnace. The flow of inert gas also moderates the partial pressure and diffusion of all vapor-phase species. Driving force is a key element in order for a crystal grow. In the case of synthesizing MoS_2, the driving forces are a temperature below the melting point of the desired crystal structure and energy liberated when adding an atom or molecule to the crystal. The reaction temperature of each reactant and their diffusion flux to the surface allows the reduction and oxidation. The following reaction occurs once sulfur atoms reduce MoO_3 [57]:

$$2MoO_3+4S\rightarrow 2MoS_2+3O_2$$

It is important to know that MoO_3 and sulfur powder has a different melting point, 795 C^o and 115 C^o respectively. Hence, each reactant requires to be placed in a different zone furnace or more than a single zone furnace needs to control the reaction environment. The most of MoS_2 studies have demonstrated a successful thin film or flake once the substrate is placed at the same temperature as MoO_3 powder while sulfur powder located upstream somewhere between central hot zone of the furnace and the room temperature[58-61] Many research groups have claimed different growth conditions with the different lateral size and thickness and it is important to know that there is no only one way to synthesize TMDC materials as it is explained earlier. The following parameters are significant to grow monolayer or a few layers flakes or films:

1. Reaction growth temperature,
2. Precursors (MoO_3 and Sulfur) growth temperature (for the case of MoS_2),
3. Precursors amount (mg),
4. Flow rate standard cubic centimeters per second (SCCM),
5. Growth time (min)
6. Cooling ramps of furnaces

Based on these parameters, the following table shows the sample of parameters used in the literature for CVD growth of MoS_2[62]

Growth Temp (°C)	MoO_3 Temp (°C)	MoO_3 Mass (g)	S Temp (°C)	S Mass (g)	Flow Rate (SCCM)	Growth Time (minutes)
700	700	550	200	700	236	10
800	300	20	180	600		
715	715	10		1000	50	15
750		10		20	200	15
700	700	20		7	15	10
700	700	14		120	10	5
800	800		150		20	
840	530		100		50	45
750	750		113	1500	175	10
700	700	5		350	10	10
850	850	15	350	1000	10	5
750	750	20		100		15
650	650	18		16	5	
750	540	35	130	600	130	30
1000	1000	13	130	1000	200	10
650	650				1	15
850	850		600	1000	200	15

Table 3 The summary of some MoS_2 studies from literature with different parameters and conditions[62]

As shown in the table, synthesizing MoS_2 has a large range of parameters with the similar results. There are a few reasons why this range is occurring during the growth. The sample preparation, the type of furnaces (single-multi zones), place of precursors and cooling ramp of the furnaces can explain the reason. Especially, cleaning a quartz tube prior to every experiment is a key parameter in terms of not removing residue. Since there is a temperature gradient in the furnace between the zones, the location of the precursors also gives rise to different results.

Nucleation and growth rate are significant phenome to insight synthesizing films or flakes. Grow rate (Gr) simply depends on the substrate temperature, the partial pressure of molybdenum and sulfur reactants. It can be represented:

$$Gr=f(TGS,Ps,PMo),$$

where TGS is the temperature at the growth surface,

$$Ps=f(Ts,SAS,FR),$$

the partial pressure of sulfur source and each parameter can be presented,

$$PMo=f(TMo,SAMo,FR),$$

is the partial pressure of molybdenum source where the partial pressures of each reactant depends on their temperatures (TS/dependrface areas (SAS/Mo), and the flow rate (FR) of inert gas. It is fact that very less amount (one microgram of each reactant)is required to cover a substrate with a monolayer of MoS_2, it is apparent that growth sensitively depends on all three of these variables [62].

2.1.2 CVD MoS_2 Applications

After having a successful CVD growth, it is important to exhibit some potential applications. Each different method of synthesizing atomically thin films yields a various range of applications. As is listed above, CVD method requires more equipment and is a more complicated process than the other methods such as micromechanical exfoliation method, therefore, the yield and consistency are greatly superior to that of the micromechanical exfoliation method. Synthesizing large area and thin nanosheet of 2D captivates the researchers to use this method more often. For instance, a few layers of CVD MoS_2 exhibits a high electronic quality and a low defect density. Moreover, since the CVD method has yielded the highest crystalline quality of monolayer islands and films, it can be promising for the future semiconductor industry.[19, 41].

Semiconductor materials such as MoS_2, 3R-NbS_2 have been used on different applications due to their unique physical properties. Especially, MoS_2 has a wide range of applications in the semiconductor industry, for instance as transistors. Some of the MoS_2 applications that have been used both in academia and in the industry are lubricant (in engines), valleytronics, microelectronics (chips), transistors for digital electronics, heterojunction solar cell (home, industry) etc.

Transistors are semiconductor devices that can be used to amplify and switch electronic signals and electrical power of electronic devices. The MoS_2 transistor is one of the most important application areas in the semiconductor industry. [55]. There are many other materials that have been used in the industry including silicon and silicon-based materials, especially, the MoS_2 transistor has been extremely studied to make them faster and thinner. Fabrication of a successful MoS_2 film for a

transistor material depends on the band gap features. The single layer of MoS_2 is much more desirable to make a transistor device since it has a direct band gap of 1.8 eV while bulk MoS_2 has an indirect band gap of 1.2 eV. The thinner film of MoS_2, the better transistor`s features. The figure below exhibits that the first implementation of a top-gated MoS_2 FET shows excellent on/off ratio of 10^8, a mobility of 200 cm^2 $V^{-}1s^{-1}$and n-type conduction.

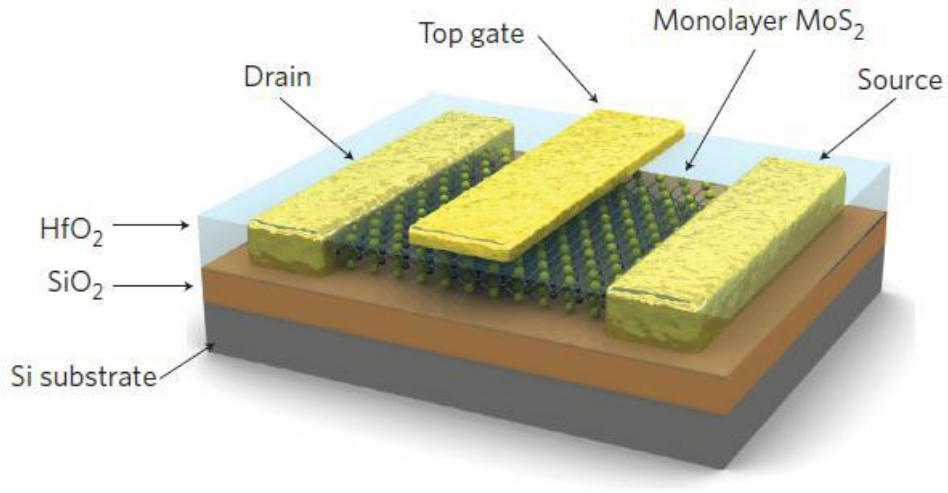

Figure 9 Top-gated MoS_2 FET with HfO2 top gate dielectric [4]

2.2 NbS_2

The electronic and structural properties of TMDCs have been widely studied for the last decades. Their unusual physical phenomena have offered many potential technological applications, especially, since two-dimensional graphene properties were discovered [63-67]. Unlike, other 2D materials such as graphene and MoS_2, there haven't been many studies on NbS_2. Thus, the properties and applications of this material have been unexplored for many years. However, the unique physical and optical properties of TMDCs have pushed the researchers to discover the new compounds of this family. The fact that the basic structure and properties of NbS_2 have been presented early 1980 `s [68], yet, there need to be many other studies to be done to reveal their features. This chapter will provide the fundamental properties and applications of NbS_2 and condense all NbS_2 studies.

NbS_2 exhibits a typical structure of TMDCs where metal atoms (M) are bonded by two chalcogenide atoms (X) to create XMX or MX_2 formula. The layers are separated by a weak van der Waals type of bonding between the adjacent layers while the atoms in a layer bounded covalently. There have been four different phases of niobium disulfide which are stoichiometric 2H-NbS_2 and 3R-NbS_2 and nonstoichiometric 2H-$Nb_{1+}S_2$ and 3R-$Nb_{1+}S_2$ [68] [69]. The excessive niobium atoms that take place between adjacent sandwiches cause the nonstoichiometric of $Nb_{1+}S_2$. The properties of these non-stoichiometric structures remarkably differ based on where excessive atoms are placed [70]. The recent studies have classified the NbS_2 structure mainly in three categories that are 1T, 2H and 3R NbS_2. While the number, 1, 2, or 3 represents the number of layers in

one unit cell, R(Rhombohedral), H(Hexagonal), or T(Trigonal) indicates the name of the crystal structure[63]. In this work, 2H and 3R NbS_2 have been investigated and their results have been shown in the experimental and result section. The morphology of NbS_2 differs based on stoichiometric NbS_2[63, 64].

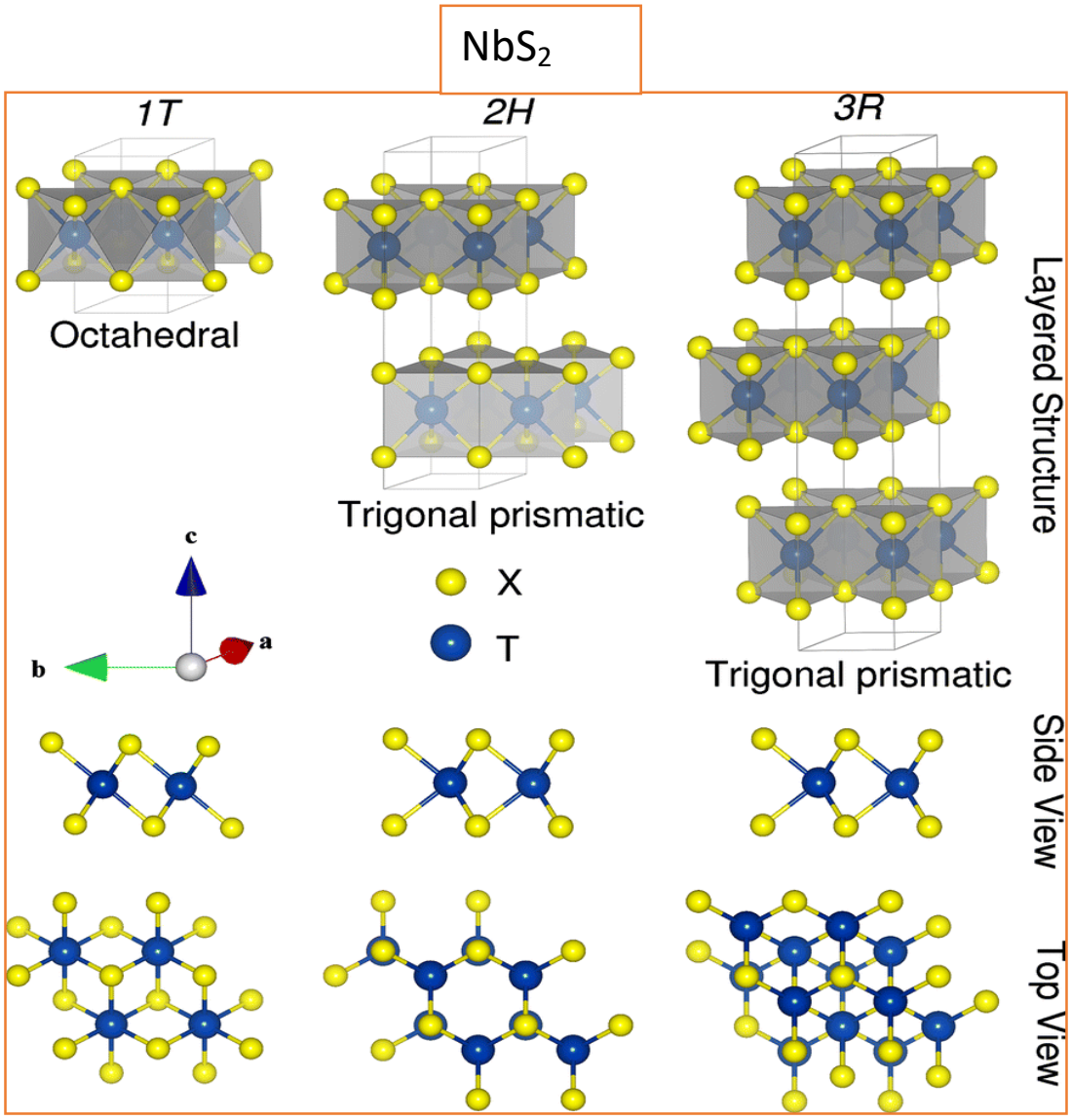

Figure 10 All polytope of NbS2 crystallographic structure with Side and Top view; T represents Nb atom while X is a chalcogen atom.[71]

Once the crystal structure is detailed, it can be observed that 2H structure consists of close-packed sulfur atoms with a repeat unit of AABB, Niobium atom is located in the half of the trigonal prismatic sites. The double layer repeat unit is shown in Figure 10 above, the structure in the xy plane is of edge-linked NbS6 trigonal prisms. The other crystallographic structure 1T possesses hexagonal close-packed sulfur atoms (AB repeat unit) with Nb filling half of the octahedral holes in every other layer. Therefore, the structure is of edge linked NbS6 octahedral. The lattice parameters of NbS_2, a, b, and c are a significant way to reveal the crystal structure and its orientation and these parameters can be calculated in terms of computing and experimental approaches[72-76].

Structure	Method	a(Å)	c(Å)	c/a	P (GPa)
$1T$-NbS_2	VASP-LDA	3.253	5.341	1.642	0
	Experiment	3.420	5.938	1.736	0
$2H$-NbS_2	VASP-LDA	3.287	11.421	3.475	0
	Experiment	3.418	11.860	3.470	0
	Experiment	3.310	11.890	3.592	0
	Experiment	3.330	11.950	3.589	0
$3R$-NbS_2	VASP-LDA	3.286	17.577	5.349	0
	Experiment	3.335	17.834	5.336	0

Table 4 The comparison of the calculated lattice constants for different NbS_2 structure

The layered structure of 2D materials allows them to slice in many ways as in the example of graphene in order to produce ribbons. Once graphene is cut, 1D stripes or ribbons can be obtained with different types of edge terminations. There are two types of edges in the case of graphene nanoribbons, are called zig-zag and armchair. These edges take place a significant role in terms of preserving the stoichiometry of the bulk structure[77].

Figure 11 As cut chains from NbS_2 layer (a) NbS_2 zig-zag. (b) NbS_2 armchair.

2.2.1 NbS_2 Synthesizing

There have been many studies reported on NbS_2 synthesizes like many other TMDCs. Based on the synthesized methods, various forms, sizes, and thickness of NbS_2 have been produced[78]. Nanotubes [79], nanowires [80], bulk powders [81] and bulk single crystal are the examples of NbS_2[78]. Even though there have been very limited studies of CVD NbS_2, synthesizing NbS_2 with CVD method is one of the most feasible methods in terms of controlling bottom-up growth characteristics. Thanks to this approach, nanoscale or even atomically controlled morphology can be synthesized.

The difficulty in sample preparation has been a serious challenge for synthesizing a good quality of NbS_2. Different preparation approach has been studied on many 2D materials like NbS_2. The choices of the precursors and the growth conditions are significant to have a large area film as well as feasible substrate matching. There have been many reports that NbS_2 has been successfully grown on the different substrates such as graphene[78], hBN [82], silicon dioxide [83]. The ideal substrate for NbS_2 has not been reported. Sulfur has used for most of these studies as a chalcogenide source with the carrier gas of nitrogen or argon to enable the reaction in an inert environment. Hydrogen has been also used in the form of argon or nitrogen mixture for the in the purpose of carrier gas as well as reducing the oxidation state of the reaction[84]. By using chloride source of Nb and the possible reaction with and without using hydrogen source as follows:

$$NbCl5 + 5/2H2 + 2S \rightarrow NbS_2 + 5HCl \text{ (with hydrogen)}$$

There are two possible reactions may occur in the system without using hydrogen source:

1- $NbCl5 + 2S \rightarrow NbS_2 + 5/2Cl2$

2- $NbCl5 + 7S \rightarrow NbS_2 + 5/2S2Cl2$ [83]

Once the hydrogen is introduced in the reaction chamber the equilibrium of the system:

$NbS_2 + x/2H2 \leftrightarrow NbHx + 2S$ [83]

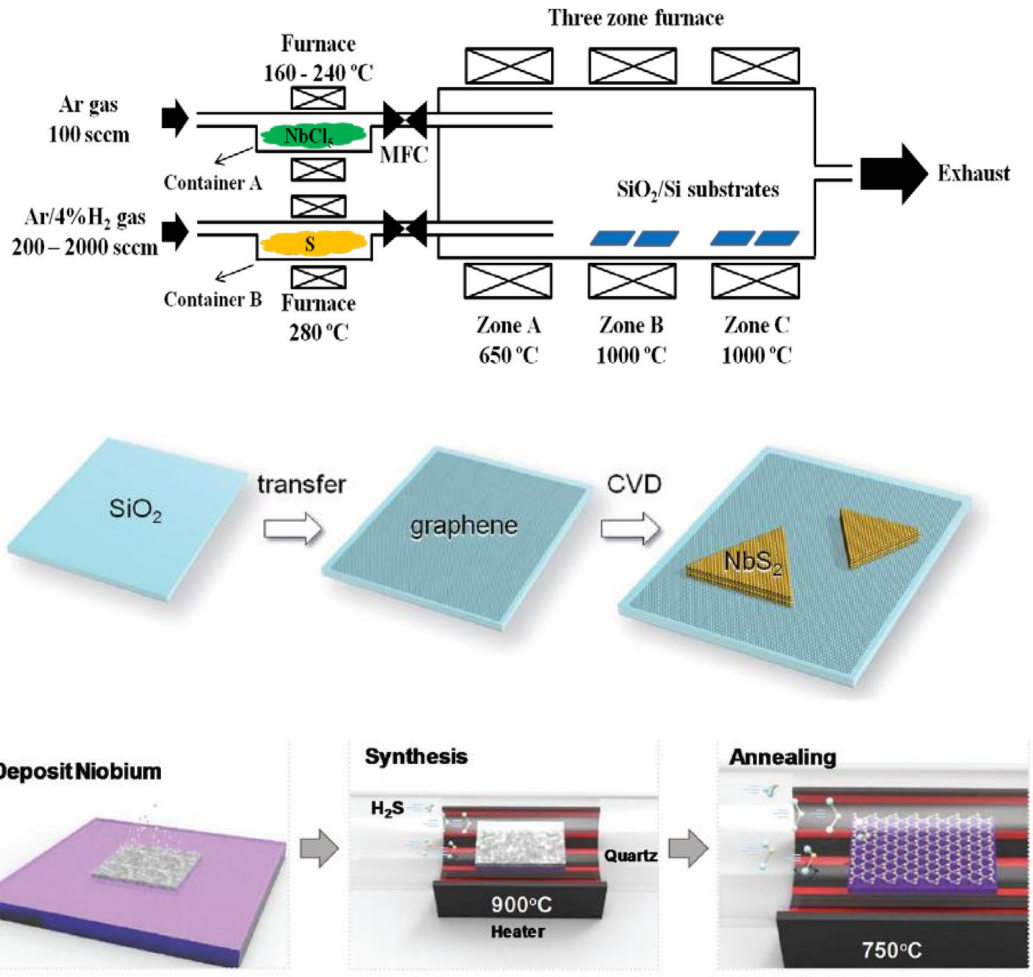

Figure 12 Schematic illustration of some synthesis methods of NbS2[84, 85]

Selecting the precursors is another key parameter to synthesize NbS2. Based on these precursors or promoters, NbS2 shows a different crystallographic structure and nonstoichiometric compound. Many studies have investigated convenient precursors to have the optimum conditions for synthesizing NbS_2 and they have used $NbCl_4$, Nb2O5, NaNbO3 and many others [86-89] to explore how the precursors affect the delicate structure of NbS_2[25, 65].

2.2.2 Intercalations of NbS_2

Intercalation is a chemical process to reversibly insert foreign species at the crystal gap. There are many factors that can determine the degree of an intercalation in 2D materials. The physical size of intercalating species, structural stability of hosting materials after the intercalations and charge stage of intercalating species are significant to be able to observe the interaction between the species and TMD layers. Many studies have revealed that intercalating transition metal dichalcogenides (TMDs) with ions gives rise to charge density waves, two-dimensional superconductivity, and interesting phase transitions[90, 91]. It is a fact that the chemical intercalation for TMD is a significant way to tune the physical and chemical properties. Novel functional of these materials provide a remarkable enhancement on the various performance when the fundamental synthesizing parameters of chemical intercalation is well studied as well as the designing and adjusting for these materials[92]

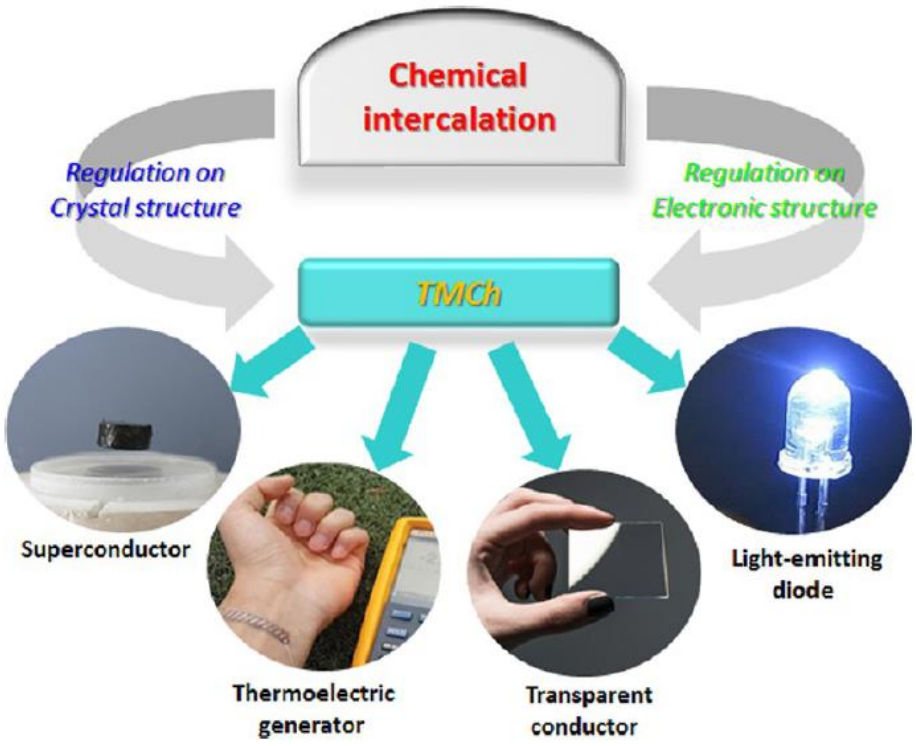

Figure 13 Once the appropriate chemical intercalation species are inserted, functional materials in the transition metal chalcogenides can be regulated.[92]

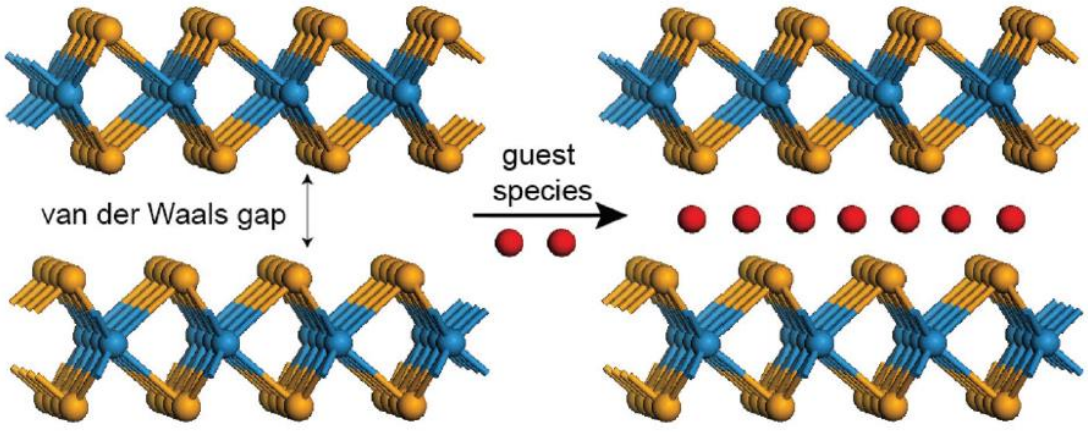

Figure 14 The illustration of intercalation in the TMD-type layered materials, where guest species can break into the van der Waals gap by diverse methods.[90]

The intercalation engineering of NbS_2 has been also widely studied and it totally depends on which polytope of NbS_2 is. It is known that 2H NbS_2 exhibit a metallic behavior and its intercalation is possible with an appropriate organic molecule such as Lewis bases. On the other hand, the 3R NbS_2 behaves as a semimetal and it is very difficult to do any molecular intercalation[93-95].

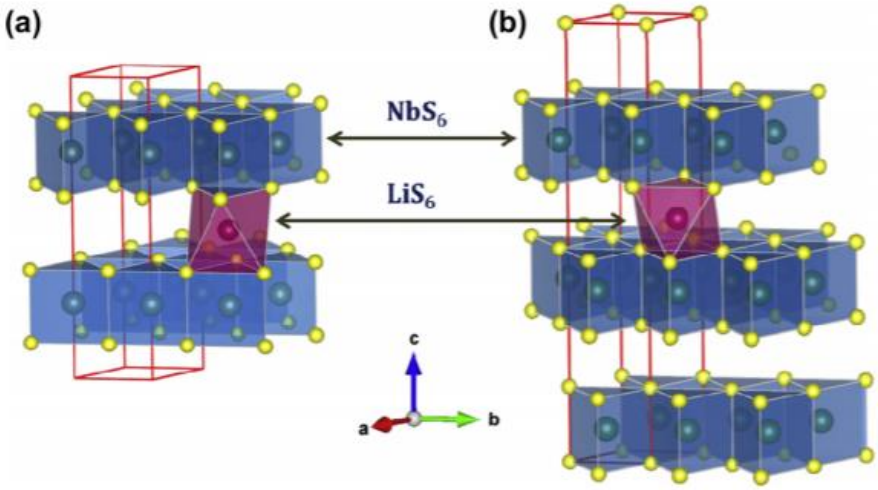

Figure 15 Both crystallographic structures of NbS_2 has been shown (a) 2H-NbS_2 (space group: P63/mmc, No.: 194) and (b) 3R-NbS_2 (space group: R3m, No.: 160) with LiS6 octahedral sites (pink in color).[94]

The intercalation engineering of TMDCs has been extensively a focus for decades. Although there have been many intercalated studies by 3d transition metals, the most common intercalation of the host alkali ions is Li^+ and Na^+ [89, 96, 97]. Once the host ions are intercalated, they significantly induce the electrochemical properties of the structure due to their size differences. The fact that NbS_2 layers are bonded weakly by van der Waals forces and this host (Li or Na) can easily intercalate into the empty octahedral sites of the gallery space in the van der Waals gap. The main difference between 2H and 3R NbS_2 structure is the stacking order of the NbS_6 trigonal prisms. As is shown above Figure 15,

Octahedral-site Li takes place between two NbS6 prisms along the c-axis. On the other hand, 3R-NbS_2 Li accommodates on a site with a NbS6 prism on one side, an empty prism on the other side [90, 98-100].

The formation of niobium disulfide may occur at the different morphology with the range from a large area monolayer thin film to a few hundred microns hexagonal or triangles flakes. The following parameters effect on the type, morphology and the thickness of NbS_2:

- ✓ The type of precursor (Sulfur or niobium source impurity effects the type of crystal structure)
- ✓ The reaction time (from a thin film to bulk crystal flakes)
- ✓ The reaction temperature (phase transformation may occur)
- ✓ The pressure (atmospheric or high pressure, vacuum – NbS_2 flake stability)

Substrate temp. (°C); sulfur precursor	Deposition time (min)	EDXA	Raman (cm^{-1})	XRD / 2θ	Contact angle (°)
600; $S(SiMe_3)_2$	5	$NbS_{1.8}$	1T-NbS_2	1T-NbS_2	95.1
600; tBu_2S_2	5	$NbS_{1.9}$	1T-NbS_2	1T-NbS_2	6.0
550; tBu_2S_2	5	$NbS_{1.8}$	1T-NbS_2	1T-NbS_2	3.5
500; tBu_2S_2	5	$NbS_{2.1}$	1T-NbS_2	1T-NbS_2	9.2
450; tBu_2S_2	5	$NbS_{2.1}$	90, 224, 285, 417, 604, 924	–[a]	87.3
400; tBu_2S_2	5	$NbS_{1.7}$	93, 226, 282, 418, 605, 924	–[a]	8.4
600; *t*BuSH	5	$NbS_{1.6}$	3R-NbS_2	3R-NbS_2	3.2
550; *t*BuSH	5	$NbS_{1.7}$	3R-NbS_2	3R-NbS_2	3.1
500; *t*BuSH	5	$NbS_{1.7}$	3R-NbS_2	3R-NbS_2	3.5
450; *t*BuSH	5	$NbS_{1.9}$	3R-NbS_2	3R-NbS_2	4.8
400; *t*BuSH	5	$NbS_{1.7}$	3R-NbS_2	3R-NbS_2	2.4
350; *t*BuSH	5	$NbS_{2.0}$	3R-NbS_2	3R-NbS_2	4.1
300; *t*BuSH	5	$NbS_{2.0}$	169, 241, 372	X-ray amorphous	4.1
250; *t*BuSH	5	$NbS_{2.0}$	187, 294, 328, 549	X-ray amorphous	14.5
600; $HSCH_2CH_2SH$	5	$NbS_{2.1}$	3R-NbS_2	3R-NbS_2	54
550; $HSCH_2CH_2SH$	5	$NbS_{1.2}$	3R-NbS_2	3R-NbS_2	87
500; $HSCH_2CH_2SH$	5	$NbS_{1.8}$	3R-NbS_2	3R-NbS_2	90
500; $HSCH_2CH_2SH$	4	$NbS_{1.9}$	3R-NbS_2	X-ray amorphous	105
500; $HSCH_2CH_2SH$	3	$NbS_{1.8}$	195, 260, 328, 383	X-ray amorphous	48
450; $HSCH_2CH_2SH$	5	$NbS_{2.0}$	186, 260, 331, 381, 535	Nanocrystalline NbS_2	95
400; $HSCH_2CH_2SH$	5	$NbS_{2.4}$	197, 239, 299, 334, 535	X-ray amorphous	95
350; $HSCH_2CH_2SH$	5	$NbS_{2.3}$	187, 242, 298, 332, 544	X-ray amorphous	21

[a] Film too thin.

Table 5 Raman spectroscopy and XRD patterns of NbS_2 thin film by using different Sulfur precursors.[101]

2.2.3 Applications of NbS_2

As a member of TMDCs family, NbS_2 has a layered structure and has been used in different applications for decades. NbS_2 `s layer structure enables us to discover its large anisotropic electrical, optical and magnetic properties. Unlike other members of TMDCs, NbS_2 does not show a charge density wave (CDW)[102]. However, it shows superconductivity at the transition temperature of T_c: 6K. Surprisingly, this transition temperature increases with the pressure change, 6K at zero pressure to ~8.9K at 20

GPa[103]. It is known that different NbS_2 shows different low dimensional behaviors and applications and its bulk form can be exfoliated to the low dimensions[72, 85]. NbS_2 has been applied as a catalyst for purification of petroleum, hydrogen evolution reaction for producing pure hydrogen, cathode materials in secondary batteries and humidity sensor[104-107]. It is a fact that NbS_2 properties haven't completely discovered yet and once the properties have been uncovered, their applications also will start to be used in various areas including academia and industry. They can also be applied on field effect transistors. Here below Figure 16 is the example of using NbS_2 as the source-drain contact to demonstrate the feasibility of using NbS_2 as a high-performance transparent electrode. It is known that Mo is a good n-type contact metal that provides lower resistance for the MoS_2 field effect transistors than other noble metals. Using NbS_2 electrodes provides a better device performance than using Mo electrodes[84].

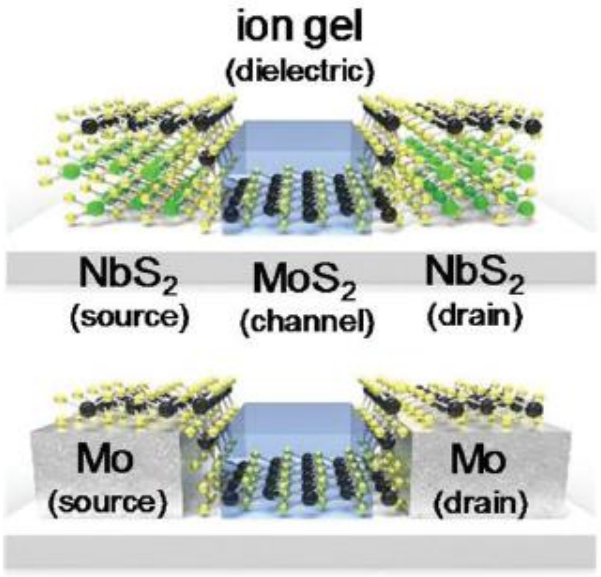

Figure 16 Electrical characterization of NbS2–MoS_2 field effect transistor (FET) devices.[84]

CHAPTER 3

3. Characterizations of TMDCs

The family of TMDCs has unique properties that can be used in different applications in terms of their electronic and optical behaviors. In order to explore their outstanding features, there have been many techniques used in research world such as Raman spectra, Photoluminescence (PL), Optical Microscope (OM), Scanning Electron Microscope(SEM), X-ray diffractions (XRD), X-ray photoelectron spectroscopy (XPS), Transition Electron Microscopy (TEM), Atomic Force Microscopy (AFM), and Energy Disperse Spectroscopy (EDS). Each TMDC has considerably gained the attention of many researchers and there have been many studies on each of this family member. However, the scope of this thesis will be predominantly on MoS_2 and NbS_2 and their data will be exhibited at the Result and Experimental chapter.

3.1 Raman and Photoluminescence Spectra of MoS_2 and NbS_2

The fact that TMDCs have many polytypes, in other words, even though they have the same compositions, their crystal structures are different. The main difference of these polytypes stems from the registry of the stacking of the layers in the lateral directions. The thickness of the films depends on the supplementary of the sources as well as reaction temperature and time. Raman spectroscopy is a form of molecular spectroscopy – the scattering of electromagnetic radiation by atoms or molecules and it is a significant way to show molecular fingerprinting. It has many advantages to indicate the molecular identity in terms of little sample preparation requirements and using transparent containers to analysis directly. Raman Spectra enables to do both qualitative and quantitative analysis very fast. On the other hand, Photoluminescence is also an important way to reveal the

composition and solid structure of a material. After the electron is in the excited electronic state or conduction band, it can undergo either radiation less decay or a photon can be emitted as the electron returns to the ground state or valence band. Once the emission occurs, this process is called photoluminescence[108]. It is a widely used technique for characterization of the optical and electronic properties of semiconductors and molecules. Using Raman and Photoluminescence spectroscopy together simultaneously is very advantageous when studying two-dimensional crystals[109].

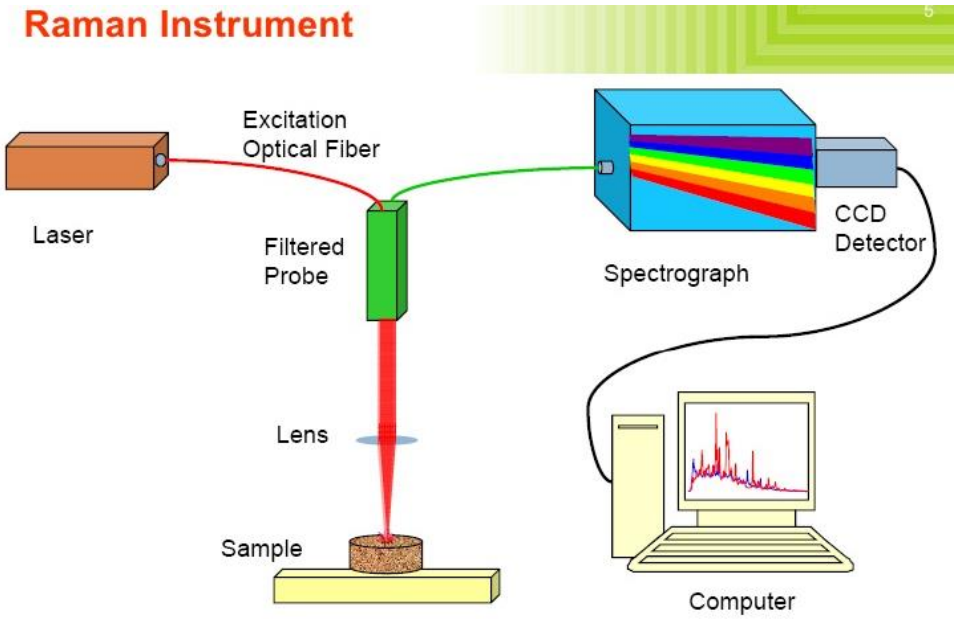

Figure 17 Illustration of the fundamental principle of Raman Spectra [109]

Molybdenum disulfide (MoS_2), a naturally occurring molybdenite, is one of the most studied and stable layered family members of transition metal dichalcogenides. It has polytypes like many other TMDCs, 1T, 2H, and 3R. But, only 2H- MoS_2 has been studied in this work without doing any phase transformation engineering. Therefore, the most of

the literature view and experimental results will be mostly on 2H-MoS_2 unless it is mentioned the different phase. MoS_2 can be easily deposited on silicon dioxide or other substrates and synthesized with different methods such as via chemical vapor deposition, mechanical exfoliation of the bulk crystal. There are two significant Raman modes of MoS_2, E^1_{2g}, and A_{1g} [110]. These two modes exhibit sensitive to layer thickness dependence with the shifted frequency of the modes. The frequency of E^1_{2g} decreases while the latter increases from single layer to bulk. This opposite frequency change is the result of Columbic interaction and possible stacking induced of the interlayer bonding[110, 111]. MoS_2 has four first-order Raman active mode, 32 cm^{-1}, 286 cm^{-1} ,383 cm^{-1} and 408 cm^{-1} which are represented by E^2_{2g}, E_{1g}, E^1_{2g}, A_{1g} respectively[112]. The different PL spectra value of MoS_2 with changing layer numbers exhibits the fact that monolayer MoS_2 is a direct bandgap material while the multilayer is an indirect material[110, 113].

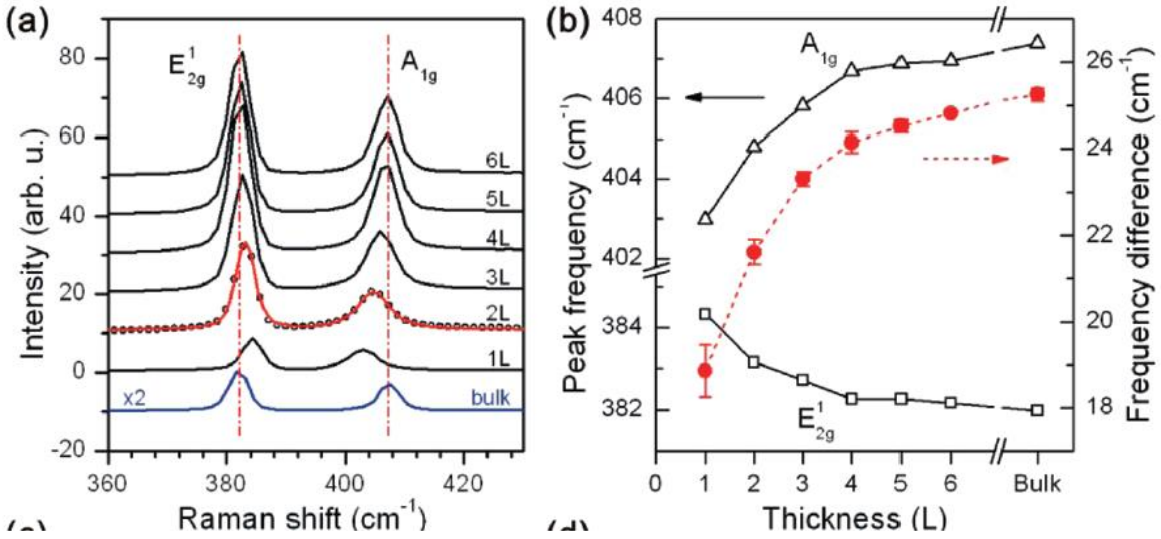

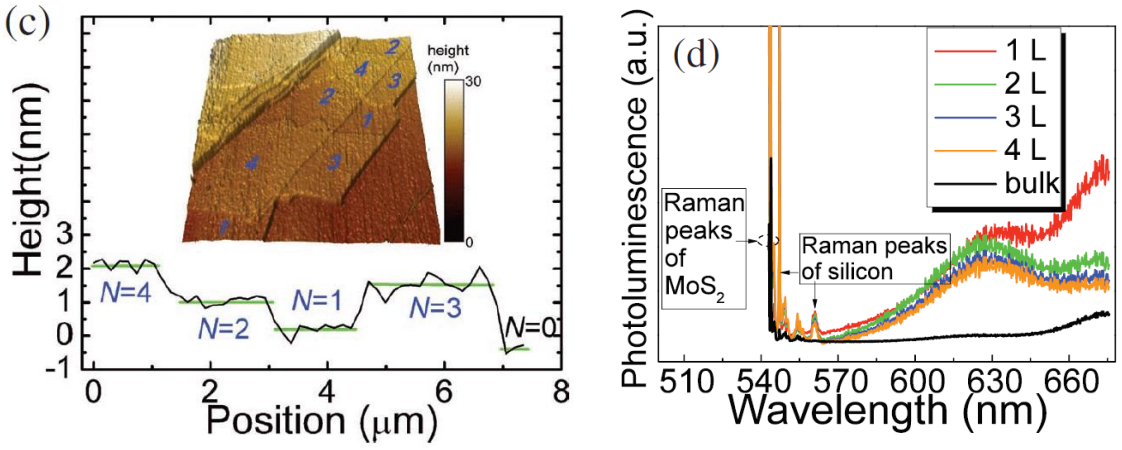

Figure 18 a) The Raman spectra of thin and bulk MoS_2 with an arbitrary unit of intensity. b)Peak frequencies with the different layer numbers c) Height profile of the film and d) PL spectra value of MoS_2 with changing layer numbers [110, 112]

It is known that NbS_2 has two major polytypes, which are 2H and 3R. The basic explanation of the numbers in front of the letters is to consist of two and three layers, in a unit cell, respectively. To differentiate these two structures might be a big challenge in some characterization methods. For instances, they almost have the same XRD patterns in the basal plane since the interlayer spacing between S-Nb-S is almost identical[114]. They also have the same value of van der Waals gap among the polytypes. It has been studied that one of the major differences for both polytypes is their electronic behavior. 2H-NbS_2 is superconducting whilst 3R-NbS_2 is not[83]. The Raman spectra is also a reliable method and have been used to differentiate the polytypes of TMDs that exhibit different intensity based on their crystal phase. 2H-NbS_2 has four Raman modes which are E^2_{2g}, E_{1g}, E^1_{1g}, A_{1g}, shows 31,260, 304 and 379 cm^{-1} respectively, 3R-NbS_2 has different four Raman modes as E_1, E_2, A_1 and A_2 at 290, 330, 386, 458 cm^{-1}[115]. The Raman spectra active modes may differ based on the method that has been selected to grow thin film and it can also depend on the precursors material for the synthesizing. The study of 3R-NbS_2 takes a significant

role in understanding the peak intensity with different thickness. It is known that there are four typical Raman active modes for 3R-NbS_2 that are E1, E2, A1, and A2. The Raman peaks at 386 and 405 cm^{-1} represent A1 and A2, respectively while A2 mode may not be observed in monolayer film. E1 and E2 peaks can be observed at approximately 280 and 327 cm^{-1}, respectively[83]. The actual vibrational mode of E2 and A1 are also shown below Figure 19 [78].

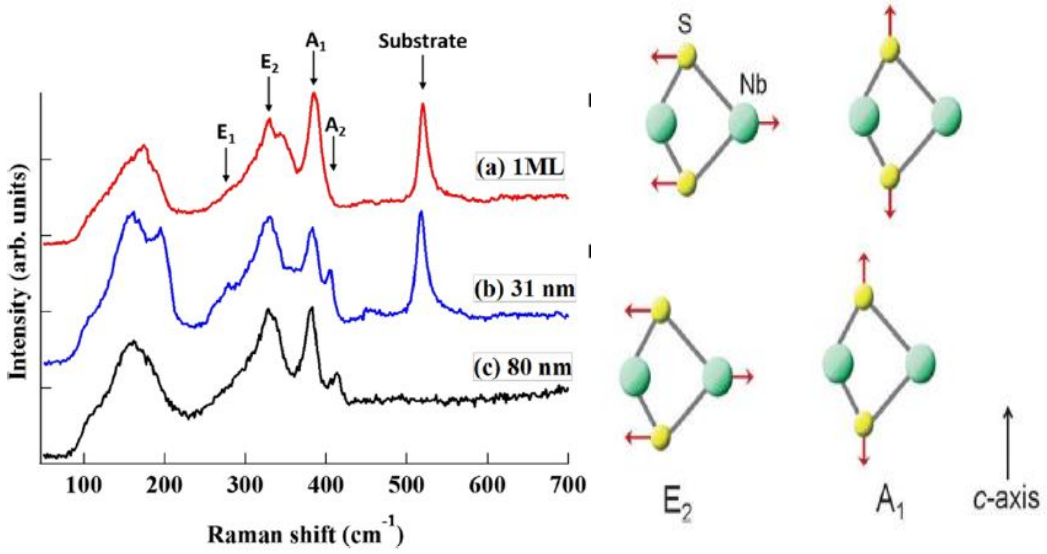

Figure 19Raman spectra of films that exhibit different thickness range from a monolayer to 80 nm (left) with the vibrational active modes of E_2 and A_1 (right) [78, 83]

3.2 XPS and XRD analysis

3.1.1 X-ray Photoelectron Spectroscopy (XPS)

XPS or Electron Spectroscopy for Chemical Analysis (ESCA) is a significant technique to obtain quantitative information about the chemical composition. Once the analysis is done, the clearer picture of relative quantities of each phase can be obtained from the test sample. By irradiating x-rays on the sample surface, and measuring the kinetic energy of the photoelectrons emitted from the sample surface, the tested sample can give

information about the elements constituting, the sample surface its chemical bonding state and its composition[116]. In order to create the information, Al Kα rays can be generally used for XPS instruments and they usually come from a few nm thicknesses of the sample surface.

XPS is very important for TMDCs to provide quantitative information especially for Mo: S and Nb: S ratio. Theoretically, the stoichiometry ration for these two materials is 1:2 even though experimentally it might slightly vary due to the synthesizing method and phase transformation engineering[116, 117].

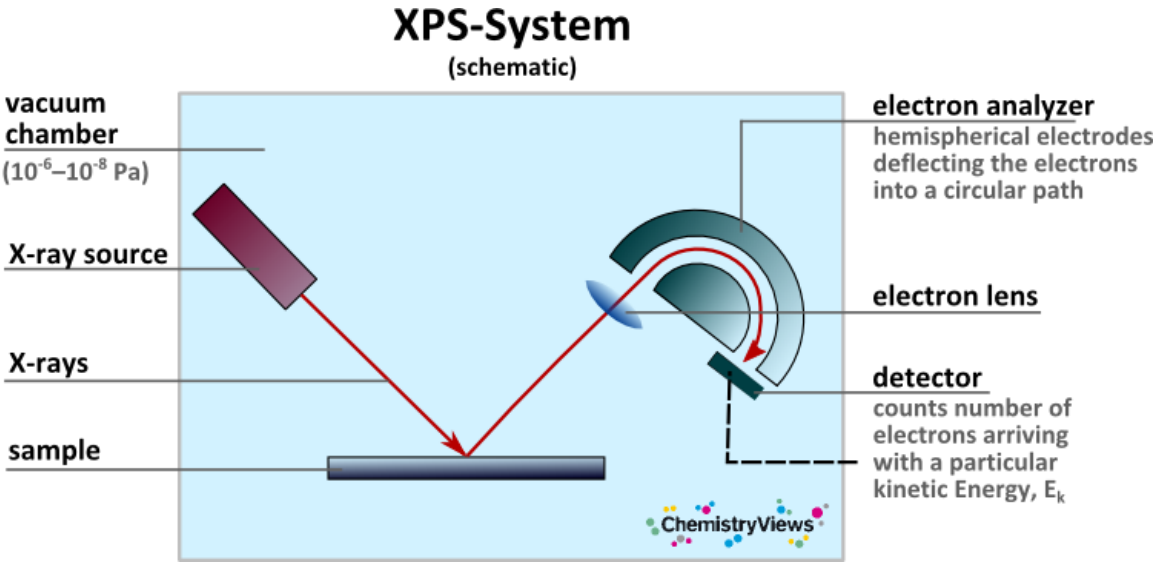

Figure 20 The schematic representation and working principle of XPS [117]

Synthesizing NbS_2 is very challenging in terms of avoiding oxygen from the surface of the films or flakes. There have been many works on synthesizing NbS_2 with oxide precursors or after growth, the oxidation layer might take place on the surface of NbS_2. In order to indicate, the amount of oxidation XPS is a crucial technique. For NbS_2 XPS analysis, there are five peaks appear on the spectrum while binding energy calculated

which are Nb 3d5/2, Nb 3d3/2, S 2p3/2, S 2p1/2, and O 1s. Nb and S elements can be observed from the elemental survey[63]

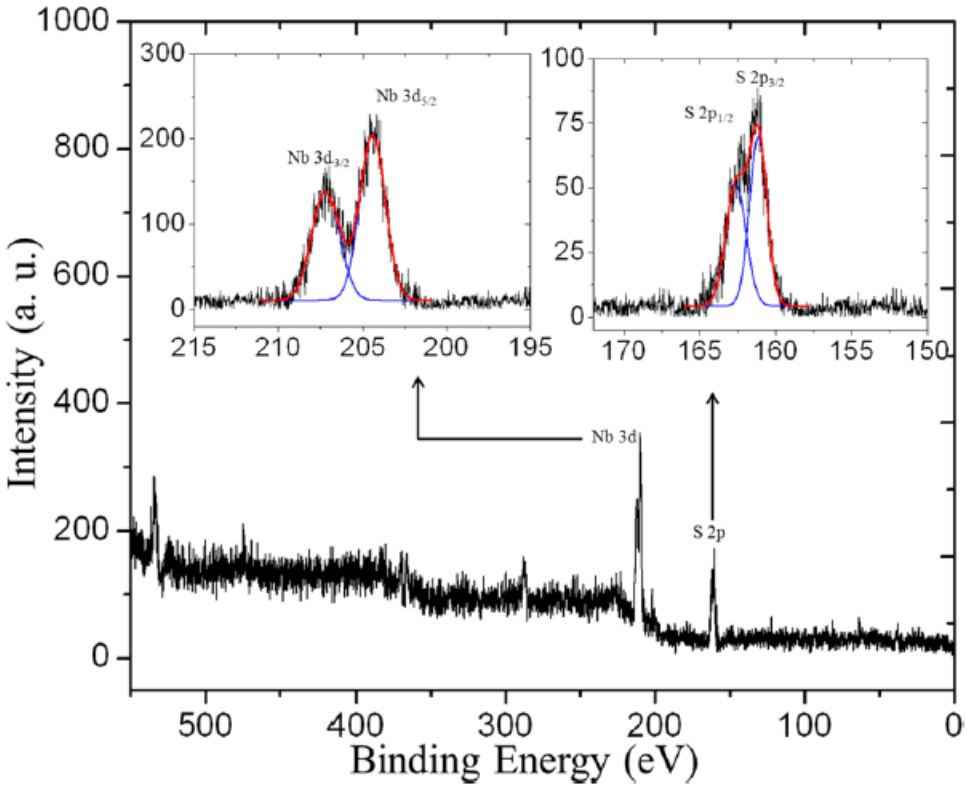

Figure 21 X-ray photoelectron spectroscopy spectrum of the synthesized NbS_2 film[63]

3.2.2 X-ray Diffraction (XRD)

X-ray powder diffraction (XRD) is another important analytical technique that is generally used for phase identification of a crystalline material and can provide information on unit cell dimensions. The following information can be revealed by this technique:

- The crystal structure,
- Chemical composition
- Physical properties of the materials and thin films.

The principal of this technique is based on the observing the scattered intensity of an X-ray beam hitting a sample as a function of incident and scattered angle, polarization and wavelength or energy[118, 119].

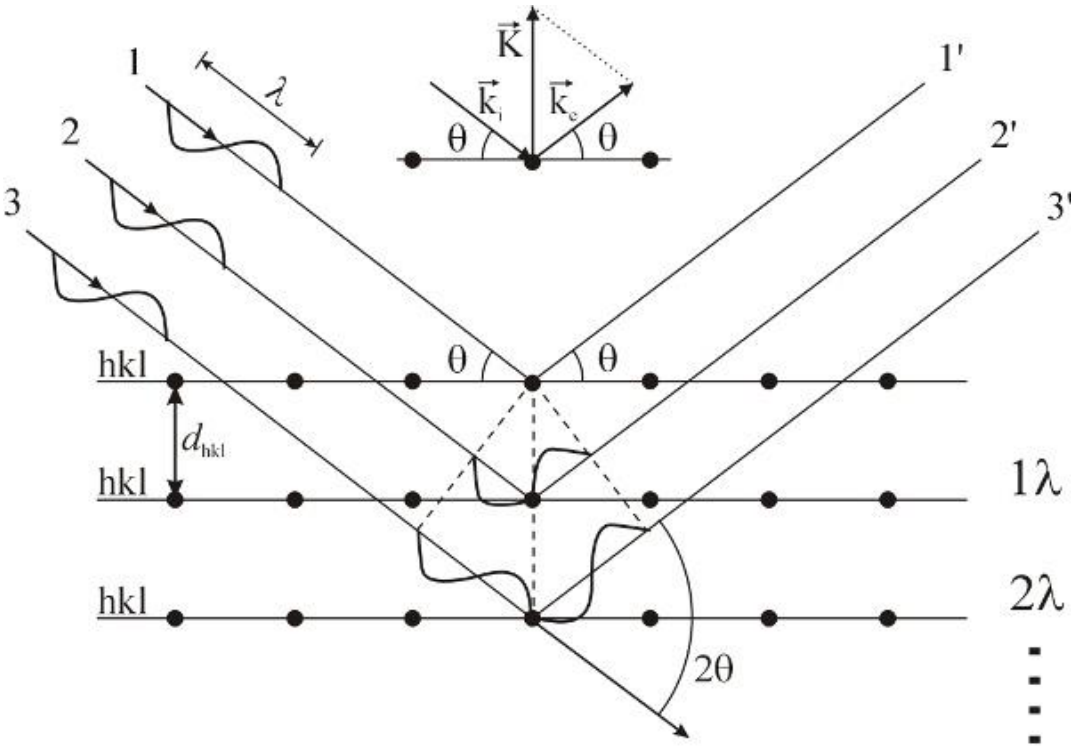

*Figure 22 vector **K = ke - ki** as the difference between the wave vector **ke** of the scattered wave, and the wave vector **ki** of the incident X-ray [119]*

The general relationship between the wavelength of the incident X-rays, the angle of incidence and spacing between the crystal lattice planes of atoms is known as Bragg's Law, expressed as:

$$n\lambda = 2d\sin\Theta$$

where n (an integer) is the "order" of reflection, λ is the wavelength of the incident X-rays, d is the interplanar spacing of the crystal and Θ is the angle of incidence[118].

Since the most of TMDCs family have polytypes, XRD is the crucial method to indicate their crystal structure which can be 1T, 2H and 3R and their lattice parameters. Especially for MoS_2, the phase transformation occurs from 2H to 1T after the lithiation treatment after a long time. Once the transformation successfully is completed, the electronic features and application of MoS_2 totally change. The intercalation of guest elements such as Na, Li, and K can also alter the chemical composition and crystal structure[120].

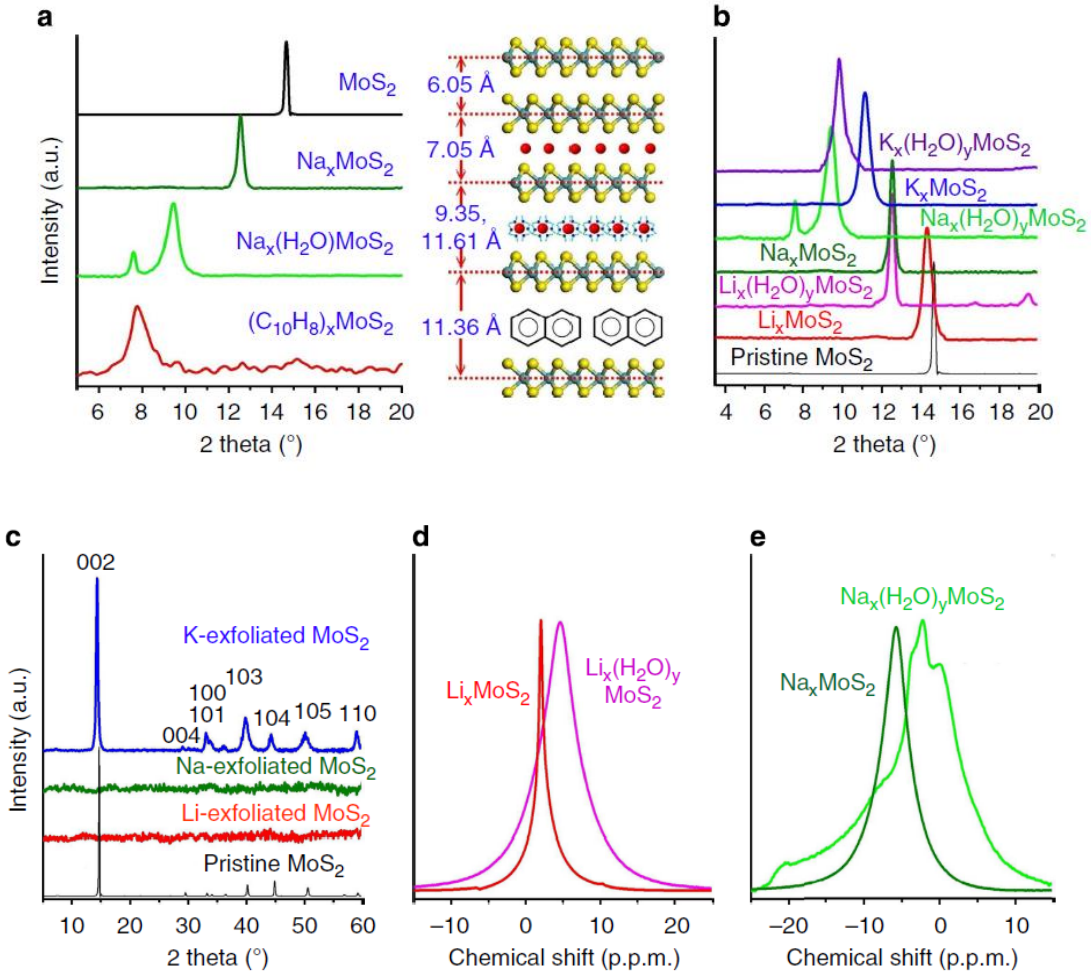

Figure 23 XRD analysis of different intercalated and exfoliated MoS_2

3.3 SEM, AFM and Optical Microscope Analysis of MoS_2 and NbS_2

3.3.1 SEM

The working principle of scanning electron, atomic force and optical microscope will be presented in this section with some examples of TMDCs. SEM stands for scanning electron microscope and it uses electron instead of light to create an image. Its development started early 1950`s, and since then, the development of SEM has reached a significant tool for the researchers to image especially atomically thin films. Compare to the traditional microscopes, SEM has a much higher resolution that is important to magnify closely spaced specimens at much higher levels[121]. Another crucial thing for SEM is that it has a large depth of field which is very important to focus many specimens at one time. Since SEM uses electromagnets rather than lenses, the degree of magnifications can be easily controlled. For TMDCs, surface morphology and its coverage are significant to be observed in terms of their features and applications, and SEM takes a key role in analyzing the materials.

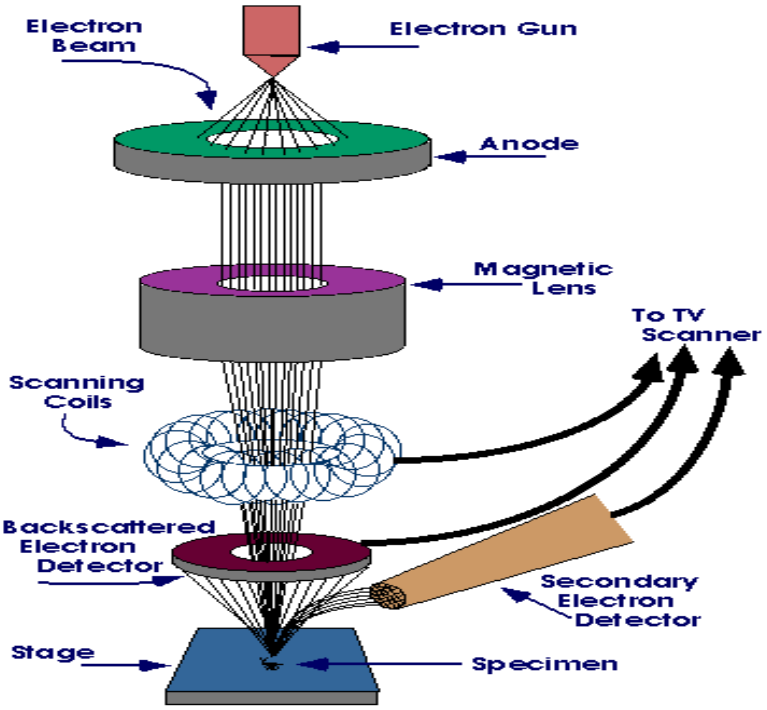

Figure 24 Scanning Electron Microscope[121]

3.3.2 AFM

Atomic Force Microscopy is a very high-resolution type of scanning probe microscopy and it provides a topological map of the surface by monitoring the deflection of a cantilever with an attached nanoscale tip that is scanned in a raster pattern across a sample surface. AFM was invented in the early 1980`s by Binnig, Quate, and Gerber. They were granted a Nobel Prize for Physic in !986 to contribute many works on both AFM and Scanning tunneling microscope (STM)[122]. The working principle of AFM is to have mechanically interaction with the surface by feeling or touching. It probes the sample surface with less interaction from electronic properties and does not rely on a tunneling current to operate. Piezoelectric elements that facilitate tiny but accurate and precise movements on (electronic) command enable precise scanning [123, 124].

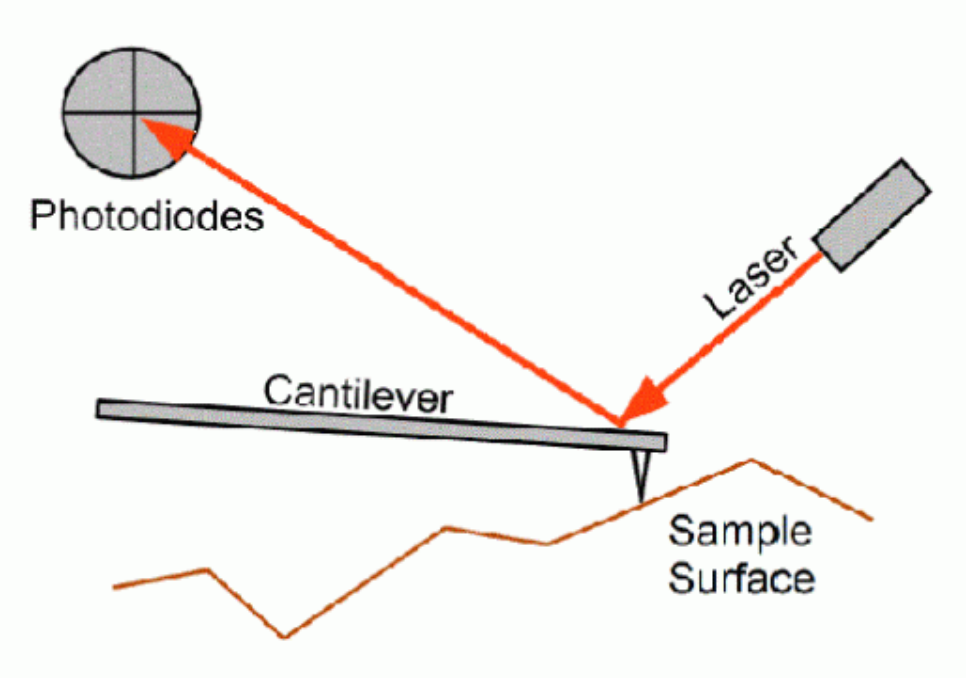

Figure 25 A schematic depicting the operation of an AFM[125]

3.3.3 Optical Microscope

Since TMDCs provides unusual phenomena based on their thickness dependency, such as single layer MoS_2 direct band, bulk MoS_2 indirect band, their thickness measurement and morphologic shape are important. Thus, Atomic Force Microscopy and Optical Microscope are significant to characterize the flake properties. The design of optical microscopy has developed recently in terms of incorporating multiple lenses, filters, polarizers, beam splitters, sensors, monitoring, and the illumination sources. Especially, for TMDCs higher resolution of the optical instrument gives a better insight into analyses of atomically thin flakes.

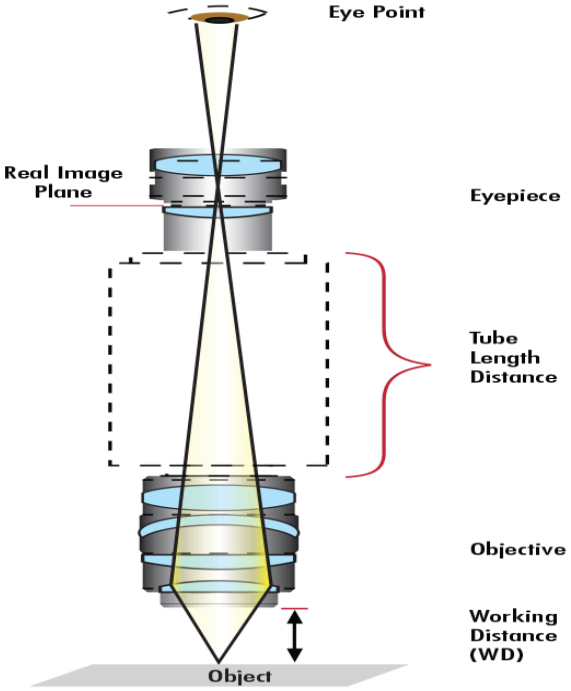

Figure 26 Components of a compound optical microscopy[126]

Here it is represented how scanning electron microscope, atomic force microscope and optical microscope have been used to get depth insight of TMDCs. The examples below are from MoS_2 and NbS_2.

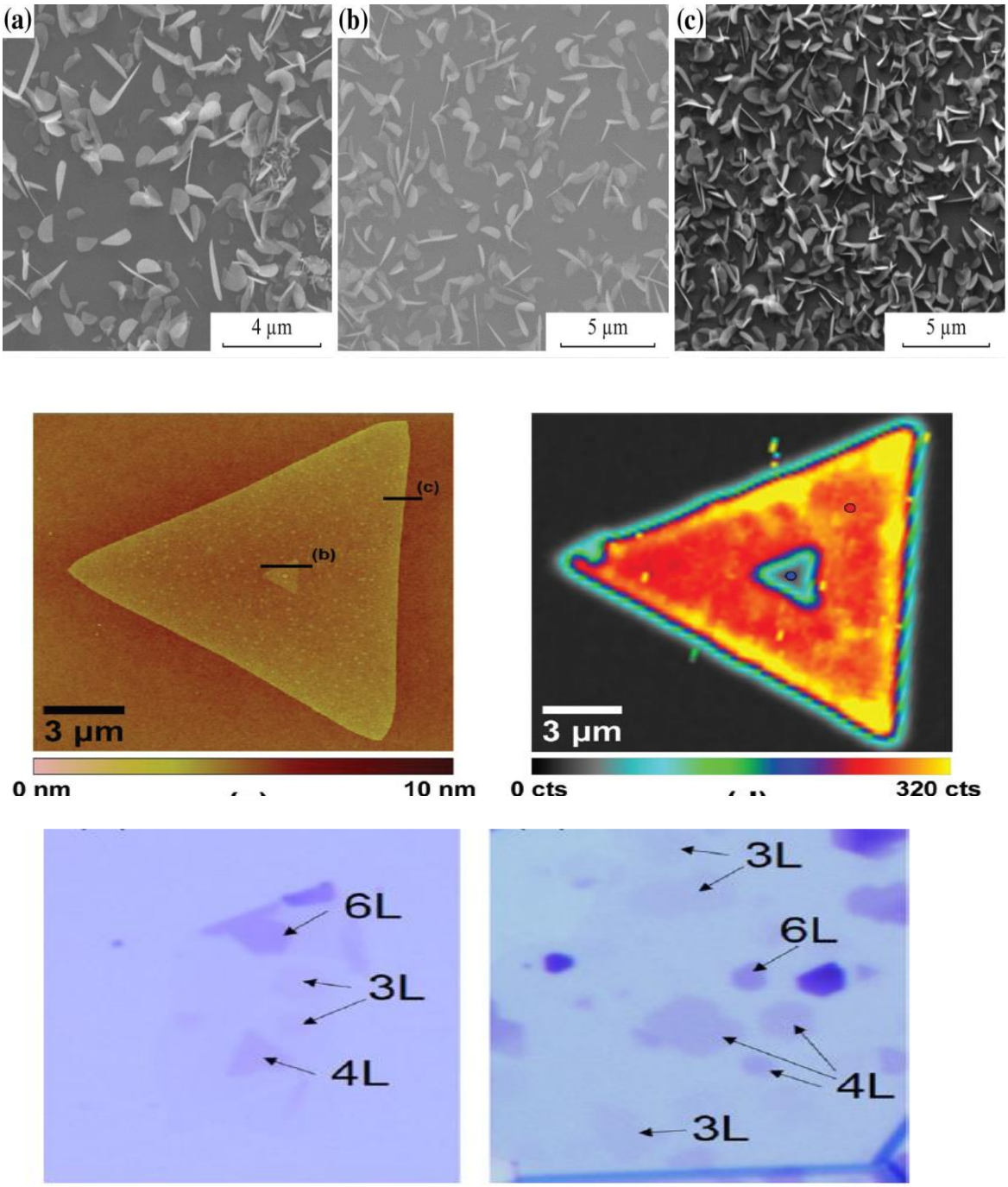

Figure 27 a,b and c shows SEM images of CVD MoS_2 on SiO2 coated Si substrate, d and e represents AFM picture of MoS_2 on Silicon dioxide substrate and the last images f and g shows NbS_2 grow on a silicon substrate, the references are shown, respectively [82, 127, 128]

CHAPTER 4

4. Experimental Works and Results

4.1 Chemical Vapor Deposition of MoS2

4.1.1 CVD MoS2 Experimental Set-up

Chemical vapor deposition of TMDCS is one of the best reliable methods in terms of having a large area of films and flakes. As we discussed earlier, there have been many studies on CVD to explore new properties of the materials with reasonable in a short time[10, 12, 129, 130]. During my research, I have utilized two different furnaces to grow MoS2 and NbS_2 since they both had different temperature gradient and cooling ramp. The set up that I modified for synthesizing MoS2 and NbS_2 was very similar to many works in literature. As it can be seen below Figure 28, the single zone clam-shell furnace with 1-inc quartz tube was used for synthesizing MoS2 thin films and flakes by CVD. There are many empirical parameters for CVD MoS2 synthesis and each of these parameters will be explicitly explained in this chapter.

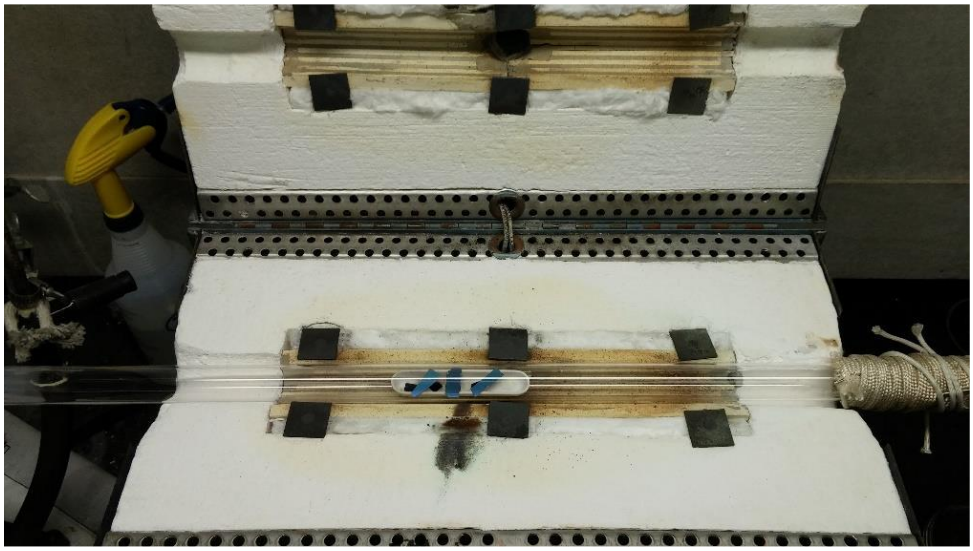

Figure 28 Single zone furnace that was used for synthesizing MoS_2, the substrates were placed in the center on the top of alumina boat with face-up position.

One of the main challenges that I had to deal with was to optimize the conditions that could be led to synthesize reproducible materials. In order to do that, it was significant to understand each key variables. My first grad year was dedicated to understand these variables from the literature and how to apply them to our lab conditions. After a deep literature survey, I finally made substantial progress towards a basic understanding of the influence of key parameters on the growth of MoS_2. Prior to having my own CVD set up, I first attempted to reproduce experimental results reported in the literature. Several precursors have been used in the literature such as Mo film[131, 132], $MoCl_5$[133], $(NH_4)_2MoS_4$[134], MoO_3[132], my initial grow study started by using the common precursors, commercially available MoO3 and sulfur powder for Mo and S reactants respectively. ≥99.5% purity MoO3 powder from Sigma Aldrich and 325 mesh (≤44 μm particle size) sulfur powder was obtained from Alfa Aesar with ≥99.5% purity.

The amount of the precursors and their locations in the furnace are one of the most key parameters of synthesizing reproducible MoS_2. Since the MoO3 has a much higher melting temperature (795 C^o) than sulfur powder (115 C^o), the MoO3 was placed in an alumina boat in the center of the tube furnace, the hottest region of the furnace. On the other hand, sulfur was placed in a region upstream, relatively cooler region and closer to room temperature zone due to its lower melting point. MoS_2 was successfully grown on the silicon dioxide substrates of which position were face down or up on the top of the aluminum boat that has Mo source. The concentration of the precursors was changed in time with increasing temperature and this change has been demonstrated clearly.

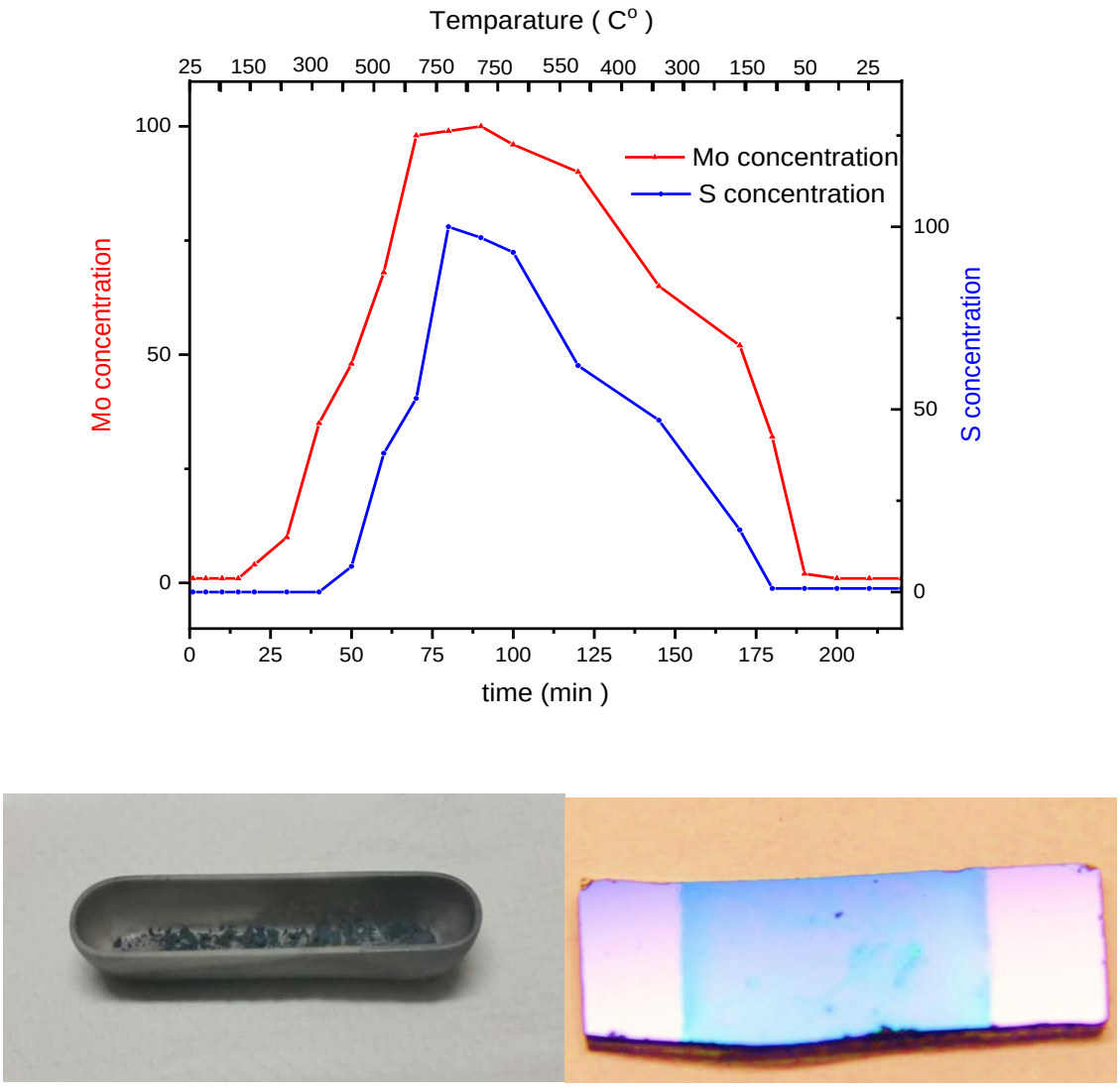

Figure 29 Concentration of the vapored gases from the precursors in time (top). Alumina boat is placed in the center of the furnace, having Mo source in it (left) and the substrate (right) shows the deposition of MoS_2 after the reaction.

Prior to beginning any deposition, it is important to have a clean tube for synthesizing any TMDC. Otherwise, the growth reaction will be influenced by initial oxygen concentration and unwanted impurities. To avoid that, the reaction tube was purged with an inert gas to minimize unwanted oxygen, dust and other impurities from the reaction environment before beginning any deposition. The furnace that I used for MoS_2 synthesizing was slightly different than the other one for the NbS_2 grow. The maximum

temperature that furnace could ramp up was approximately 900 C^0 while the other one was over 1200 C^0. Once the set up was ready, the temperature of the furnace was slowly ramped up to the growth temperature that was approximately 800 C^0 at a rate of 20 - 25 C^0/min for MoS_2 growth. Then, the temperature was held at that temperature the amount of 10-45 minutes based on the desired film thickness. Once the reaction was over, the tube furnace was allowed to cool to room temperature before the samples were removed for further characterization. It is important to know that the modifying cooling rate is significantly important to have a uniform, large area films. During MoS_2 growth, the furnace was allowed spontaneously to the room temperature in approximately 2 hours. The possible reaction has been taking place in the reaction chamber as follows:

$$2MoO_3 + 7S \rightarrow 2MoS_2 + 3SO_2$$

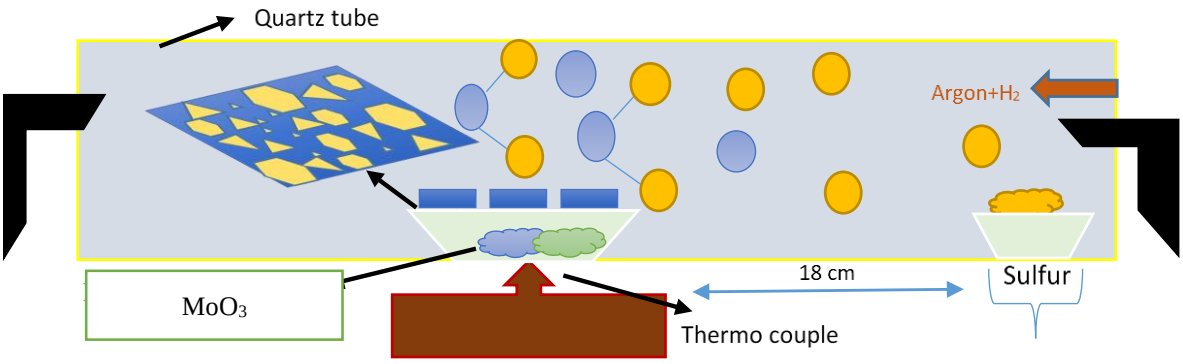

Figure 30 CVD MoS_2 growth set up. The precursors are located in the different region, 18 cm distance from each other, the silicon is at the face-up position on the top of alumina boat.

The experimental set-up that has shown above, the most of the time led to successful deposition of MoS_2 with having a different thickness on the substrate surface. Inhomogeneity and variable thickness on the sample surface was the main challenges to

overcome. The formation of MoS_2 has differed in many ways once the parameters were slightly changed resulting to have different crystal morphology and their forms, monolayer to bulk. With the substrate-face-down approach typically led to having thicker film and flakes compare to placing the substrate face up on the aluminum boat. Monolayer MoS_2 were found on the surface where silicon dioxide made contact to alumina boat. Increasing monolayer area of MoS_2 was the most difficult challenge to characterize the film for further applications. Modifying the time-temperature variant was not the only parameter to reduce the solution simply. Many CVD published worked claimed that 5 minutes of growth time would be enough to have a monolayer region of MoS_2. On the other, having that less of growing time is not sufficient enough to vaporize the precursors and allow unwanted components to leave the reaction. Due to the fact that the precursors are placed in the different region in the tube, their vaporizing time and temperature will be different. MoO_3 vaporizes long before appreciable sulfur is produced. Since the experiment takes place in the single zone furnace, the relative partial pressure drastically changes. Once MoO_3 starts to vaporize, the relative partial pressures shift dramatically from sulfur deficient to sulfur-rich in a short time. While the reaction continues, the partial pressures of the precursors change with the flow of the inert gas. This and the huge variation in experimental parameters cause to have different thickness and morphology of MoS_2 after the reaction. To reduce the effect of the variant and achieve reproducible products, some researchers have used heating tape. The aim of using the heating belt is to control sulfur temperature by placing it outside of the furnace temperature zone. However, this might bring another parameter to the system especially once it is started to use slightly different time than the previous experiment or placing it differently on the quartz tube. In this work, the heating

tape was not used for any deposition of MoS_2 and NbS_2 in order not create another uncontrollable variant.

4.1.2 Parameters for CVD growth

There have been many variables for the CVD growth of any TMDCs materials and some of them were mentioned briefly earlier. However, it is crucial to focus on the highest contributing ones so that the reproducibility of CVD grown samples can be engineered for phase transformation and characterizations. The following parameters are significant for successful CVD growth:

- Temperature (precursors vaporizing, reaction growth)
- Mass (the amount of the precursors, needs to be milligram or less)
- The surface area of the reactants
- Inert gas flow rate (even though the type of the inert gas does not effect on the deposition for CVD, its flow rate is extremely important- 100 sccm ideal)
- Substrate position (usually the substrate is placed at the center but its position- face up or face down- effects on the growth)
- Cooling rate (the temperature is spontaneously brought down to room temperature, the faster cooling rate causes an undesired crack on the flakes)
- Time (longer growth time usually results in thicker films although monolayer flakes can be obtained in shorter time depending on the materials)
- Temperature zone of the furnace (the larger zone furnace is desired in terms of keeping the heat longer with higher efficiency)

There are many more factors for CVD growth that are harder to manage including using cleaner substrates, the height differences between the precursor's source and the

substrates, roughness of the surface for the substrates, humidity of the precursors. The last but not the least, the type of the substrates impacts on CVD growth of any TMDCs. As it can be observed, the CVD method is much more complicated than it seems. I have meticulously focused on each of these parameters during my project. The journey of synthesizing a successful film and its characterization has been successfully demonstrated in this section.

4.1.3 Characterizations of CVD MoS_2

Synthesizing a high quality and large area of CVD MoS_2 directly depends on the amount of sulfur. Sulfur takes two important key roles during the CVD reaction, the first, it makes a bond with Mo atoms to create a MoS_2 structure as expected, the second is to reduce oxygen in the reaction by creating an SO_2 bond. $MoOS_2$ compounds might take a place on the substrate surface once there is an insufficient amount of sulfur as shown Figure (a). The Raman spectra of this compound have given extra peaks around 200 cm^{-1} besides 385 and 404 cm^{-1} which corresponds to a single layer of MoS_2, $E_{2g,}$ and A_{1g} respectively. A closer examination on the thickness analysis has been done by atomic force microscopy (AFM). Typically, the thickness of a single layer of MoS_2 measured by AFM ranges between 0.6 and 1 nm. In this work, the thickness of the flakes measured 0.98 nm which is a good match to the thickness value of monolayer MoS_2 in the literature. The AFM image and the thickness analysis has been shown in Figure 31 below.

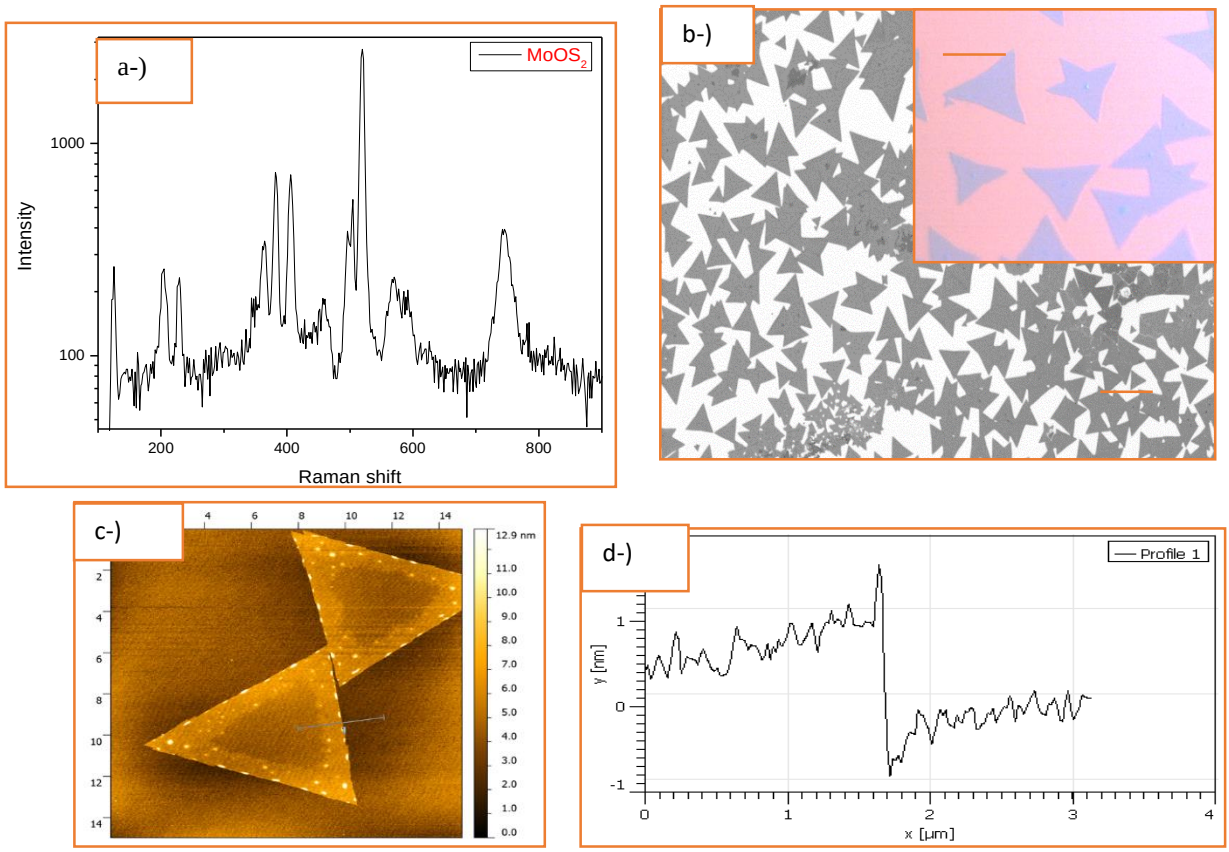

Figure 31 The oxidation state of MoS_2 once insufficient sulfur in the reaction (a), optical and SEM images of the flakes, scale bar of 30 microns (b), The AFM picture of the flakes (c) and its thickness is approximately 1 nm, which corresponds to a monolayer of MoS_2 (d)

The qualitative information about the film and flakes can be obtained by Raman spectroscopy and the structural data including phases, a number of MoS_2 layers can be clearly determined via the vibrational spectrum as discussed earlier. Raman spectra have been employed on the same sample at the different regions to have a better picture of the sample as shown below. The experiment was done at 700 C^o – 45 minutes by using 0.4 gr of sulfur with 100 mg of MoO_3 powder. The different thickness of CVD grown MoS_2 has been synthesized with clear E_{2g} and A_{1g} peaks as well as PL peak which shows pronounced

emission peak of 677 nm for CVD MoS_2. On the other hand, X-ray photoelectron spectroscopy (XPS) is a very useful device to give information about the chemical composition of the materials with a better picture. In this project, the Thermo Scientific K-Alpha spectrometer was used to do further characterization for CVD-grown MoS2 samples. In addition, all spectra were taken using an Al Kα micro-focused monochromatized source (1486.7 eV) with a resolution of 0.6 eV and a spot size of 400 μm. XPS to correlate experimental parameters with resultant film stoichiometry. Survey spectra from XPS show that the presence of S, Si, O, C, and Mo have been obtained in all CVD experiments**.**

The atomic ratios of each element can be easily compared by fitting Gaussian curves. The calculation can be done directly on their areas above the baseline of this fitting. As seen below Figure 32, the relative areas of each element peaks yield the ratio of Mo and S. The ratio indicates the stoichiometry of MoS_2 films. By scanning for specified photon energies more slowly, higher resolution binding energy peaks are obtained. The Mo3d scan contains two peaks at 233.5 eV and 230.2 eV as well as a small S2s peak at 227.5 eV. The sulfur scan resolves two overlapping peaks at 163.5 eV and 162.5 eV. The atomic ratio of Mo: S was approximately 1:2 indicating that the region where the substrates located might show the different ratio. The ratio is directly dependent on the sulfur or Mo-rich region. The striking finding from the XPS analysis was that measurements made on the same exposed central region of a sample sometimes showed drastically different S: Mo ratios. For instance, once the substrate was located at the center of the furnace- right above the MoO_3 source, the ratio showed the highest average of S: Mo = 2.33 while it was 0.72 once the samples were placed closer to the reaction cold zone. Based on the XPS the result, it

can be said that the ratio is dependent on a few parameters, which are the substrate location, the precursor's location, the alumina boat location and the flow rate of the carrier gas. The reaction temperature is another key parameter in terms of consuming all the precursors during the reaction.

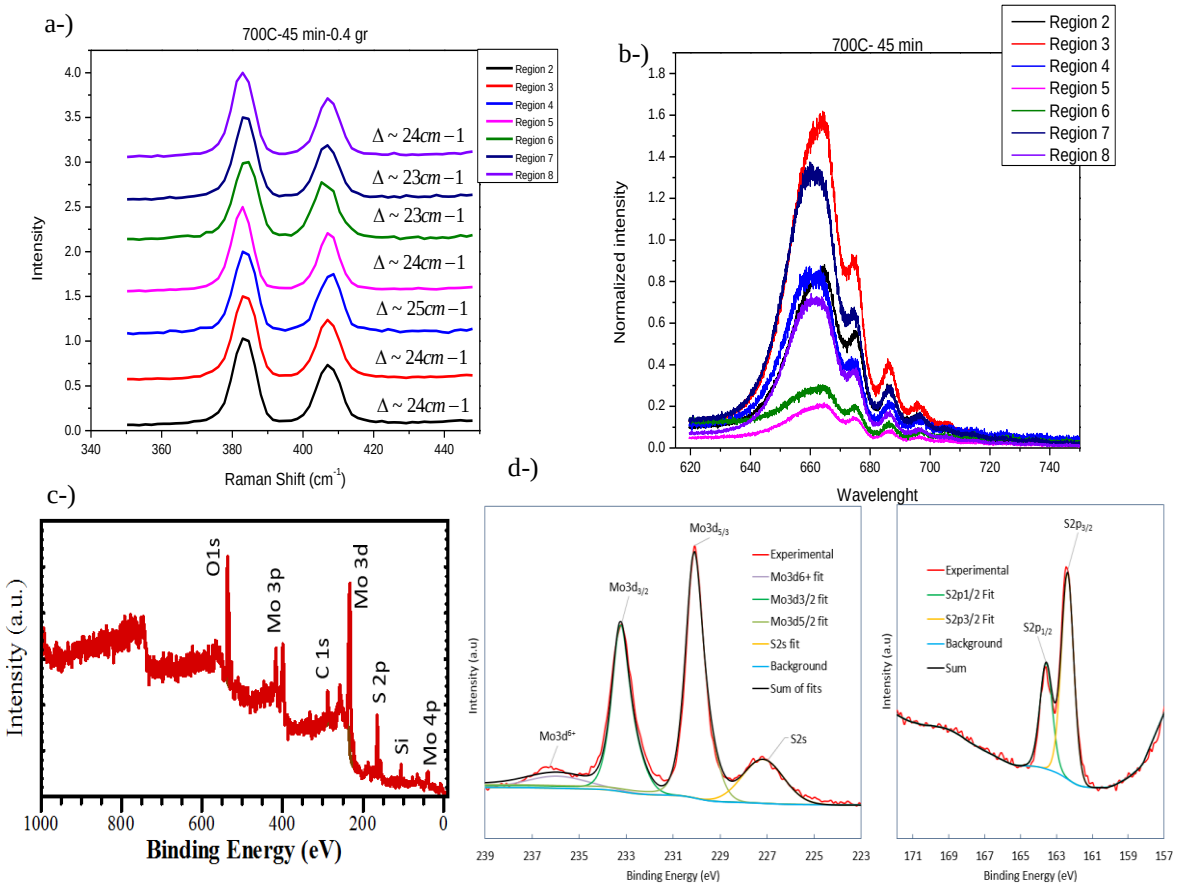

Figure 32The Raman spectra (a) and PL measurements (b) of the flakes. The measurements have done on the same sample at the different location by using 514 nm laser wavelength with a 1-micron diameter size of the laser. XPS survey of CVD-grown MoS_2 (c) Mo3d and S2p XPS scans (d)

4.2 Shape evolution of CVD- grown MoS_2

Once the successful growth is achieved via CVD method on TMDCs, the flakes can take many different domain shapes. Those domain shapes have been shown in the literature including triangles, hexagons, truncated triangles, three-point stars and six-point stars[135-137]. Even though there has been great attention on TMDCs applications and synthesizing, understanding of the shape evolution of MoS_2 or any other domains is still limited. In this section, the study of shape evolution will be straightforwardly explained and this approach can be applied to any other TMDCs materials. In order to show the shape evolution, different morphology and evolution of MoS_2 have been demonstrated in this section. This experimental method to study the shape evolution of the CVD grown MoS_2 domains is employed on the Si substrates with a 300 nm silicon dioxide surface within the same growth conditions after each growth. The shape evolution approach is employed to comprehensively study the crystal structure of MoS_2 and it has been supported many techniques including Raman Spectroscopy, Scanning Electron, and Optical Microscopy and Atomic Force Microscopy. The different crystal growth mechanism with shape transformation have been illustrated with the dependence on Mo: S atom ratio. The fundamental principles of crystal growth, the shape of a crystal is determined by the growing rate of different crystal faces[138]. To elaborate on this, the slowest growing faces causes the largest face of a morphology. On the other hand, the rapidly growing faces either become smaller or disappear altogether. This mechanism can be explained by surface free energy for 2D materials. Based on these edge energies, the final morphology can be shaped in triangles, hexagonal or any other forms. Prior to any shape, the crystal morphology is initiated with a nanoscale hexagonal nucleus and it finalizes the morphology.

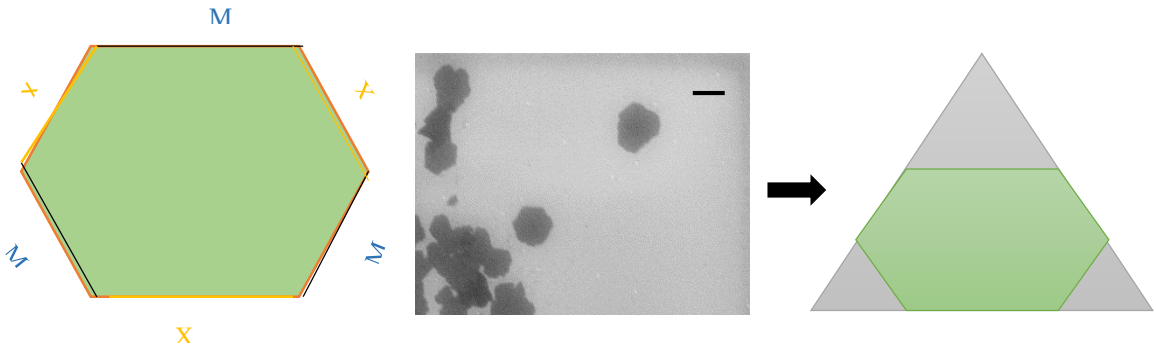

Figure 33 The nucleation and grows starts with nanoscales flake and continues its final shape based on the highest energy edge terminations, the lateral size of the hexagon flakes is approximately 100 nm. (scale bar 100nm)

The surface free energy pertains to the edge free energy in this case. Since the low-energy faces tend to grow slowly, the final shape evolution of MoS_2 is related to the growth rate of different edge terminations. In the case of MoS_2, the most commonly observed terminations are Mo-zigzag and S-zigzag terminations, Mo-zz and S-zz respectively. Those two terminations are known the most energetically stable structures[135]. As it can be seen below, these two terminations have zigzag edges. However, the position of S and Mo atoms differ. The S atoms are exposed to the outside and each S atoms has two bonds with Mo atoms. On the other hand, for Mo-zz terminations, the Mo atoms are exposed to the outside and each has only four bonds with S atoms.

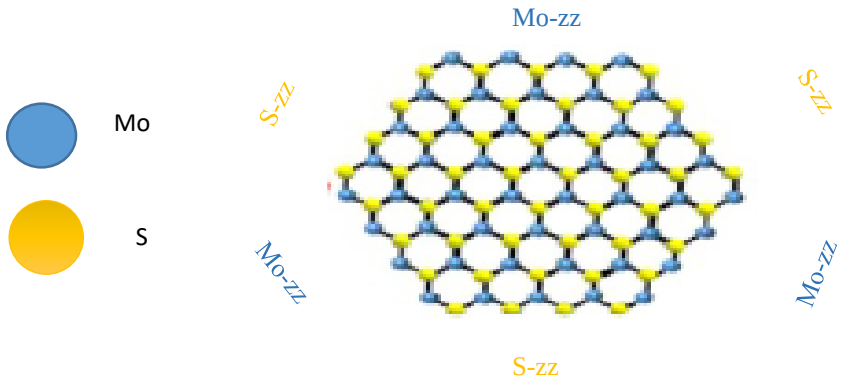

Figure 34 The most energetically edge terminations, Mo-zz and S-zz, the first nucleation starts and grows.

4.2.1 Case 1 (Mo: S >1:2)

Mo-zz and S-zz terminations and their energy are responsible for the final morphology. We can categorize this in three conditions which are If Mo: S >1:2 If Mo: S =1:2 and If Mo<S 1:2. As we mentioned that earlier, all shapes of domains start growing from the nanoscale hexagonal nucleus. In the first case, Mo: S>1:2, since Mo atoms are rich in the environment, S-zz terminations grow faster than Mo-zz terminations. Indeed, S-zz terminations with unsaturated S atoms exposed to the outside are more energetically unstable than Mo-zz terminations. In addition, the fact that there is a higher probability of meeting and bonding with free Mo atoms for S-zz terminations. Under this condition, hexagonal nucleus starts to grow from S-zz terminations and the final morphology is three sides of Mo-zz terminations.

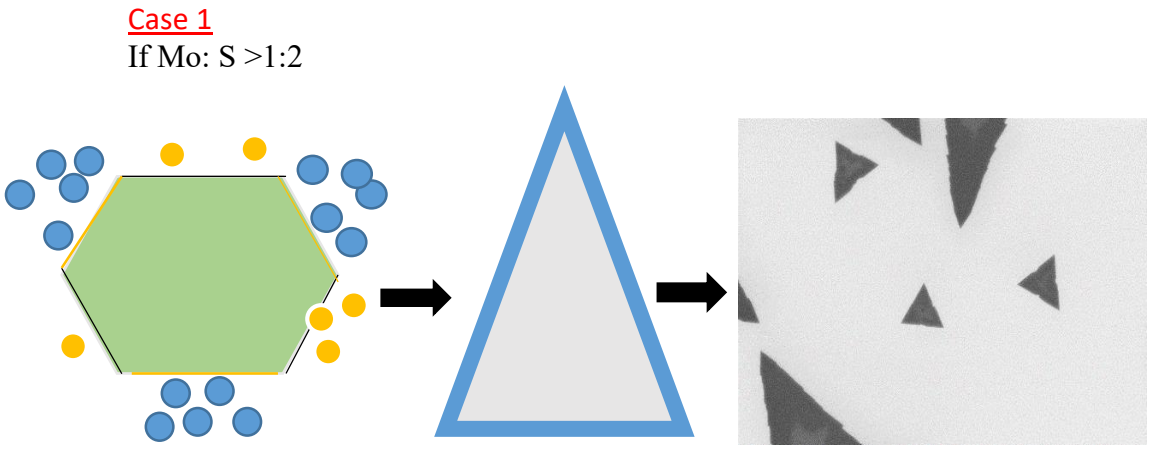

Figure 35 The domain shape will change from a hexagon to a triangle with three sides of Mo-zz terminations since the S-zz terminations grow faster.

4.2.2 Case 2 (Mo: S =1:2)

In the second case, there is a similar growth rate where Mo: S =1:2 corresponds to the stoichiometric ratio of MoS_2. The free atoms that meet in sufficient environment of Mo and S have the same termination stability and probability. Since both terminations grow rate are similar, the hexagonal morphology is observed at the end of the reaction. The lateral size is relatively larger than the first hexagonal nucleus.

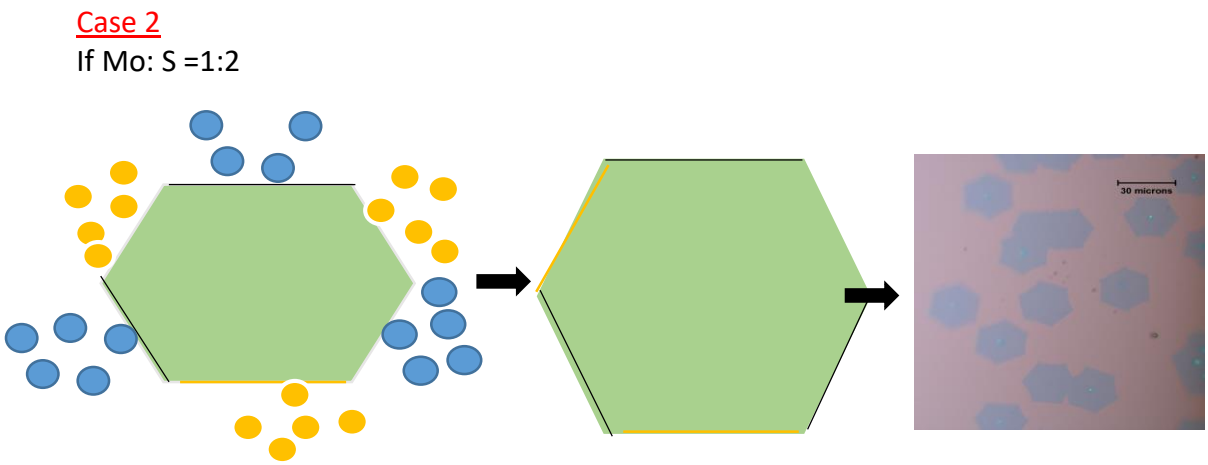

Figure 36 The domain shape will not change but the lateral size will. Mo-zz terminations and S-zz terminations grow similarly.

4.2.3 Case 3 (Mo: S <1:2)

Under the final condition, where S atoms are rich in the reaction environment, the result is similar to the first condition in terms of the final morphology. The S-zz termination will take place at the final stage instead of Mo-zz termination. The growth rate differences between Mo and S is the main parameter of MoS_2 ratio that is influenced by the energy stability of Mo-zz and S-zz terminations.

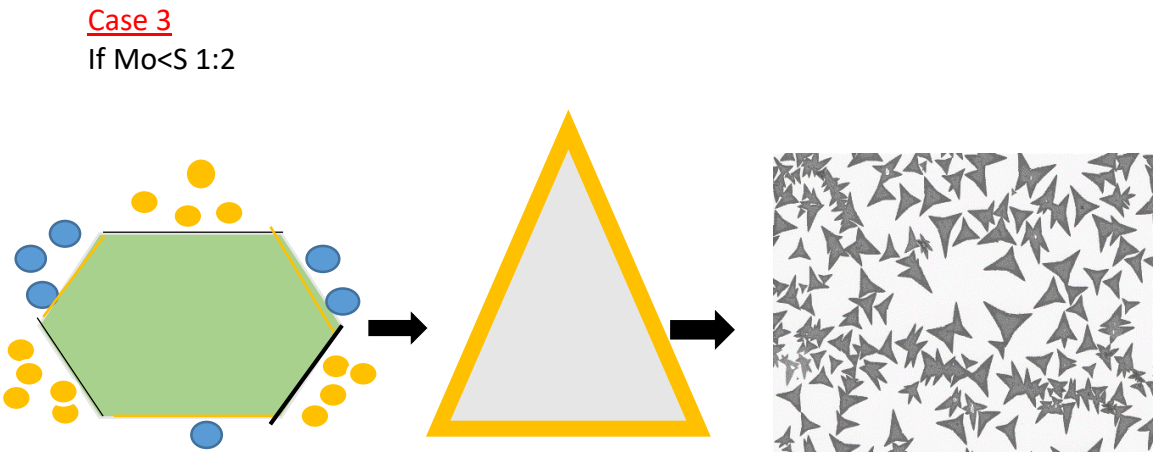

Figure 37 Mo-zz terminations grow faster than the S-zz terminations grow under the third case. Final morphology shapes sulfur edge triangles.

There are many parameters that effect on the shape evolution morphology, including the amount and the location of the precursors in the furnace, type of the precursors, the distance between the precursors and the growth temperature. the correlation between the domain shape and Mo: S ratio has been proved with previous studies[136, 139] and our approach of different shapes of MoS_2 domains evolution has been exhibited the similar

results to the other TMDCs including NbS_2, the further information will be provided upcoming chapters[140].

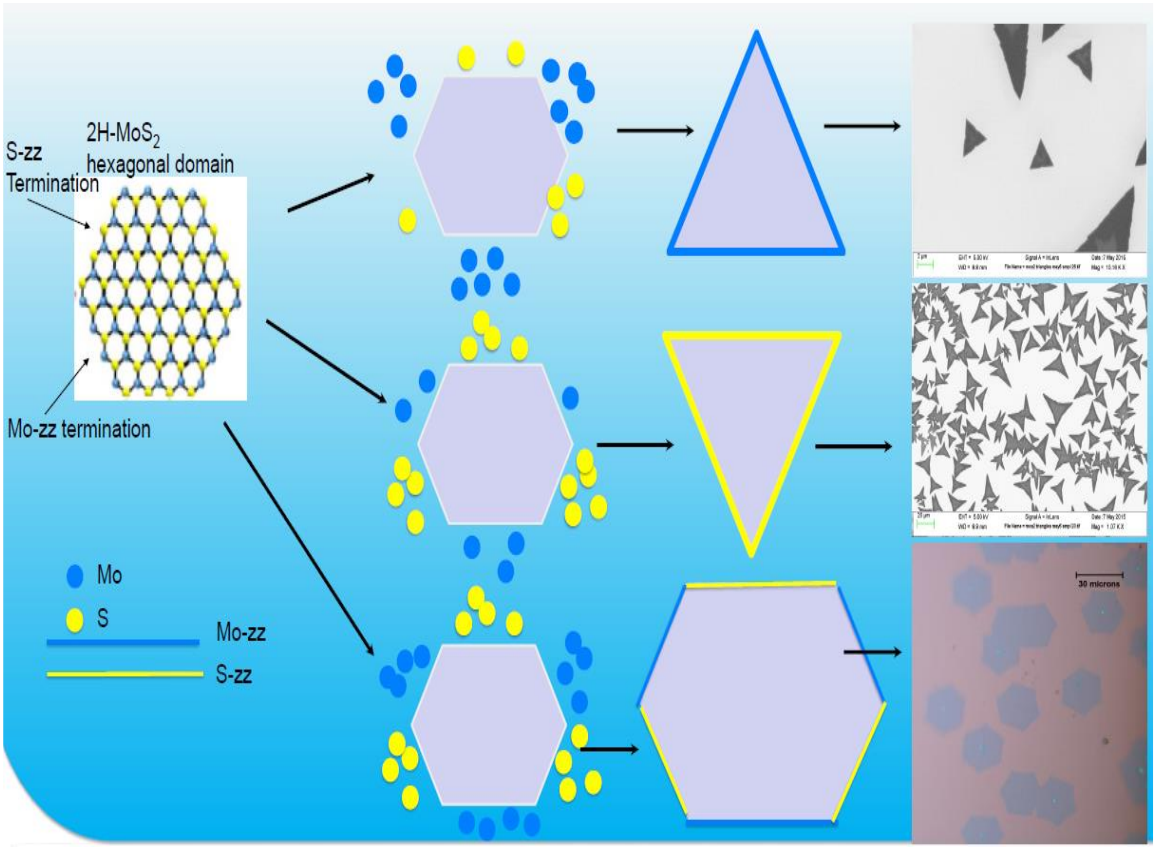

Figure 38 The summary of all three conditions is illustrated with the different final morphology - presented at NASA New Jersey Space Grand Consortium, Rutgers University 2015

4.2.4 Precursors and gas flow effect on shape evolution

The number of parameters that effects on the shape evolution of CVD MoS_2 have demonstrated that Mo: S atomic ratio along the substrate surface is significantly important to explore the final morphology of the crystals. Not only the distance that is between the precursors and the heat zone but the precursor's distance to each other takes a key role for the nucleus to grow. If Mo: S ratio is >>1:2, this means that S-zz termination grow much

faster than that of Mo-zz making crystal domain transform to a triangular shape in a very short time. This will cause to form the star shapes of flakes. On the other hand, the truncated triangles will be formed within the same period of growing time once Mo: S ratio is slightly above 1:2 atomic ratios. The figure below shows the change of the shape evolution once the distance between the precursor's increases, from stars to truncated triangles is formed with the different average of the flake size including the standard deviation of the flakes size for each condition. The sulfur distance to MoO_3 source exhibits the optimum flake size and triangle shape once the distance to each other is approximately 19 cm. Increasing the distance between the sources leads to relatively smaller flake sizes.

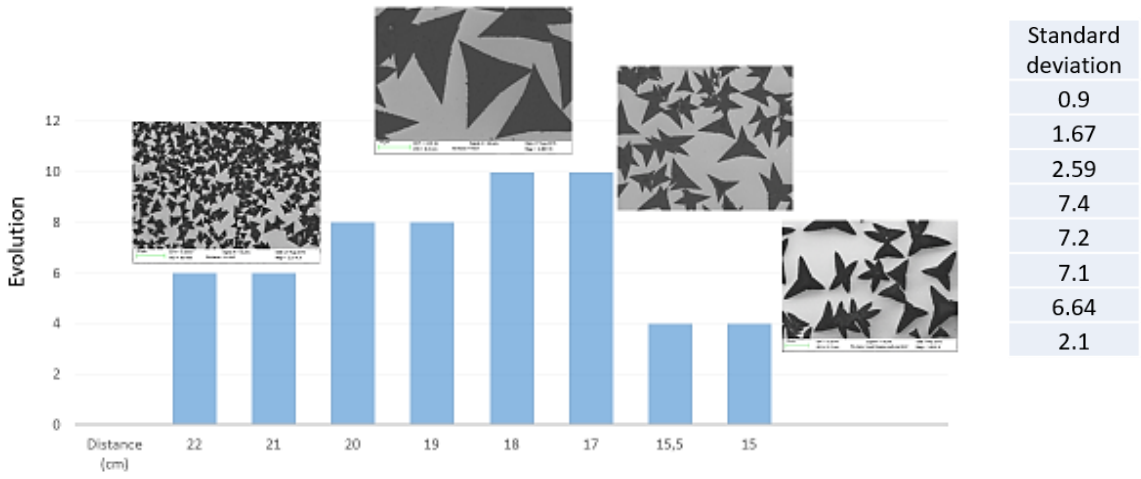

Figure 39 The top figure presents the distance between the sources vs the average size of the triangles, the optimum size, and distance of about 19 cm. The figure below shows the shape morphology vs distance between the precursors.

A carrier gas is one of the main components during CVD reaction. Career gases are generally selected depending on the application and they help to achieve the best separation in the whole process since they are inert, don't react with any reactants. They have used in

many chemical reactions including CVD process. The choice of the carrier gases is related to their usage either in the industry or individual performing the process. Their accessibility and price are also important parameters to select them as well as obtaining maximum efficiency[141]. The linear velocity of the gas and its purity are the major factors to use them as a carrier gas due to the fact that a minor impurity can affect the results significantly for CVD or any other chemical reactions[142]. Several gas carriers have been used in this work, nitrogen (99,9%), argon (99,9%), the argon-hydrogen mixture ((90% argon and 10% hydrogen) with different flow rate during the CVD growth. Although using the type of carrier gases did not affect the deposition amount on the silicon/silicon dioxide substrate, the flow rate of the carrier gases moderated the final morphology during the CVD reaction. The Figure below shows the final morphology of MoS_2 flakes versus changing the flow rate.

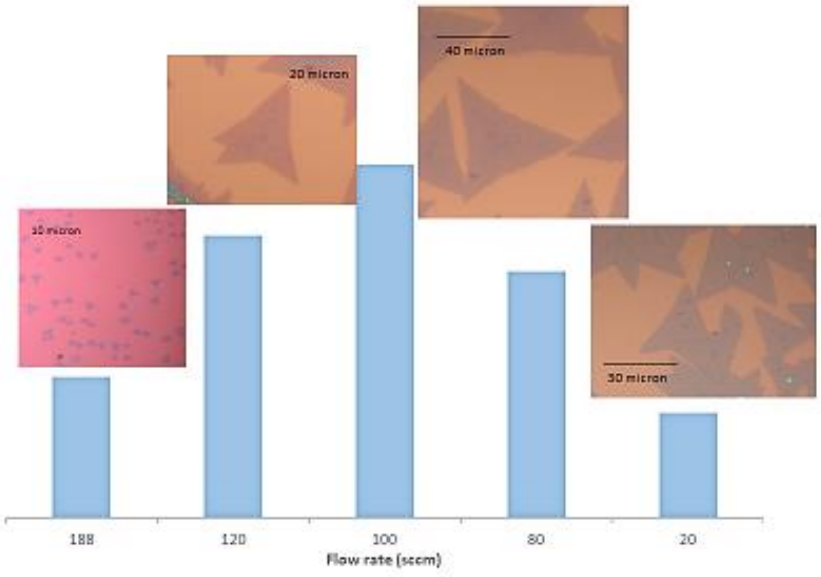

Figure 40 The flow rate between 80 -100 cubic centimeters per second (SCCM), has shown decent size and coverage of the triangles. Each experiment was done under the same time condition, approximately 30 minutes.

4.3 Substrate effect on CVD MoS_2

Thin film deposition technology engineers applying a thin film with good step coverage. The technology employs between a few nanometers to about 100 micrometers or in some cases, the thickness of a few atoms. Many materials can be deposited with this technology resulting in the range of different thickness[143]. Choosing the substrate for thin film technology is considerably important for the final materials and their thicknesses. It is a fact that the thin film manufacturing process is the heart of today's semiconductor industry. Thus, the choosing optimum substrate for each material gives rise to a successful CVD growth. Nucleation and growth mechanism occur on the substrate surface where the deposition and further island evolution form the nucleation and cluster. There are certain places on the surface where the possibility of deposition is higher. The first place is called kink; the following second deposition takes place on the step. The terrace is the third favorable place for atoms to deposit and create an island for further growth process[144].

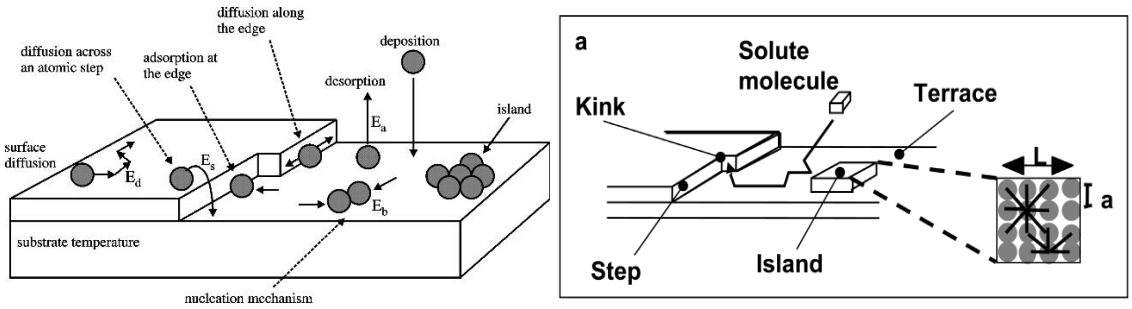

Figure 41 Deposition and surface deposition diffusion process of adatoms, nucleation mechanism on the substrate.[144]

4.3.1 Substrate locations for CVD MoS_2

In this work, selecting a feasible substrate for each CVD growth process of MoS_2 and NbS_2 was one of the most challenging issues that I had to overcome. The deposition of MoS_2 and NbS_2 were done with the different substrates such as silicon, silicon dioxide, sapphire, gold, quartz, doped silicon, glassy carbon in order to create an efficient surface chemistry for CVD growth. In the CVD process, the substrate is placed in the quartz tube chamber either face-up (the polish part positioning up), face-down and sometimes side position. Silicon dioxide was the most used substrate for further characterization. However, the result of other substrates will be also presented in terms of a better understanding of the substrate effect on CVD growth. After each deposition using the different substrates, the further characterization will be presented in the next section. The fact that the reaction chamber is isolated, there is a limited region in the quartz tube where the substrates can take the position of.

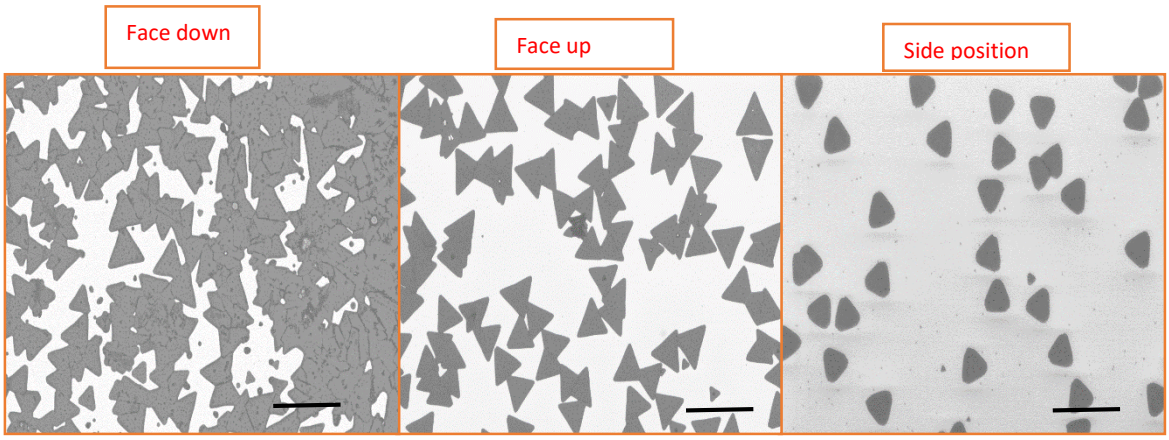

Figure 42 The possible positions of the substrate can place in the quartz tube. Three different positions of silicon dioxide substrate in the quartz tube for CVD MoS_2 growth, the scale bar is 20 microns for the SEM images.

Using the optimum substrates and its location in the reaction chamber is a key to understanding the mechanism of CVD system. After trying each position of the substrate in the quartz tube, the face-up position has given much more controllable coverage and deposition compare to other two positions, face-down and side. To clarify this better, Figure above and figure below has been demonstrated to have an insight on the substrate surface. Once the substrate is placed in the quartz tube with face-down position, the partial pressure of MoO3 is relatively higher than any other two positions resulting in having a large and dense coverage on the surface. The vaporized molecules from the MoO3 powder meets with vaporized sulfur with higher possibility. In addition, the diffusion of these molecules along the substrate surface causes a high gas flux in a short time span. The large range of deposition from bulk to monolayer is still formed. However, the region where a few layered and monolayer flakes are occupied is limited and isolated. On the other hand, the side position gives relatively a better form. The gap between the flakes is reasonably decent for making a contact to do further applications. Nevertheless, the size of the flakes is smaller in the range of a few microns to 10 microns. Therefore, the applications and further characterizations of these flakes might be a challenge for the side position. Placing substrate face-up position gives a desirable flake size including from a few microns to up to 100 microns at the same experimental conditions. As shown figure below Figure 43, the regions are labeled to explore each location features and morphology for a better understanding.

The semiconductor device applications and hydrogen evolution reactions require to have an applicable size of the flakes starting from 10 microns lateral size. The partial vapor pressure of the gases and their diffusions along substrate have enabled to make a

sufficient environment. Due to the fact that the activation energy is the lowest on the edge of the substrate to overcome the energy barrier for nucleation and growth, the gases initiate to deposit on the edge first, then later, they diffuse along the substrate surface based on their surface energy. The dangling bonds are one of the main reasons why nucleation and growth continues along the substrate surface. Once unstable and high energy molecules reach the substrate surface, they desire to release their energy to become stable. Adsorption and desorption reactions continuously take place on the surface until the reaction is over and the furnace temperature is brought to the room temperature.

4.3.2 Substrate mapping

Controllable coverage density for CVD mechanism has easily been developed by using the substrate face-up position. The figure below presents the information about the substrate surface by labeling the regions. The region number 3 and 11 are predominantly bulk (>100 nm) while the flakes are usually formed a single layer or bilayers on number 1,5,9 and 13 regions. Since the diffusion and mass transport of the precursors gas form are limited on the region 6,7 and 8, the insufficient deposition and uncompleted growth take place in the middle of the substrate. Multilayer deposition generally is formed on number 4 and 10 regions.

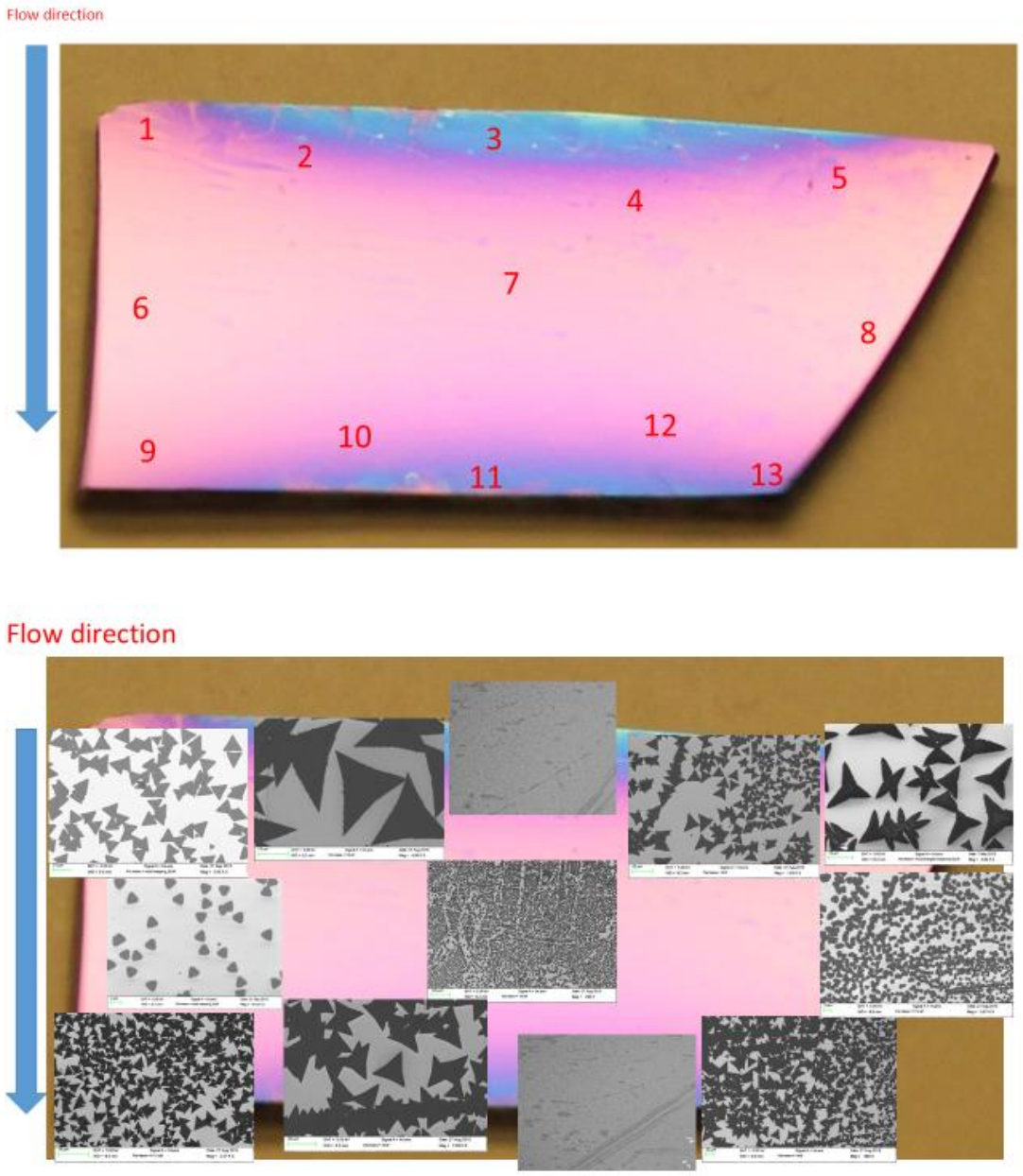

Figure 43 Substrate mapping with the face-up position, SEM images represent each region coverage and morphology

The face-up substrate positions also makes the further characterization possible due to their desired lateral size. As mentioned previous chapter, one of the most important challenges for CVD growth is to synthesize reproducible film and flakes. Therefore, a great deal of attention has dedicated to the film and flakes formation on the substrate surface in

order to have a successful and reproducible CVD growth. This evolution has been demonstrated below with more detailed information. The average size of the triangles varies from region to region. Note, however, that the formation of the film and flakes on silicon dioxide may show a different evolution for other substrates. Even though this formation difference will be explained in the following section, it is important to know that the correlation between the substrate surface atoms and the vaporized precursors molecules must have chemically and thermodynamically convenient reaction on the substrate surface.

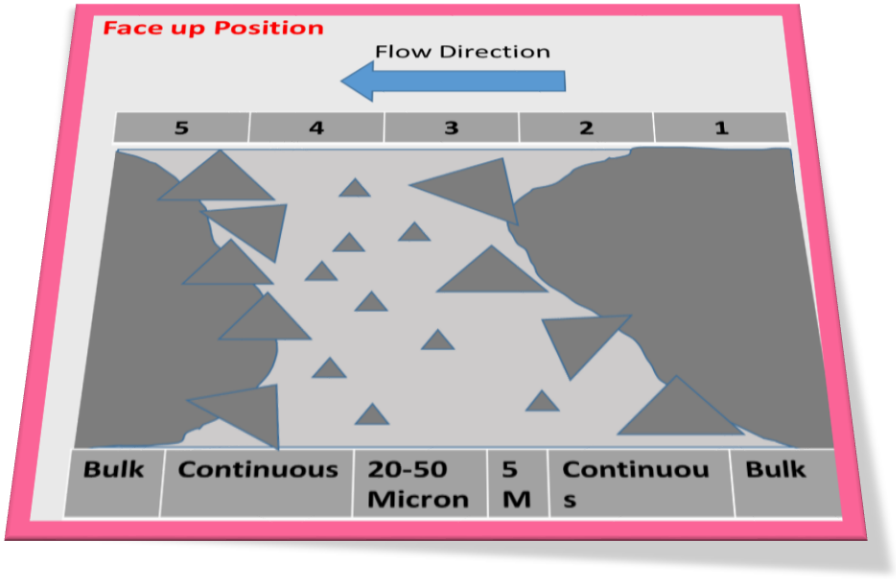

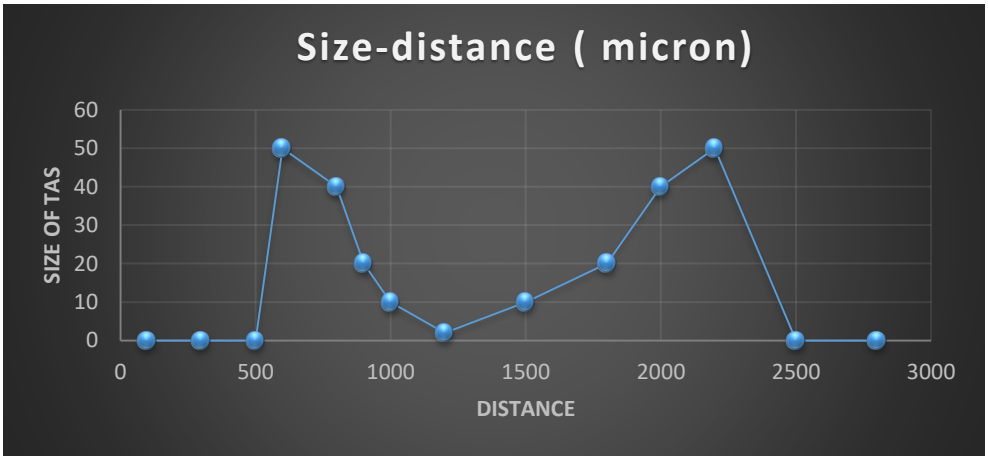

Figure 44 The average size of the triangles has been formed on the different regions of the substrate, from bulk (substrate edges) to monolayer (generally close to the middle of the substrate) formation- the distance is represented by microns.

4.3.3 Synthesizing CVD MoS_2 on different substrates

Silicon dioxide is the most preferable substrate for much different growth mechanisms including, CVD, PVD, mechanical exfoliation, ALD and many more in terms of their reasonable accessibilities. Several studies have been also dedicated to synthesizing TMDCs on different substrates such as silicon, silicon nitride, quartz, graphene, boron nitride, sapphire and gold foil[53, 54, 56, 145, 146]. Not only in the literature studies but also in this work, the single step synthesize method has been observed, there was no pretreatment of either the precursors or the substrate.

4.3.3.1 Characterizations of CVD MoS_2 on different substrates

The ability of this readily synthesize these samples on a range of the substrates makes possible to use them directly implemented on the different applications, including in a variety of nanoelectronic, optoelectronic and catalytic systems. In addition, the deposition on the different substrates is easily characterized by many atomic scales characterization techniques such as Raman Spectroscopy, SEM and AFM. In this work, in order to have a better insight CVD growth mechanism has been employed on silicon dioxide, quartz, doped silicon, graphene oxide, and the gold substrate. Based on the results, the growth of CVD on silicon dioxide has shown a better film and flake formation compare to other substrates since there is a perfect matching between silicon dioxide surface atoms and the vaporized precursors and the surface energy of the molecules are thermodynamically more stable.

In order to prevent the contaminations from the previous reaction, each experiment has been done in a different quartz tube. For instance, the melting point of gold foil (~850 C^0) is very close to the reaction temperature (750 C^0). The quartz tube was also meticulously cleaned prior to each experiment to avoid any residue and its reaction.

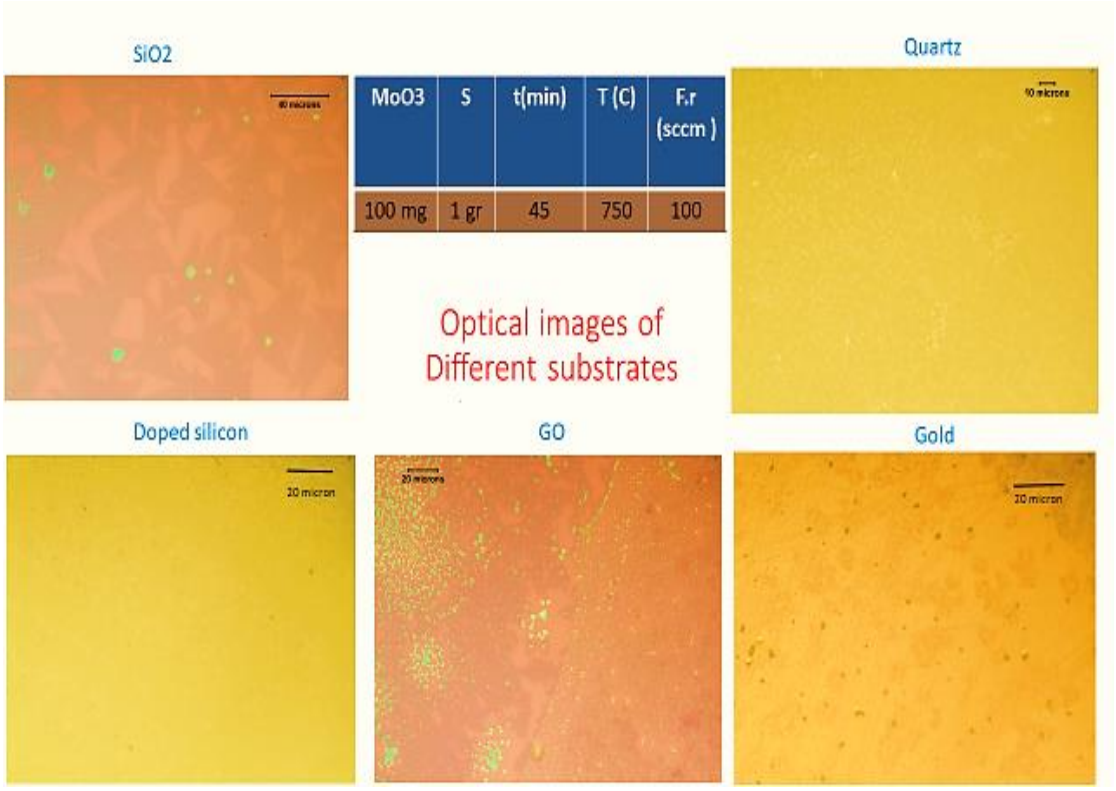

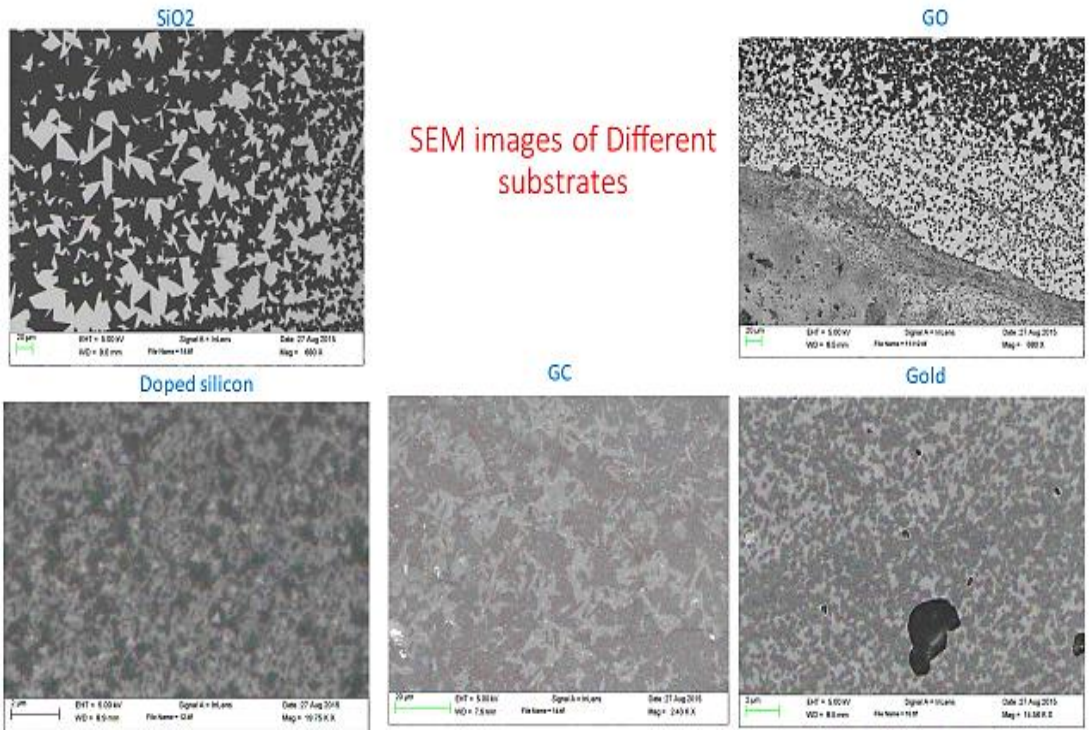

Figure 45 The growth mechanism of CVD MoS_2 on different substrates, the formation can be range from nanoislands to triangles crystals using the same recipe. (The optical images are shown the top, SEM images are shown bottom)

The different thickness of CVD MoS_2 samples was successfully synthesized by direct sulfurization of MoO3 as a precursor without any treatment to the precursor or the substrates. Due to the fact that pretreatment of the precursors might be detrimental to the intrinsic properties of any 2D materials, not using any treatment to the substrates, except that acetone or IPA is required for the substrate cleaning, is quite useful in terms of having the maximum efficiencies from their applications. As shown figure below, the average size of the flakes for CVD growth by using silicon dioxide is much bigger than the other substrates at the same experimental conditions since the possibility of creating a dangling bond on the surface of the substrate is the highest for silicon dioxide substrate. Another key important point for the growth is the substrate conductivity resulting in that the conductive or insulator substrate has not been favorable for CVD MoS_2 growth. The

semiconductor substrate, silicon dioxide, has offered a larger and applicable size for further characterization and applications.

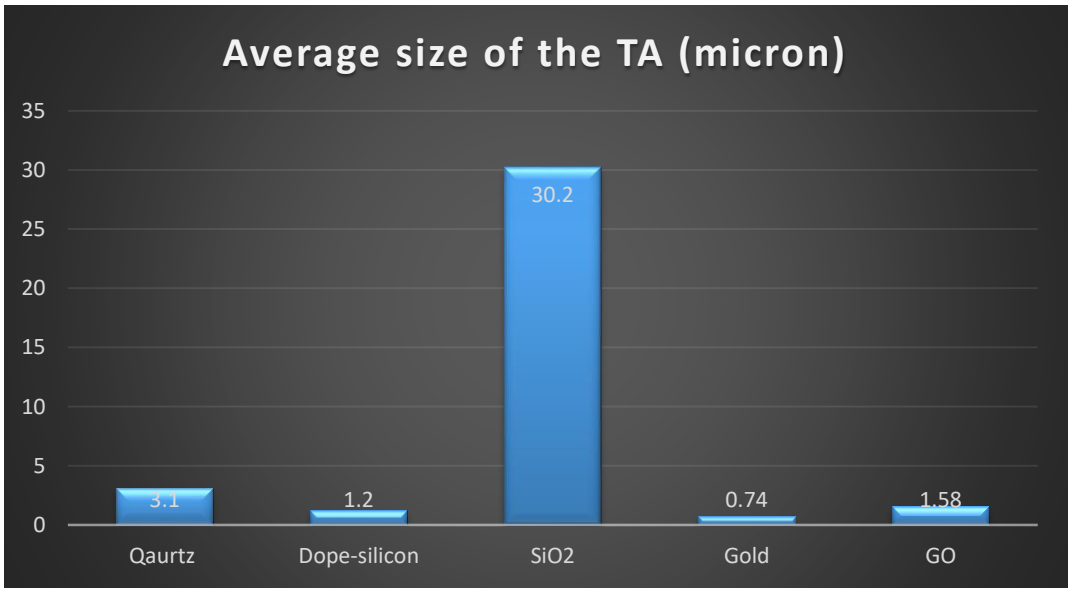

Standard deviation
0.48
0.29
6.02
0.26
0.31

Figure 46 The average size of triangles has been presented by using a different substrate. Approximately 400 flakes have been analyzed for each substrate growth condition.

Raman spectra and photoluminescence has been employed on the synthesized film and flakes for further characterizations. It is known that Raman spectroscopy provides information about the structure including the type of phases and number of the layers on 2D materials. This qualitative information enables analyzing crystal quality of the flakes. By using the vibrational spectrum, this information can be measured.

The Renishaw Invia with a 514 nm laser has been used for this thesis work to do further characterization. The device produces a spot of approximately 1μm in diameter that allows having information even from relatively small flakes. As explained in the previous chapter, Raman Spectra exhibits a unique means of exploring the vibrational modes and electromagnetic scattering mechanism for TMDCs. There are two specific vibrational modes for MoS_2, E_{2g} and A_{1g} modes- 385 cm^{-1} and 406 cm^{-1}, respectively. These two main peaks have been obtained from each substrate with different intensities as well as PL

intensity. The perfect stoichiometry of MoS_2 is 1:2 for any growth mechanism. However, it is experimentally quite difficult to obtain this structure due to the fact that there is always a defect formation in the material structure resulting in the nonstoichiometric compound.

The nonstoichiometric formation of MoS_2 has been observed by using the different substrates while searching the optimum substrate for CVD MoS_2. Excessive Mo or S atoms caused the intensity different and Raman shift. Especially, the reason why the Raman peak quite low on the gold substrate is that the flake formation is too small to be determined by the laser. On the other hand, the PL spectra were not obtained from the films that were synthesized on gold and glassy carbon substrate as expected since these two substrates are conductive and probably the laser was distorted while extracting the phonons for analyzing. Nevertheless, the film synthesized on silicon dioxide and graphene oxide have provided the signal at approximately 1.85 eV which is a good fit with many works in the literature.

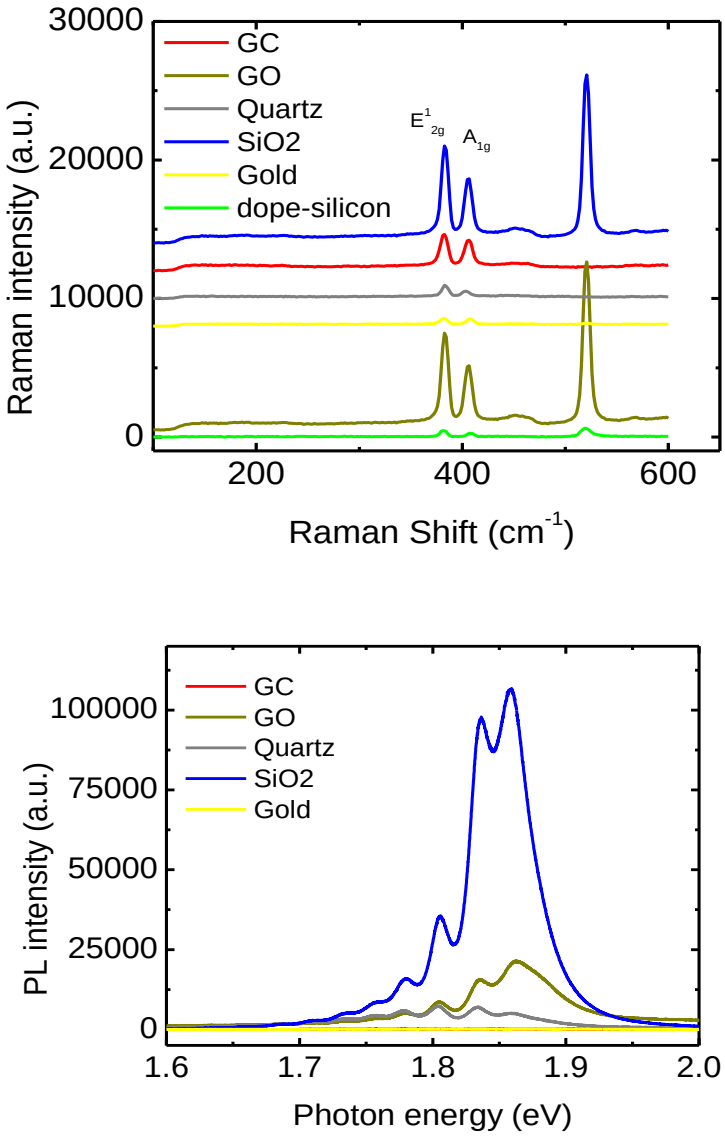

Figure 47 Raman spectra and PL values of the different substrates of the same experimental recipe and conditions. As expected, silicon dioxide has provided a better signal for Raman and PL.

4.3.3.2 A statistical study of CVD MoS_2 on different substrates

Once CVD thin film or flakes of MOS_2 is successfully synthesized, there are a few methods to analyses the thickness. The most reliable method that has been used for decades in both industry and academia for thickness analysis is an atomic force microscope (AFM). However, there are a few methods that can still give roughly information about material thickness. Raman spectra are one of these techniques to do thickness characterization in the absence of AFM. Raman peak location and intensity of their two main vibrational modes, E_{2g} and A_{1g} exhibit a weaker signal once the film becomes thinner. The other method is to calculate peak spacing, which is called **Δ**. Once the difference is 20 cm^{-1} or lower between, E_{2g} and A_{1g} peaks, it is assumed that the film is monolayer[111, 112, 147, 148]. The last method is to calculate the intensity ratio between the characteristic peaks from MoS_2 and silicon peaks:

E_{2g} / silicon peak = 0.05 (monolayer)

E_{2g} / silicon peak = 0.09 (double layer)

The calculating of the peak spacing between E_{2g} and A_{1g} was used to analysis the thickness differences of MoS_2 by using the different substrates. The monolayer film was successfully produced on only silicon dioxide substrate while others provided predominantly bilayer or multilayers of MoS_2. The Δ value of silicon substrate was 20 cm^{-1} whilst that value of the others was quite high meaning that the single layer of MoS_2 was not successfully grown on other substrates.

Based on the Raman spectra, PL optical and SEM images, it can be said that silicon dioxide is the optimum substrate for synthesizing CVD MoS_2. The controllable material thickness and easy transferability lead silicon dioxide to the most preferable and used

substrate in the semiconductor industry. On the other hand, making a gold substrate or using a piece of the glassy carbon is a harder process to make and handle compared to silicon or silicon dioxide. The last but not least, the pricing is another important parameter both in academia and industry considering tight budgets in both areas. The price of a silicon wafer is in many ways cheaper than sapphire, glassy carbon, quartz and gold substrate. Therefore, all of these reasons make the silicon dioxide substrate convenient for any applications.

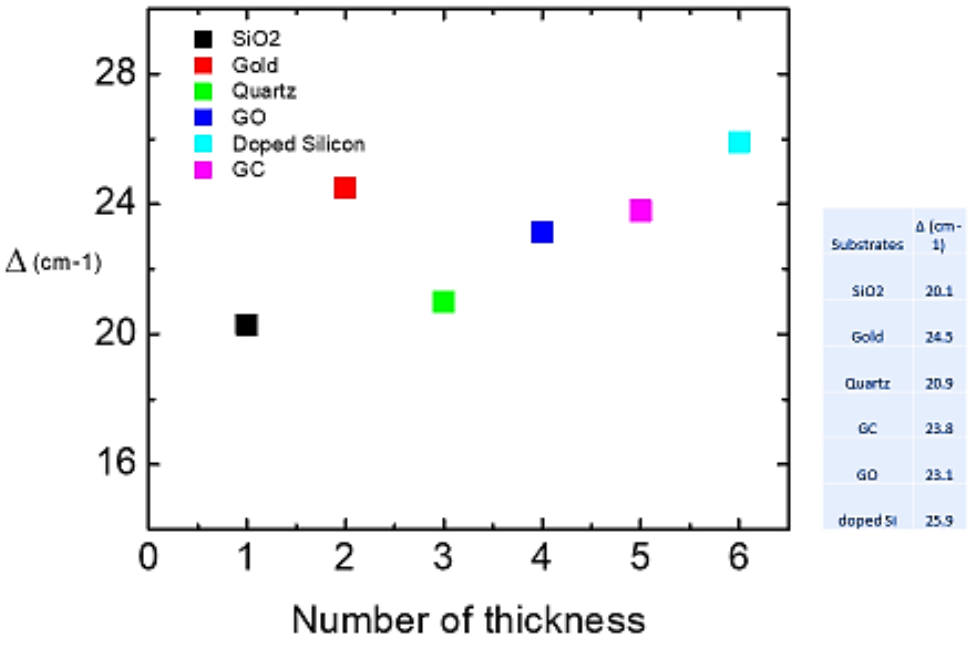

Figure 48 The illustration of the thickness differences with Δ which usually gives information about the thickness roughly, lower than 20 cm-1 corresponds to monolayer by using the different substrates.

4.4 Nb-doped effect on CVD- grown MOS_2

Studying a defect engineering has widely opened a new research area for many scientists. Creating a defect in the crystal structure or doping with another material to

TMDCs have gained a great deal of attention in terms of understanding the structure chemistry and improving the material properties[149, 150]. Many studies have been devoted to enhancing doping engineering and analysis of that in practical applications[151]. Like other TMDCs, MoS_2 can be also doped since it shows unipolar characteristics. There are two main charge carriers for semiconductor materials which are holes and electrons. The majority of the charge carriers are electrons for MoS2 due to the existence of native sulfur vacancies[152].

MoS_2 is an n-type and intrinsic semiconductor, but since field effect transistors made from MoS_2 are Schottky-barrier FETs it is the work function of the metal used for the contacts that determine the polarity of the device. There are many transition metal elements, however, only niobium has been theoretically and experimentally demonstrated to be an effective p-type dopant in MoS_2[153, 154]. Based on the works from the literature, the motivation was to synthesize a large area MoS_2 film with Nb-doped by the CVD method. The successful growth with Nb-doped has also shown an enormous increase on magnetic features.

4.4.1 Experimental set-up for Nb-doped CVD MoS_2

To have a successful CVD grown MoS_2 with Nb-doped, the experimental set up was slightly modified based on the desired product. $NbCl_4$ (≥99.5% purity powder from Sigma Aldrich and 325 mesh) has been used to produce Nb source as a dope agent while MoO_3 and sulfur source were the same as typical CVD MoS_2-grown before. The Nb and sulfur source placed very close to each other in the quartz tube since their melting point was very similar, 205 C^0 and 116 C^0, respectively. The substrates have placed a face-up position and right above the MoO_3 precursor after they were exposed to acetone for 30

minutes in the sonication for the cleaning. Argon was used as a carrier gas with the flow rate of 100 sccm.

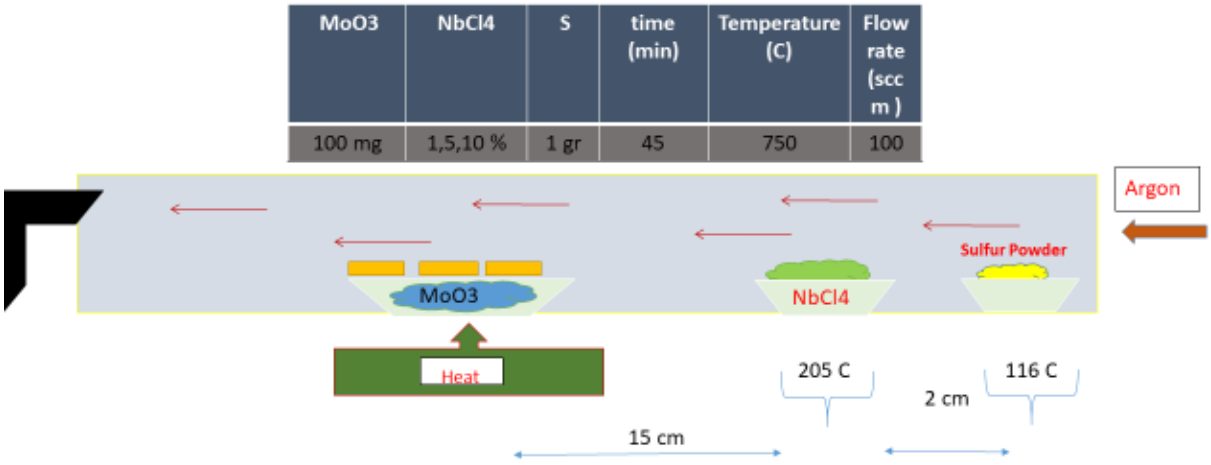

Figure 49 The experimental set-up of Nb-doped CVD grown MoS_2. The recipe (top) was very similar to the typical MoS_2 CVD growth.

The doping was systematically done with different percentage of the MoO_3 amount in order to analyze the effect of amount versus the shape evolution and growth. The amount of Nb source was slightly increased and was used 1,5 and 10% of the Mo source in sequence. With 1% Nb-doped, there was no big effect on the growth evolution of MoS_2 while increasing the amount changed the surface coverage and density. Truncated triangles and multilayers hexagonal flakes were produced with increasing the Nb amount to 5 %. A few microns of the triangles were synthesized once the Nb source reached to the 10% of the MoO_3. There are a few key parameters to explain why this growth and shape evolution mechanism differs, however, the main reason is that sulfur reacts with chloride and creates the new chemical compound of SCl_2 during the reaction. This new chemical reaction is more favorable by sulfur. SCl_2 is produced rapidly and leaves the reaction without any other interaction. Therefore, the possibility of meeting Mo molecules with

sulfur molecules drastically decreases. Finally, the size of the triangles or hexagonal flakes were reduced by this reaction.

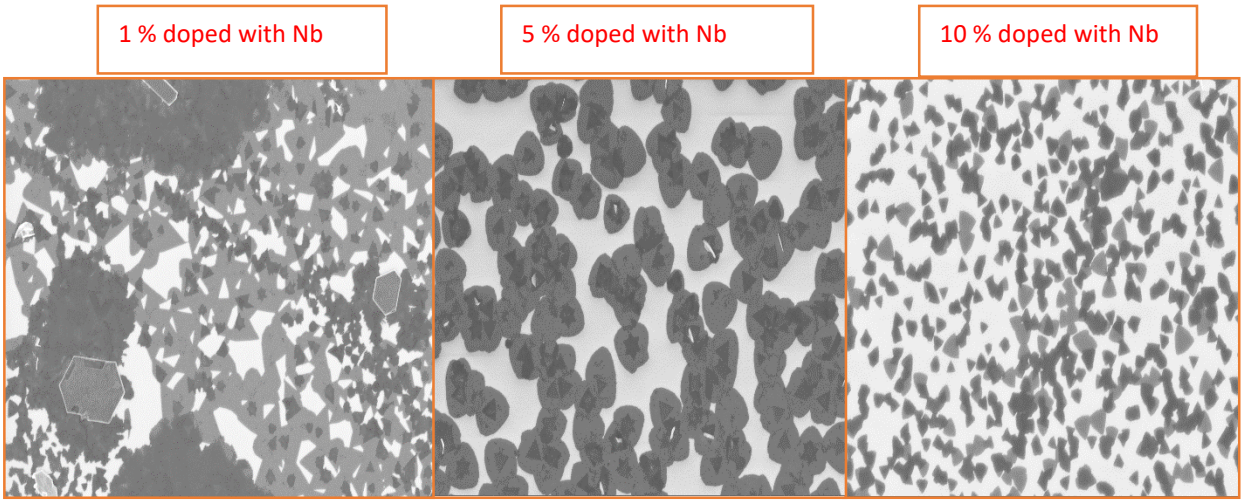

Figure 50 The different Nb source doped CVD MoS_2 has been successfully synthesized with the amount of 1,5 and 10 % $NbCl_4$ of MoO_3. The shape evolution of MoS_2 differs with increasing the amount of the Nb source.

4.4.2 Characterization of Nb-doped CVD MoS_2

The Raman spectroscopy and PL have been employed on the doped CVD growth MoS_2. Each condition has shown clear MoS_2 peaks at 385, 408 and 520 cm^{-1}, $E_{2g,}$ $A_{1g,}$ and silicon peaks respectively. 1% of Nb source doped MoS_2 has given a sharper and more intense peak as expected due to the less interaction between the MoS_2 layers and Nb atoms while the weak peaks were observed at 10 %. PL spectra were approximately 1.82 eV for each condition with the different intensity.

It is expected that PL intensity decreased while the amount of Nb source increased. This is because the metallic behavior has improved once the amount of Nb was increased in the system. The doping of Nb studies in this work has shown that the shape evolution and growth behavior of MoS_2 has changed in the presence of the doped element.

Further characterization is required for a better understanding of the Nb-doped mechanism. This will be shortly discussed in the future work section in the last chapter.

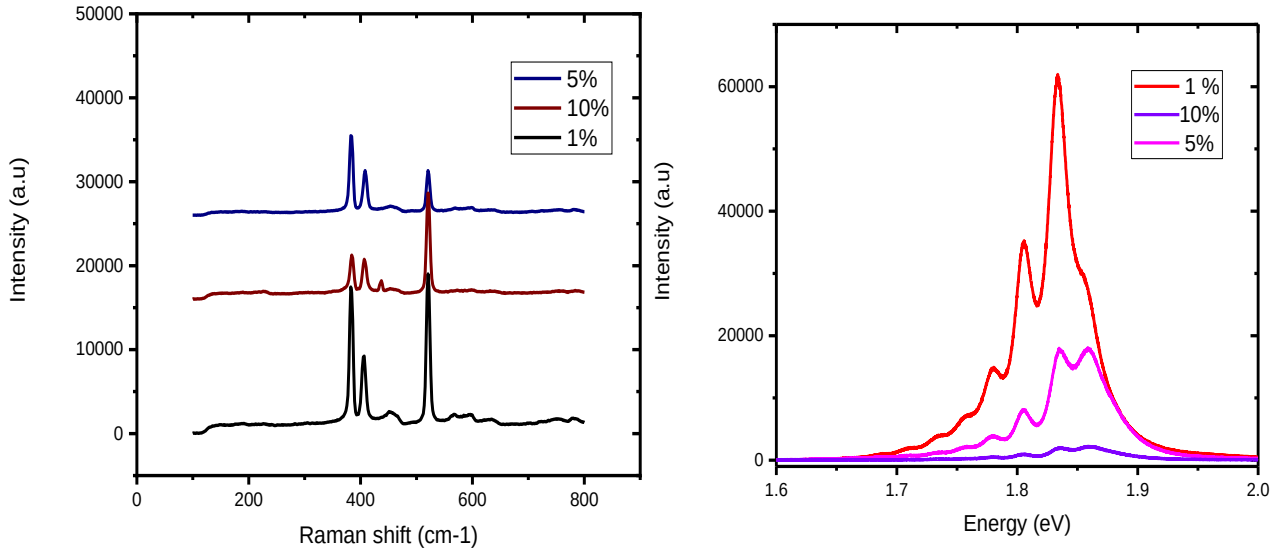

Figure 51 Raman spectra and PL values of the different amount of the doped Nb at the same experimental recipe and conditions. The measurements have done on the same sample at the different location by using 514 nm laser wavelength with a 1-micron diameter size of the laser.

4.5 CVD NbS_2

4.5.1 Experimental Set-up for CVD NbS_2

TMDs can be synthesized by top-down and bottom-up methods as discussed earlier. Mechanical and liquid exfoliation is the example of the top-down method[155] while chemical vapor deposition and hydrothermal synthesis are typical bottom-up strategies.[156] Chemical vapor deposition(CVD) of the metal oxides has been used for decades to synthesize high quality, uniform films or flakes. It typically uses oxide form of the metal compound MoO_3, WO_3 as a metal precursor and elemental sulfur and selenium.

At high temperature, sulfurization or selenization of the oxide metals proceeds, forming of MoS_2 or WS_2. However, this traditional metal oxide- sulfurization method is not convenient for CVD NbS_2 growth due to the fact that the metal oxide of Nb has a high melting point (Nb_2O_5 -Niobium pentoxide/Melting point -1512 C^o). Therefore, I pondered to find an alternative way to synthesize a large area film for CVD NbS_2. First, I started to use a different furnace that can go up a higher temperature in case that the NbS2 reaction takes place at high temperature. The picture below shows the new CVD furnace -max temperature 1250 C^o.

Figure 52 The new single-zone furnace was used for CVD NbS_2 growth. Even though it has relatively a smaller temperature zone, the higher (1250 C^o) temperature can be reached at.

Like CVD grown MoS_2, the oxide precursor was used to synthesize a large area and highly crystalline NbS_2 by atmospheric pressure (APCVD). Sulfur (99.5 % from Alfa Aesar) and Nb_2O_5 powders (99.9% from Sigma- Aldrich) were used as the precursors. One of the main challenges was to eliminate the oxidation state since the vacuum system was not a

favorable way for CVD-grown NbS_2. In addition, the precursor had more oxide in the compound that required a higher reaction temperature as well as the oxidation state. To overcome this problem, the mixture of Argon–H_2 (90-10 %) carrier gas was used to avoid the oxidation. Since the precursor has the oxide and the reaction temperature is about 1000 C^o, the oxidation state has been observed after the reaction on the substrate. In order to eliminate it, the argon-hydrogen gas mixture was used to reduce the oxygen.

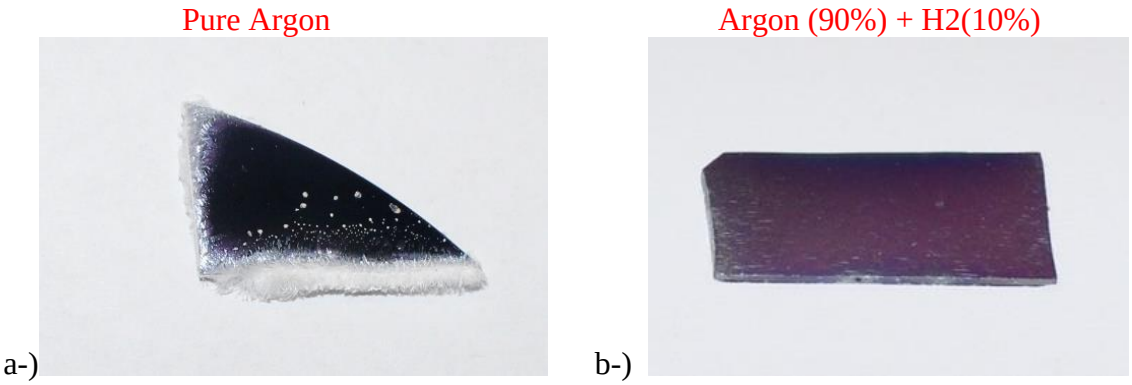

Figure 53 The oxidation state has been observed without hydrogen gas by using pure argon (a). Hydrogen gas gives rise to oxygen reduction (b) and tailors the NbS_2 flakes.

4.5.2 Halide group effect on CVD NbS_2

The growth of CVD NbS_2 was not as easy as CVD grown MoS_2 since the oxide form of Nb has a higher melting and evaporation point comparison to MoO_3 (795 C^o). Based on the melting point difference, some alternative ways were needed to be discovered to understand this new material features. After doing a long time literature survey, I came across that the alkali halide group has been used in the chemistry for decades as a promoter. In addition, the group also enhances the mass transport during the reaction since they can be used as a transport agent. The role of alkali promoters is to create a new eutectic point for the precursor's mixture in order to decrease the melting temperature of the mixture and produce more volatile oxides.[157] Three important missions of the halide group have been

demonstrated below. It is important to know that each alkali halide group has their own characteristic features and they assist to nucleation and growth process based on these features.

Nb_2O_5	Halide group	S	t(min)	T (C)	Flow rate (sccm)
70 mg	30 mg	100 mg	45	900	100

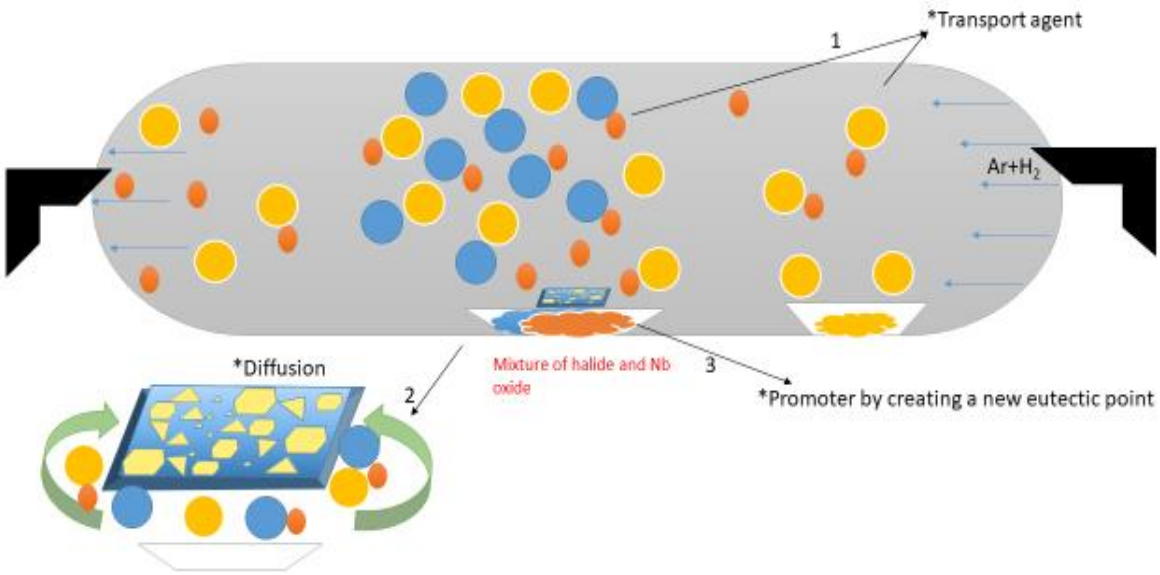

Figure 54 The new experimental set-up and the recipe for CVD grown NbS_2 with alkali assisted. The role of the alkali group was briefly explained in the figure.

In this study, various alkali promoters were used including KI, NaCl, KBr, KCl. Their melting points are different, 681 C^o, 801 C^o, 734 C^o 770 C^o, respectively. All the experiment was conducted with the same experimental condition to explore the optimum condition for CVD NbS_2 growth. However, potassium iodide (KI) was found to be the best

alkali promoter. Iodine has been used as a transport agent on different reactions for decades.[158, 159] When the KI decomposes to its components, Iodine helps to mass transfer during the reaction, and alkali ions such as Na, K, enhance the thermal stability[160].

NaCl and KCl have higher melting points compare to other two halide group used resulting in more vaporized oxide precursors and their partial pressure. Nevertheless, the substrate etching has occurred on the surface of the silicon dioxide substrate over 1000 C^o reaction temperature. Using KBr as a promoter for CVD NbS_2 led to the similar result to KI promoter. However, the flake size of KI assisted samples were larger compared to the KBr ranging from a few microns to 100 microns. That is more favorable to transfer the KI assisted samples for further characterizations and applications. Chlorine compounds also caused uncompleted crystal structures as well as having holes on the surface of the flakes. Optical microscope of NbS_2 with KI at the different grow temperature has been shown below. Increasing temperature allows to evaporate and deposit more mass of the precursors with the result of the different size of the NbS_2 flakes.

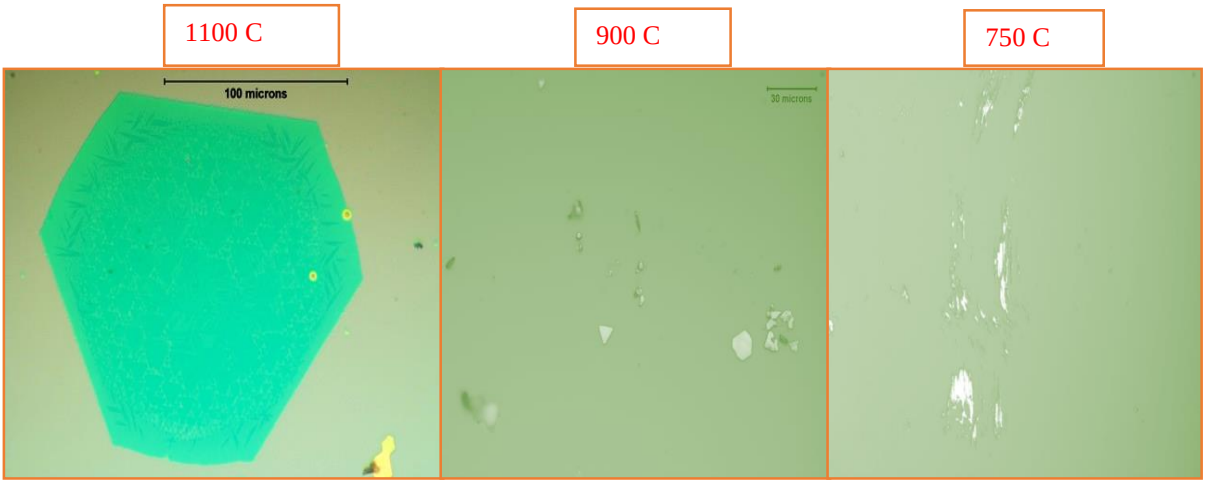

Growth Temperature (C°)	Growth time (min)			
	5	15	30	45
	Result	Result	Result	Result
750	No deposition	No deposition	No deposition	No deposition
900	Very less deposition with nano islands regions	Relatively bigger submicron of NbS_2 flakes	A few microns of NbS_2 flakes	Smaller flake size because of the precursor's consumption
1100	Successful deposition with a few microns NbS_2 flakes	Good amount of deposition with descent flake size	Over 100 microns of NbS_2 flakes	Precursors consumption relatively smaller NbS_2 flakes

Table 6 The optical images of different temperature growth (750, 900 and 1100 C o) at the same experimental conditions and the summary of growing condition at the different time and temperature show the uniformity and coverage of NbS_2 on SiO2 substrate on Si (001) with alkali assisted CVD grown

4.5.2.1 Using different halide group

Once further characterization was employed on the alkali-assisted CVD NbS_2 including X-ray photoelectron spectroscopy (XPS), Raman scattering, atomic force microscopy (AFM), High-resolution transmission electron microscopy (HRTEM), scanning electron microscopy (SEM), Only CVD KI-assisted samples were used to characterize the NbS_2 flakes to learn the composition, structure, and morphological information. As will be discussed in the next section, the thickness of the flakes is also significant for any type of TMDCs materials. For instance, MoS_2 Raman spectra from a monolayer to multilayers or bulk drastically change with increasing thickness. By critically assessing and comparing the performance and applications of these two materials, the hybrid composition of NbS_2- MoS_2 systems can be enhanced for digital electronics and

optoelectronics. However, there has not been many reports from this hybrid system. This part of the thesis will be on understanding the growth mechanism of CVD NbS_2 to explore their physical properties. The following figures show how using the different halide group effects on the CVD NbS_2. To summarize, it can be said that using different halide group (a)NaCl, (b)KCl, (c) KBr and (d) KI shows different grow behaviors. Cl destroys uniformity and quality of NbS_2 flakes. In terms of the flake quality and uniformity, KI gives the best result.

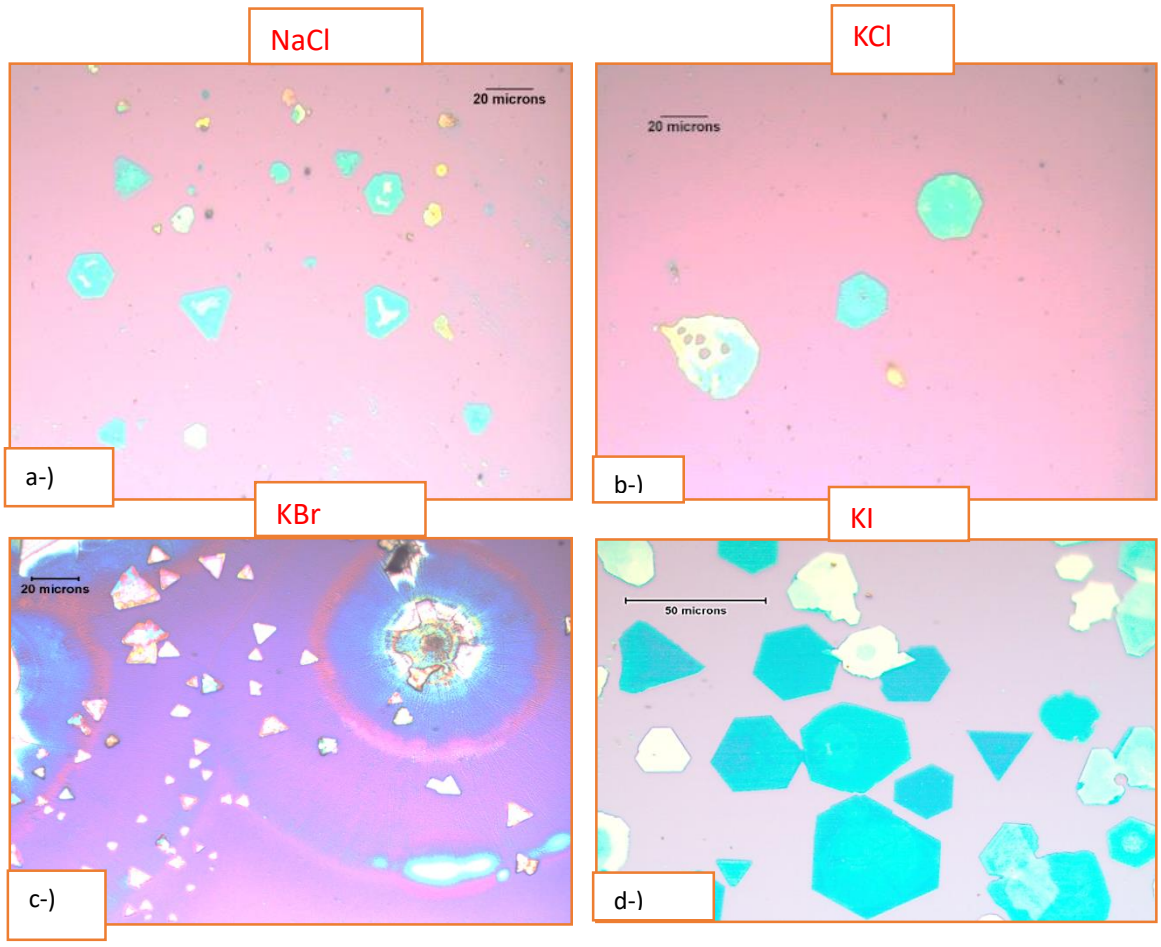

Figure 55 Using different halide group for CVD grown NbS_2 has shown a different range of the flake sizes and the shape evolutions. a-) NaCl and b-) KCl have caused etching on the substrate surface while c-) KBr and d-) KI were more favorable in terms of having a larger flake size.

4.5.2.2 Optimizing precursors with alkali-assisted NbS_2

One of the biggest challenges associated with the synthesis of NbS_2 is (i) to control the delicate balance of the stoichiometry and (ii) to choose the correct precursors for high quality NbS_2 flakes (iii) optimum reaction time and temperature for decent size of the flakes for further characterization and applications[161, 162]. Various form of NbS_2 with the different morphology such as nanowires, nanobelts, nanoflakes have been observed using different types of the precursors.[86, 162].

In order to have a controllable growth mechanism of NbS_2, other sources of Nb including $NbCl_4$, $NaNbO_3$ (1420 C^o) were also used to find the optimum precursor for CVD NbS_2 growth. The different precursors have studied to synthesize high-quality NbS_2 flakes as shown below. In terms of impurity and growth conditions, Nb_2O_5 was the ideal one as a precursor since $NbCl_4$ was sensitive the air and exposed to oxidation very fast, on the other hand, removing Na was a big challenge for $NaNbO_3$.

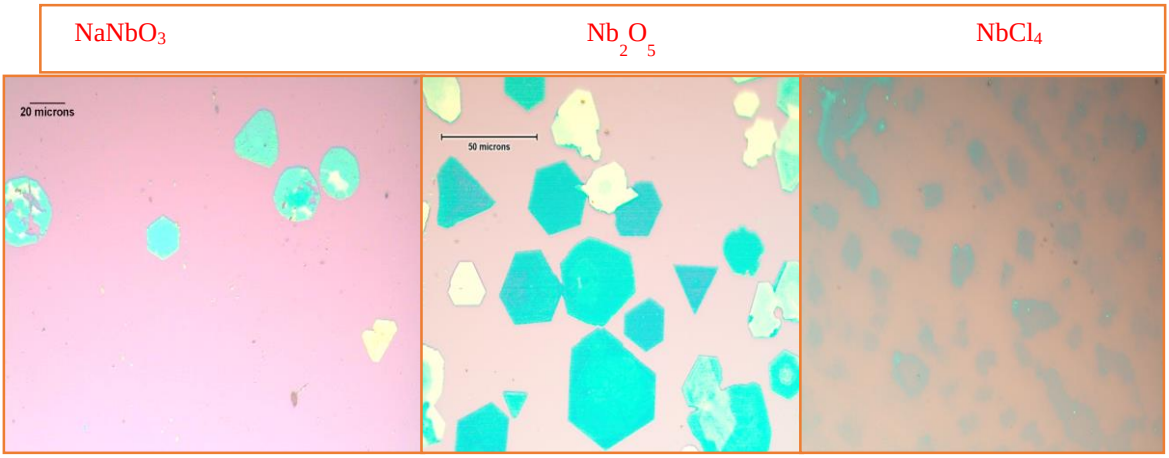

Figure 56 The images show using the different precursors of Nb sources. The Nb oxide precursors led to having larger flake size ranging from 10 microns to 100 microns with alkali halide group-assisted.

4.5.2.3 Different substrate effects on alkali-assisted CVD NbS_2

Like CVD MOS_2, choosing a correct substrate for CVD NbS_2 is significant to have the maximum amount of coverage on the substrate surface. Since every atom has a different surface energy and its interaction with other atoms, several substrates studies have been conducted for CVD grown NbS_2 in order to discover the optimum substrate. there have been used many different substrates for this aim including Quartz, Sapphire, Glassy carbon, Silicon, Graphene Oxide and Silicon dioxide. Prior to sharing the result, it is worth mentioning that each experiment was conducted at the same experimental setup and condition except that quartz tube was changed prior to each experiment in order to avoid the contamination that might cause an unsuccessful growth process.

As it can be seen the figures below, the optimum substrate was silicon dioxide as expected for many TMDCs materials in terms of having maximum coverage density and the flake size while the others showed almost uncompleted nucleation and growth mechanism. Glassy carbon was the second favorable substrate to have a decent size of the flakes, however, handling the substrate after the growth was a big challenge to do further characterizations and applications.

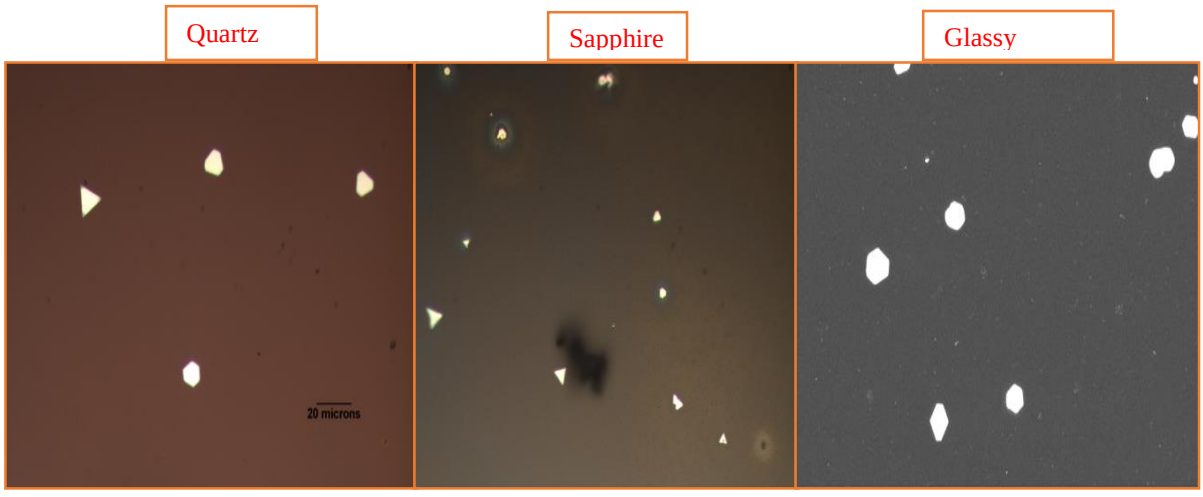

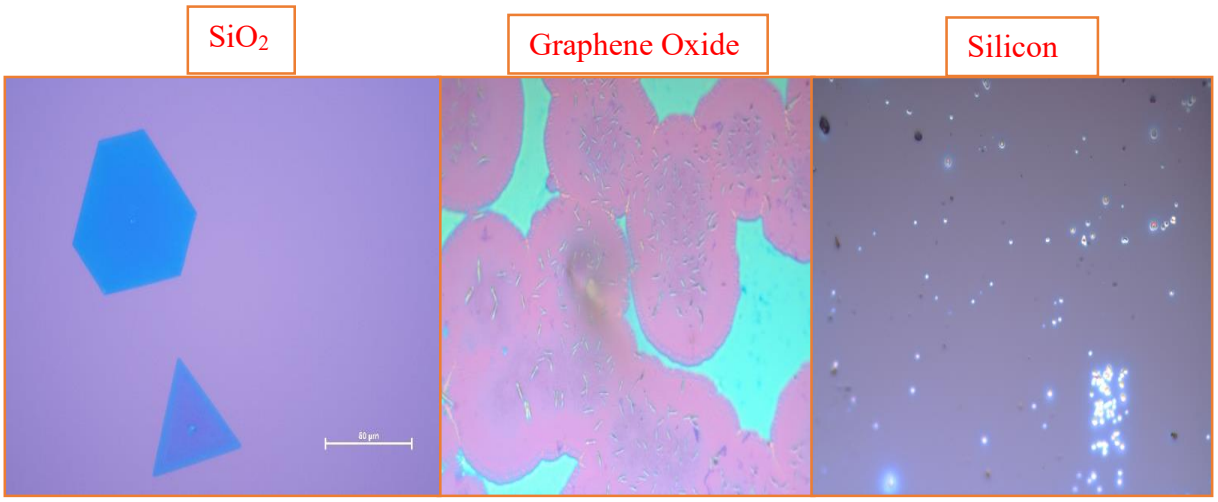

Figure 57 Optical Microscope images of the different substrates of NbS_2 flakes on SiO_2, sapphire, glassy carbon, silicon, quartz has shown a large range from a few microns' small islands to over 150 microns' flakes.

4.5.2.4 Characterizations of alkali-assisted NbS_2

Raman spectra with 532 nm green laser were utilized to analysis NbS_2 peaks which are 2H and 3R. 2H-NbS_2 has four Raman modes which are E^2_{2g}, E_{1g}, E^1_{1g}, A_{1g}, shows 31,260, 304 and 379 cm^{-1} respectively, 3R-NbS_2 has different four Raman modes as E_1, E_2, A_1 and A_2 at 290, 330, 386, 458 cm^{-1}. The more detailed of Raman work will be presented in the next chapter, however, it is important to mention that Raman peaks were not successfully detected on the graphene oxide and silicon substrate since the lateral size of the flakes was not large enough to achieve the correct detection. Especially, graphene oxide that was deposited on the silicon dioxide was not favorable for CVD NbS_2.

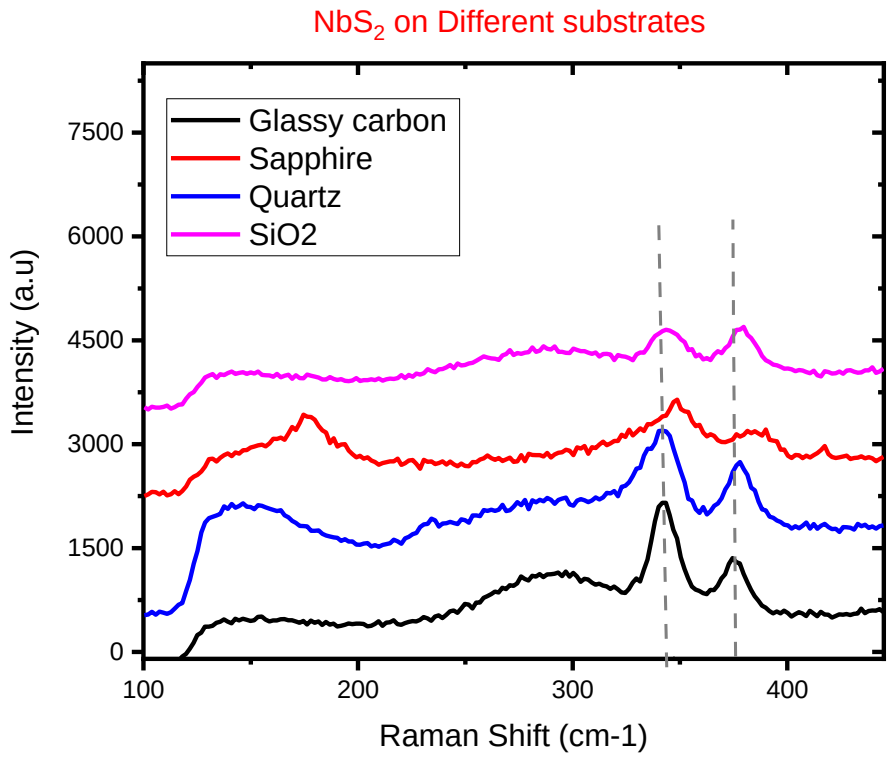

Figure 58 Raman spectra of NbS_2 on different substrates. Characteristic two Raman peaks were observed by using the Horiba Raman Spectrometer with 532nm green laser were employed for the analysis.

4.5.3 CVD NbS_2 without alkali promoter

As discussed earlier, there were two different approaches applied to growing CVD NbS_2 flakes. This first approach consists of the mixture of Nb_2O_5 and alkali promoter from halide group compounds (KI, NaCl, KBr, KCl-(BioUltra >99.5% from Sigma-Aldrich)). The second approach was to synthesize the flakes without any alkali assisted using sulfur (99.5 % from Alfa Aesar) and Nb_2O_5 powders (99.9% from Sigma- Aldrich) as the precursors., In both approaches, the sulfur powder was located upstream while the substrate and Nb_2O_5 (and mixture with alkali promoter) was located at the center of the furnace. The second approach was pretty similar to the first one in terms of the experimental set-up that

has been demonstrated below. The mixture of the precursors takes place at the center of the one zone furnace while the sulfur source is 18 cm far away from the center of the furnace. The mixture of the gas (Argon 90%, Hydrogen 10%) is purged during the experiment and till it cools down the room temperature. Hexagonal and triangle shape of the flakes are deposited on SiO_2 on Si (001) substrates. It is known that there are three polytypes of NbS_2, 1T, 2H and 3R-NbS_2. The mixture of 2H and 3R-NbS_2 have been synthesized with these two approaches. The recipe for each grow parameter (CVD NbS_2 growth and CVD NbS_2 growth with alkali-assisted) will be demonstrated in the near future section.

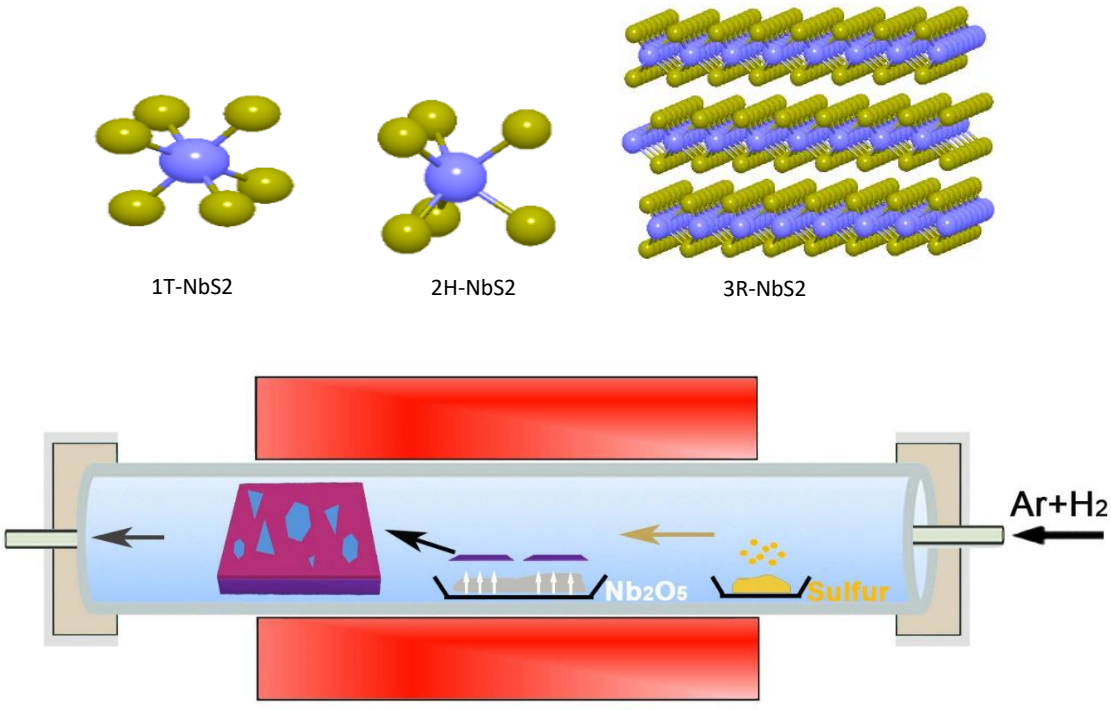

Figure 59 Schematic experimental set up of NbS_2 flakes and three different polytypes have been shown. The mixture of the gas (Argon 90%, Hydrogen 10%) is purged during the experiment and till it cools down the room temperature.

4.5.4 Comparison of CVD NbS_2 with and without alkali promoter

The following experimental paths have been applied on the synthesizing CVD grown NbS_2 and CVD grown NbS_2 with alkali assisted. First, Niobium Oxide: Nb_2O_5 (150 mg) was placed in a ceramic boat while sulfur powder was placed 18cm away from the center of the Quartz tube. For alkali promoter incorporation method, the KI (100 mg) was mixed with metal oxide in the ceramic boat. The silicon dioxide substrates were located above the ceramic boat upstream while the experiment was under an ambient condition with Argon–H_2 (90-10 %) carrier gas mixture. The furnace first was set at 200^{o}C for 30 min to remove the moisture and any possible impurities from the quartz tube prior. Then, the reaction temperature was adjusted to 1000^{o}C in 30 minutes and was hold another 30 minutes at that temperature in order to exactly decompose and consume KI, which was grinded to be evaporated faster before placing in the quartz tube. The carrier gas was continued to purge until the reaction was completed and allowed to cool down to the room temperature in 3 hours. The summary of experimental growth conditions has been tabled below to understand each approach much better.

NbS_2 grow	With KI	Without KI
Temperature (C°)	900	1100
Time (min)	15	90
Ar/H2 Gas Flow (sscm)	100	100
Average Flake Size (microns)	40	5
Flake thickness (nm)	~10	~5
Morphology	Triangle and hexagonal flakes	Triangle and hexagonal flakes
Phase	2H and 3R together , dominantly 2H phase up to 10 nm	2H and 3R together , 2H more dominant at thinner flakes
Raman Shift and intensity	Mixture of 2H and 3R phase -2H dominant	Mixture of 2H and 3R phase -2H dominant
TEM result	2H phase	2H phase
XPS	K and NbS_2	Only NbS_2

Table 7 The growth condition of alkali assisted NbS_2 and NbS_2 exhibit slightly different features after the synthesizing at the different time and temperature on SiO2 substrate on Si (001).

4.5.4.1 Flake size and thickness comparison

4.5.4.1.1 Flake size comparison

These two approaches led to having successful NbS_2 large area thin films and flakes. In this section, the comparison between these two methods has been presented in many ways including their thickness differences, lateral size, and the compositions. Both methods have some advantages and disadvantages in some ways. Large flake size of NbS_2 can be easily synthesized with alkali- assisted method. However, it might bring an undesired impurity to the system since it is sometimes difficult to remove the residues from

the halide group. On the other hand, high-quality crystalline flakes can be produced with the traditional CVD method without any alkali promoter assisted. Nevertheless, not the thickness of the flakes, the size of the flakes might be too small for some certain electronic and optoelectronic applications as well as further characterizations of the NbS_2 flakes. There are some energy applications including hydrogen evolution reaction (HER) that do not require large flake sizes besides electronics and optoelectronics of two-dimensional transition metal dichalcogenides. The CVD grown NbS_2 without alkali-assisted flakes can be employed on this type of applications. The thickness and lateral size analysis were done from the same substrate and growth.

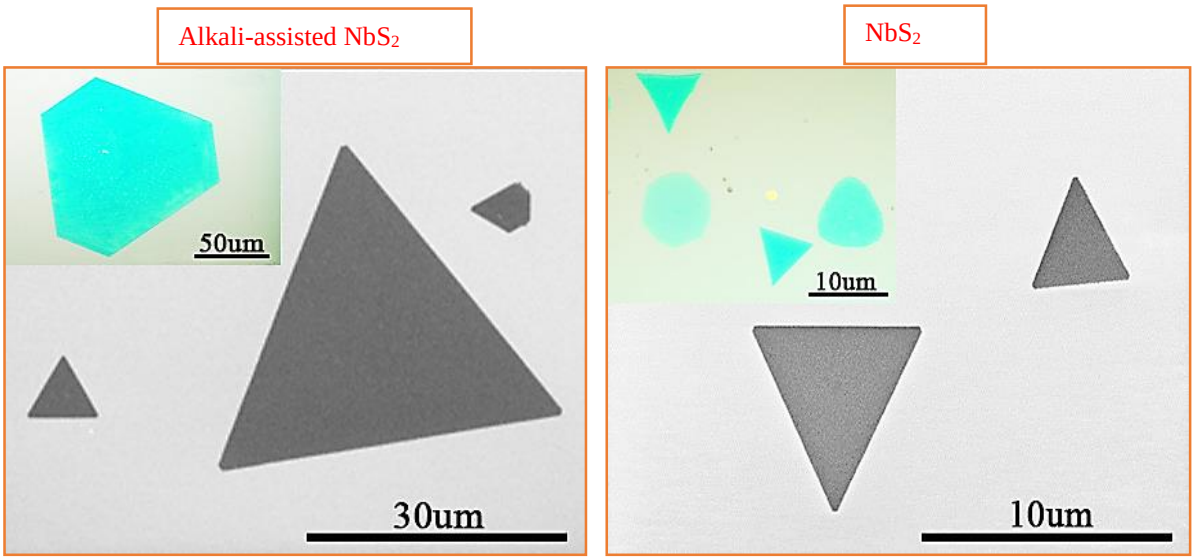

Figure 60 SEM images (optical image in inset) clearly shows the difference between two approaches of NbS_2 synthesizing. The most of the flakes are about 30 microns with alkali assisted NbS_2 while the average size for traditional CVD NbS_2 grown without using any promoter is less than 10 microns.

The statistical work of thickness and flake size analysis were employed by measuring approximately 250 flakes with the alkali assisted promoter and without any promoter assisted NbS_2 on SiO_2. The lateral flake size studies show very large variety from submicron to over 100 microns flake size from the different regions of the substrate. NbS_2

crystals take place anywhere on the substrate, predominantly on the edge where the activation energy barrier is lower than any other place on the substrate. On the other hand, it was straightforward to analyze that the average size of flakes without using any alkali promoter was much smaller. The most of the flakes without any promoter was under 10 microns the average size.

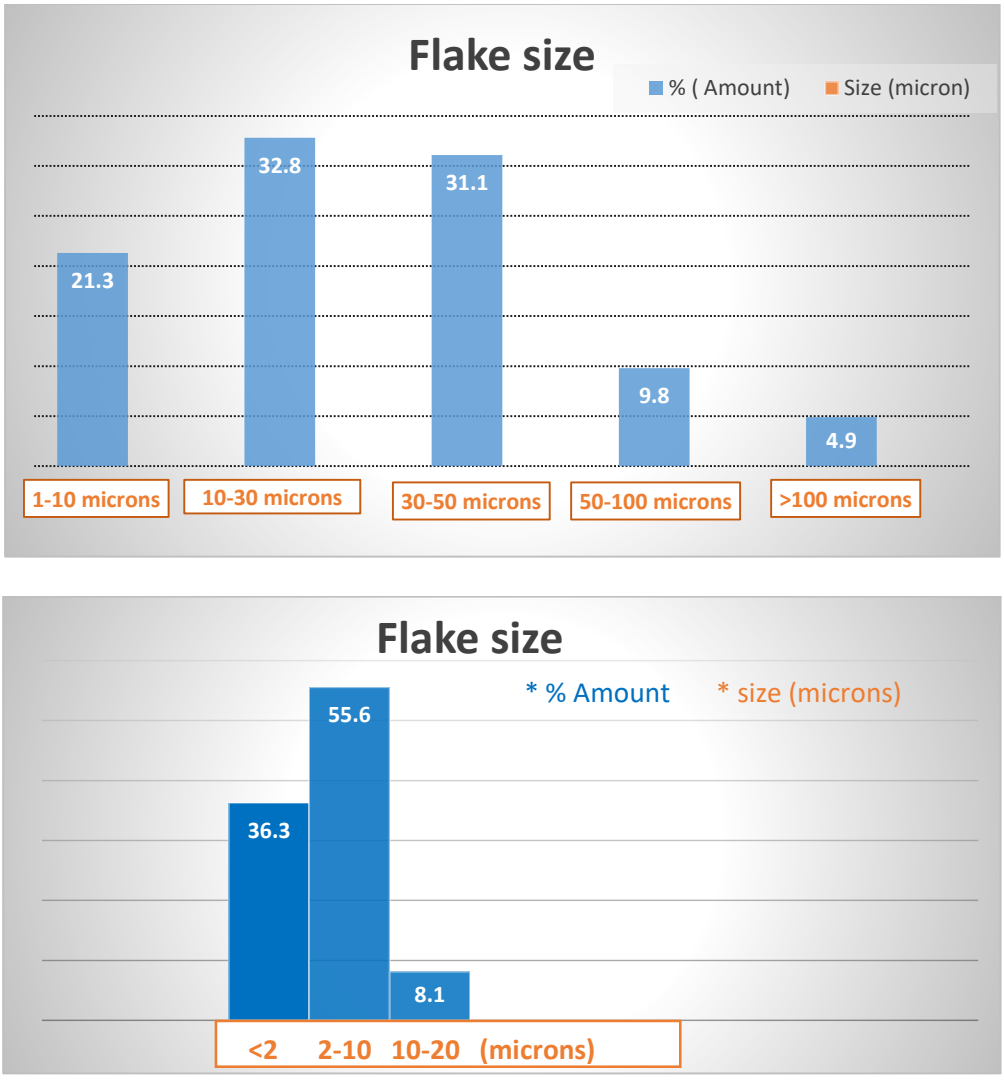

Figure 61 The size of NbS_2 flakes on SiO2 shows very large variety from submicron to over 100 microns with alkali-assisted. (top) Most of the NbS_2 crystals takes place anywhere on the substrate with the size of a few microns with no promoter help (below), predominantly on the edge since the activation energy barrier is lower than any other place on the substrate.

4.5.4.1.2 Thickness comparison

Atomic force microscopy is a reliable method to measure nanoscale tribological properties of a semiconducting and metallic monolayer of MoS_2 and NbS_2 to explore the influence of electronic structure on synthesizing and shape evolution behavior. In addition, various multilayer semiconductor or metallic polytopes of MoS_2 and NbS_2 were studied to elucidate the photonic contribution to the layer engineering. Electronic and photonic properties of MoS_2 and NbS_2 have been still a challenge to discover their full properties although several studies, especially on NbS_2, have been devoted to understanding their thickness dependence versus phase formations. In this work, surprisingly no big differences between two different synthesizing methods have been observed. Although the thickness distribution from this two method will be explained upcoming section, here, it is worth to say that many more flakes with alkali assisted NbS_2 were synthesized under 5-nanometer thickness.

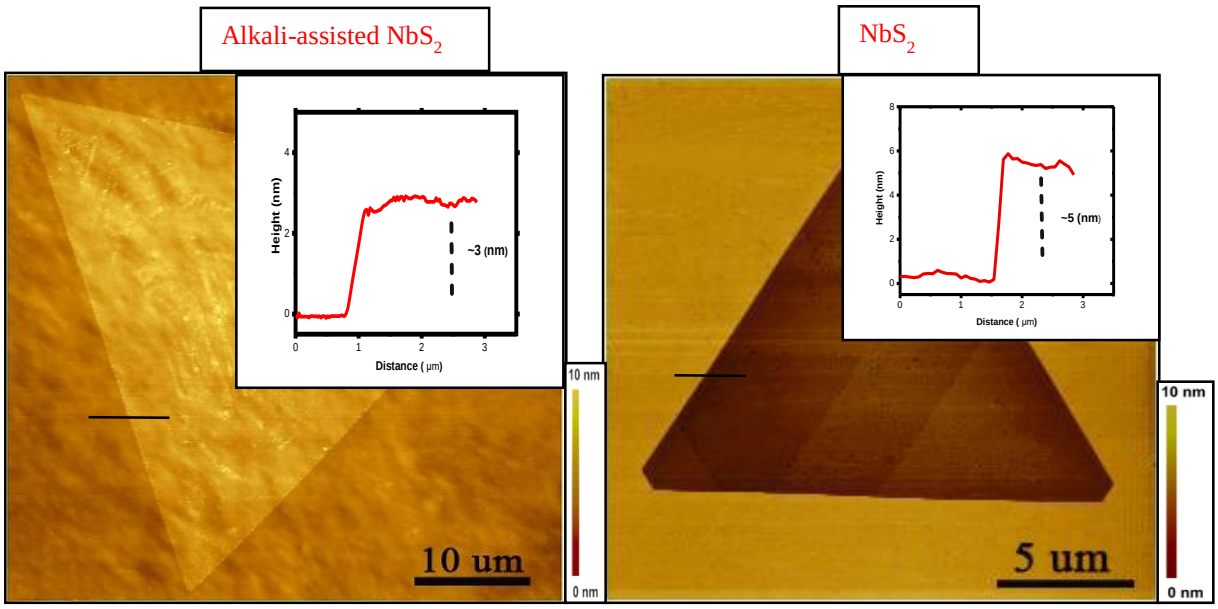

Figure 62 AFM thickness does not exhibit a big difference, in both cases, multilayers flakes are synthesized approximately 5 nm NbS_2 and 3 nm alkali-assisted NbS_2 flakes

AFM thickness measurement was studied to analysis the thickness distribution of these two methods. As explained earlier, interactive forces between the tip and atoms in the sample generate the bonding motion of cantilever and resultant feedback via photodetector. AFM responds to forces generated at an atomic level. Therefore, it reveals the critical amount of information about the materials.

In this study, analyzing approximately 40 flakes for each condition reveals different thickness distributions. NbS_2 flake thickness distribution is in the range from 2 nm to 100 nm with alkali-assisted NbS_2. Most of the flakes thickness on the substrate is about 10 nm and a bulk form of NbS_2 is placed as well without alkali-assisted. In both experiments, Image J software was used for analyzing the lateral size and the thickness of the flakes.

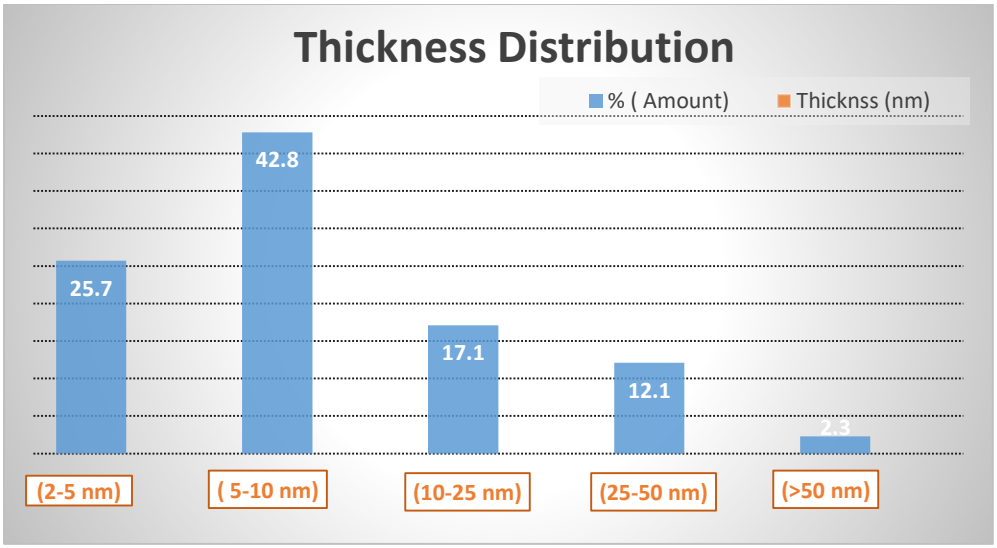

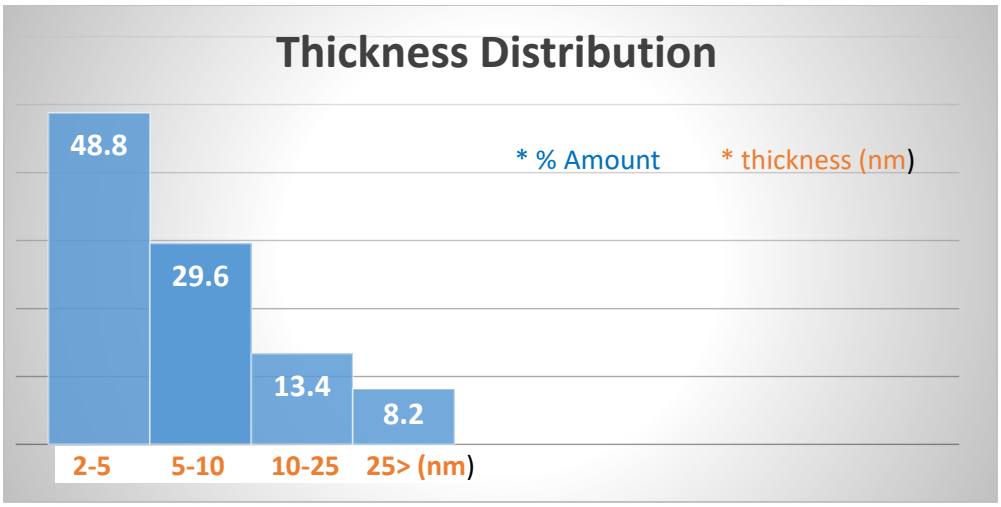

Figure 63 Two different synthesizing methods present a various range of the distribution. The most of the thickness of the sample was under 10 nm with alkali assisted (top) while approximately 5 nm average size of flakes were successfully synthesized without any promoter (down)

4.5.4.2 Characterizations with and without alkali-assisted NbS_2

4.5.4.2.1 Raman Spectra Comparison

The Raman spectra is a reliable method and have been used to differentiate the polytypes of TMDs that exhibit different intensity based on their crystal phase. The difference stems from the stacking of the layers in lateral directions. It has been studied that there are two major polytypes of NbS_2 which are 2H and 3R. 2H-NbS_2 has four Raman modes which are $E^2_{2g,}$ $E_{1g,}$ $E^1_{1g,}$ $A_{1g,}$ shows 31,260, 304 and 379 cm^{-1} respectively, 3R-NbS_2 has different four Raman modes as E_1, E_2, A_1 and A_2 at 290, 330, 386, 458 cm^{-1}.[163] Raman spectra for NbS_2 grown with and without alkali-assisted methods are shown in Figure 2. Whilst, for 1-2nm thick NbS_2 only 2H Raman modes, were observed, as shown in Figure 2a. 2H Raman modes are the dominant mode for NbS_2 flakes up to around 10nm thick. However, thicker flakes have stronger 3R Raman modes, as shown in Figure 2 b and c. There are three key ways to take an important role for a phase transformation engineering

that is temperature, pressure, and intercalation of the host materials. Since the reaction occurs at the ambient pressure environment, both the temperature and possible intercalation may cause the phase transformation or having both 2H and 3R phase together. Similar to other TMDs[112, 164], the Raman spectra might slightly shift with the different thickness for NbS_2.

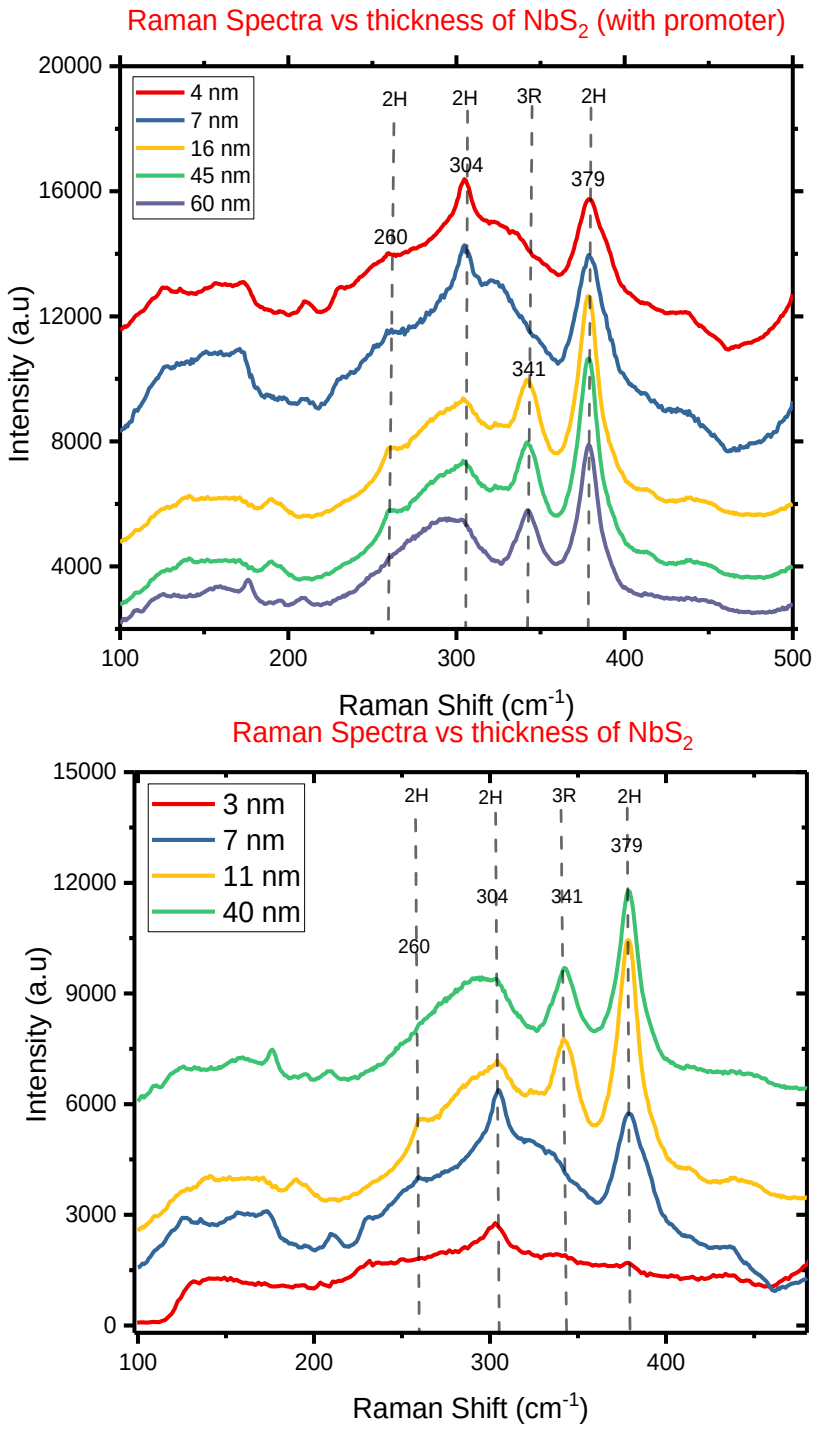

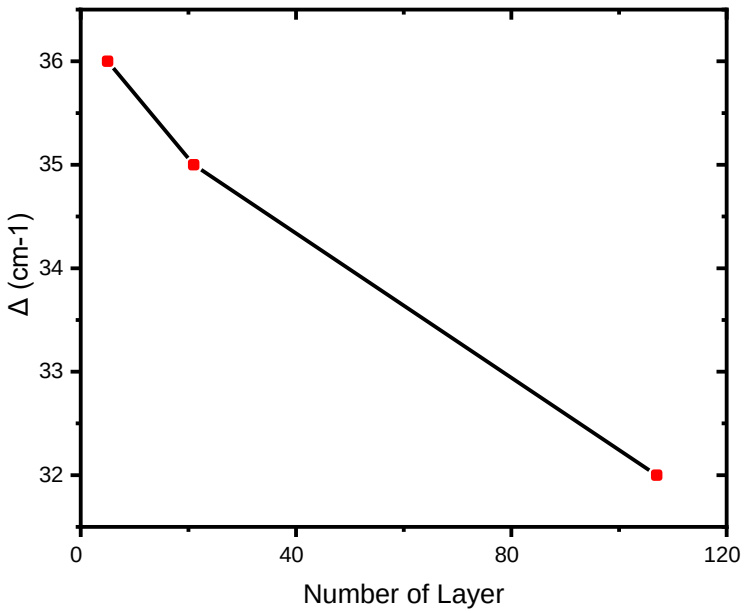

Figure 64 The Raman spectra shows that when it becomes multilayers, 3R-NbS_2 peak also appears for both cases (top). The peak positions of different phases are clearly labeled on both graphs, with and without a promoter, respectively. Raman spectra for NbS_2 with different thickness versus delta (bottom). The Horiba Raman Spectrometer with 532nm green laser was employed for the analysis.

4.5.4.2.2 EDX analysis

EDX, energy disperse X-ray analysis or energy disperses X-ray microanalysis, is a technique that elemental or chemical characterization of the sample can be analytically detected. As its name indicates, it relies on an interaction of some source of X-ray excitation. Due to the fact that each element has a unique atomic structure, its electromagnetic emission spectrum analyses a set of peaks. The sample preparation differs, the most of EDX devices in both academia and industry are used with SEM devices because of the similar work principal. The detection limit of EDX analysis, especially when is built with SEM, totally depends on the composition of the sample being analyzed. The range of

this detection is between 0.1-0.5 wt.%. Therefore, it is a very significant method for both major and minor element analysis[165, 166].

EDX is also known as a non-destructive analytical technique which means that the samples can be analyzed repeatedly many times. However, since an electron beam is used and sometimes can be very powerful, some samples can be damaged under some circumstances. Most of TMDCs have been synthesized atomically thin flakes or films in many different methods. Analyzing them with powerful electron beams might create a defect in the structure that can be either vacancies or disorientation of the layers. To avoid that, the EDX analysis was done several times but with different samples in this work. The results have been presented the different element surveys based on the precursors. As expected, potassium was detected at very low intensity while iodine was completely consumed with KI-assisted NbS_2 flakes. It is important to mention that most of the flakes were atomically thin, that is, a few nanometer thicknesses of the flakes was employed. Hence, silicon dioxide peaks were also observed as well as all expected peaks including Nb, and sulfur. The atomic percentage of NbS_2 without alkali-assisted was close 1:2 Nb: S atomic ratio, which is very well correspondent to the literature studies. The weight and atomic percentages of each element have been tabled that oxygen amount is the higher element comparing to the others due to the silicon oxide surface oxygen treatment.

a-)

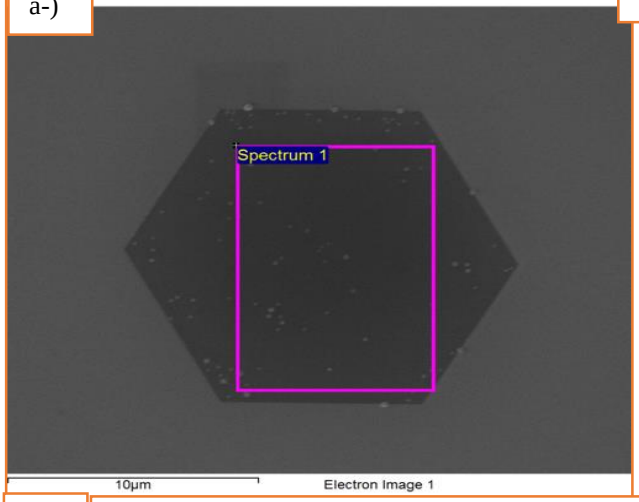

b-)

Element	Weight%	Atomic%
O K	52.54	68.07
Si K	38.37	28.32
S K	3.73	2.41
Nb L	5.37	1.20
Totals	100.00	

c-)

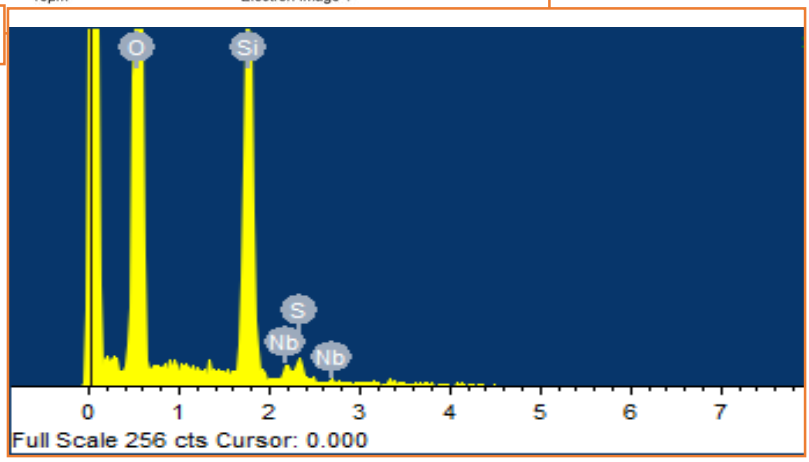

Figure 65 Energy-dispersive X-ray spectroscopy shows the imaging (a), percentage (b) and the elemental analysis of NbS_2 without alkali-assisted (c). The flakes of NbS_2 is relatively smaller size with the good uniform of 1:2 stoichiometry ratio.

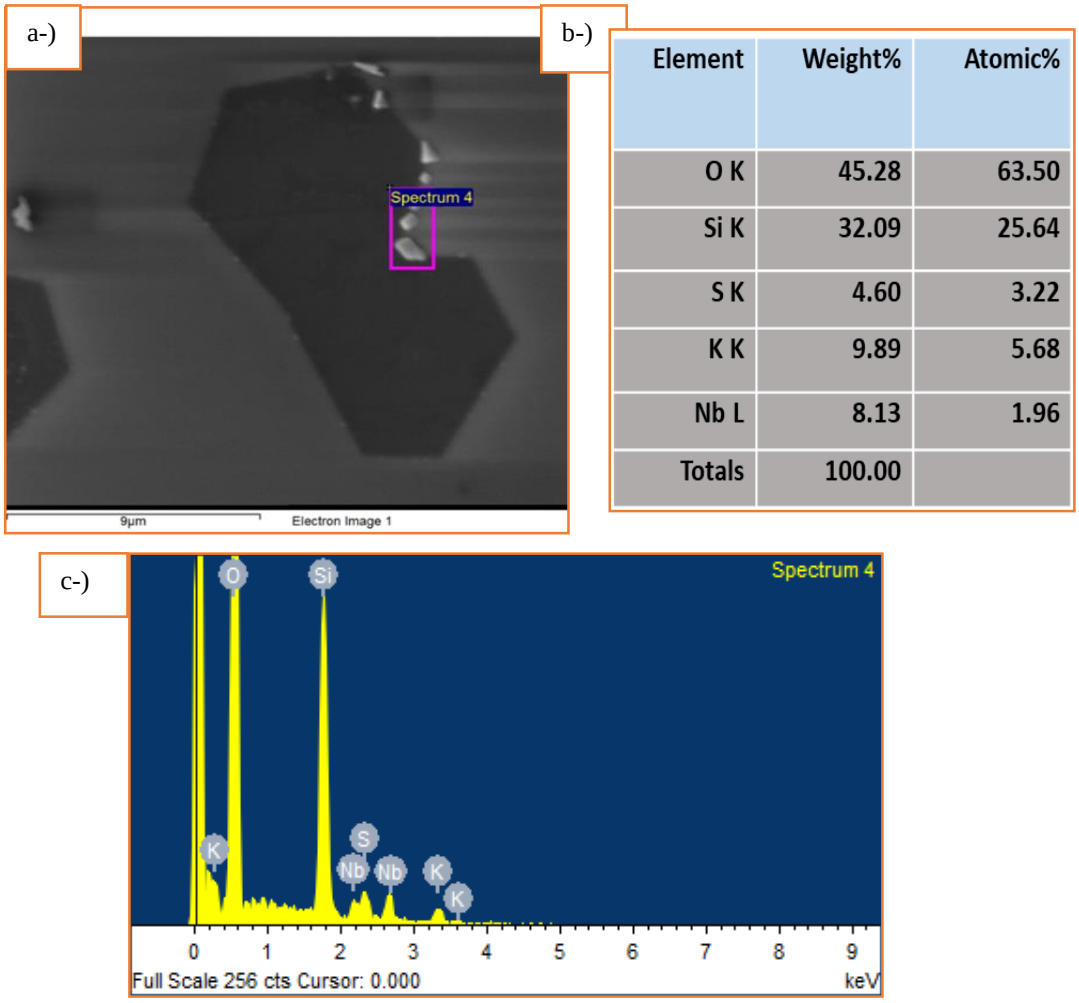

Figure 66 Energy-dispersive X-ray spectroscopy shows the imaging (a), percentage (b) and the elemental analysis of NbS_2 with alkali-assisted (c). The flakes are NbS_2 while submicron K flake may appear on the edge of the NbS_2 crystal flake.

4.5.4.2.3 XPS analysis

To further understand the relative differences in sample characteristics resulting from NbS_2 with and without alkali promoters, X-ray photoelectron spectroscopy was utilized to determine the chemical composition and stoichiometry of NbS_2 flakes. The elemental composition results are shown in Figure 67,68 and Table 8. K element was only detected in samples synthesized using alkali promoters, while all the samples do not have

Iodine. The binding energy of Au foil at 84.0eV was chosen as the reference for energy scale calibration. Non-flake area for samples using both methods was studied. As shown in Figure S7 a Nb_2O_5 thin film covered on substrates. The Nb core level spectrum is well fitted with two peaks which are in good agreement with Nb_2O_5 at 207.07 and 209.77eV for Nb_2O_5 $3d_{5/2}$ and Nb_2O_5 $3d_{3/2}$.[167] Figure 67 shows the XPS spectra of Nb and S cores level in NbS_2 flakes grown via the two different growth methods.

According to Raman spectroscopy results, most of the NbS_2 flakes are a mixture of 2H and 3R phases. The XPS results imply that the NbS_2 flake grows on Nb_2O_5 thin film and contains 2H and 3R phases. The XPS background intensity of each peak was first subtracted using a Lineal background subtraction, and the peak area was fitted using a Gaussian intensity distribution. The area ratio of $3d_{5/2}$ and $3d_{3/2}$ is 3:2, and that of $2p_{3/2}$ and $2p_{1/2}$ is 1:2. The spin-orbit splitting between Nb $3d_{5/2}$ and Nb $3d_{3/2}$ is 2.7eV, and the splitting between S $2p_{3/2}$ and S $2p_{1/2}$ is 1.18eV. As shown in Figure 68, three doublets of Nb $3d_{5/2}$ and $3d_{3/2}$ were observed in the XPS spectrum of NbS_2 for Nb_2O_5, 2H-NbS_2 and 3R-NbS_2. Detailed fitting parameters used for the Nb 3d and S 2p spectra decomposition are provided in Table 9. These peak positions for Nb_2O_5 $3d_{5/2}$, Nb_2O_5 $3d_{3/2}$, 2H-NbS_2 $3d_{5/2}$, 2H-NbS_2 $3d_{3/2}$, 3R-NbS_2 $3d_{5/2}$, 3R-NbS_2 $3d_{3/2}$, S $2p_{3/2}$ and S $2p_{1/2}$ are consistent with those of previous reports from the literature.[167-169] The area ratio of 2H-NbS_2 and 3R-NbS_2 in Nb 3d scan is the same with that in S 2p scan. This is consistent with the Raman results which show the presence of both 2H and 3R phases. Due to Nb_2O_5, the chemical composition of Nb and S for NbS_2 might be a big challenge to calculate.

Sample	Nb (%)	S (%)	K (%)	Si (%)	O (%)	C (%)
NbS_2 (K)	7.94	5.55	2	42.28	37.34	4.89
NbS_2 (no K)	2.76	1.54	0	50.5	38.95	6.25

Table 8 Elemental composition of NbS_2 flakes with K and without K based on XPS analysis.

	Nb_2O_5			2H-NbS_2		3R-NbS_2	
Sample	Non-flake area	NbS_2 (K)	NbS_2 (no K)	NbS_2 (K)	NbS_2 (no K)	NbS_2 (K)	NbS_2 (no K)
Nb $3d_{5/2}$	207.07 (1.7)	207.07 (1.6)	207.08 (1.8)	202.81 (0.8)	203.2 (0.9)	203.67 (1.1)	204.1 (1.2)
Nb $3d_{3/2}$	209.77 (1.8)	209.78 (1.6)	209.68 (1.5)	205.53 (0.9)	205.89 (1)	206.54 (1.3)	206.8 (1)
S $2p_{3/2}$				160.34 (0.65)	160.5 (1.3)	161.06 (1)	161.2 (1.2)
S $2p_{1/2}$				161.56 (0.65)	161.68 (1.4)	162.27 (1)	162.39 (1.2)

Table 9 Binding Energy (eV) and Widths (full width at half maximum in brackets) of the measured core electrons of Nb and S

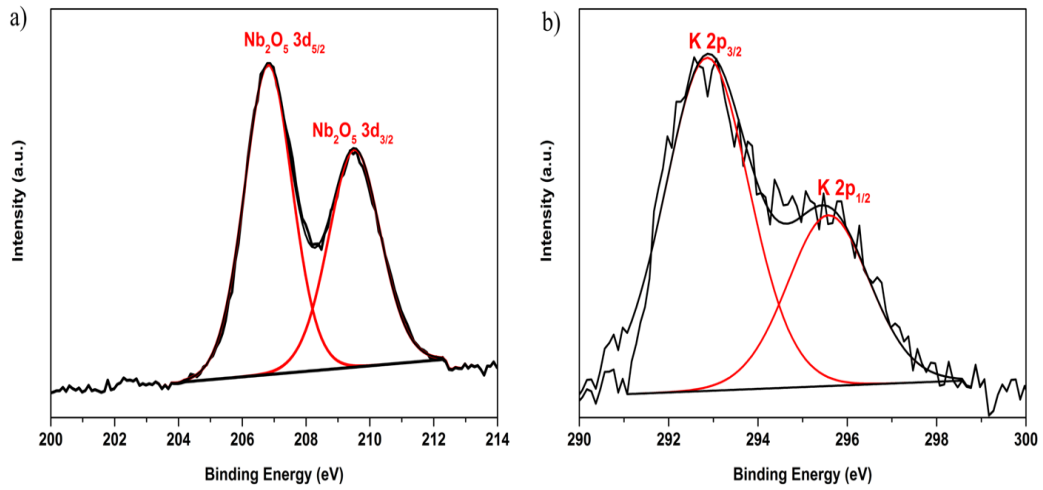

Figure 67 a) XPS scan of Nb 3d for the non-flake area of the NbS_2 with and without K samples. b) XPS scan of K 2p for the NbS_2 with K flake.

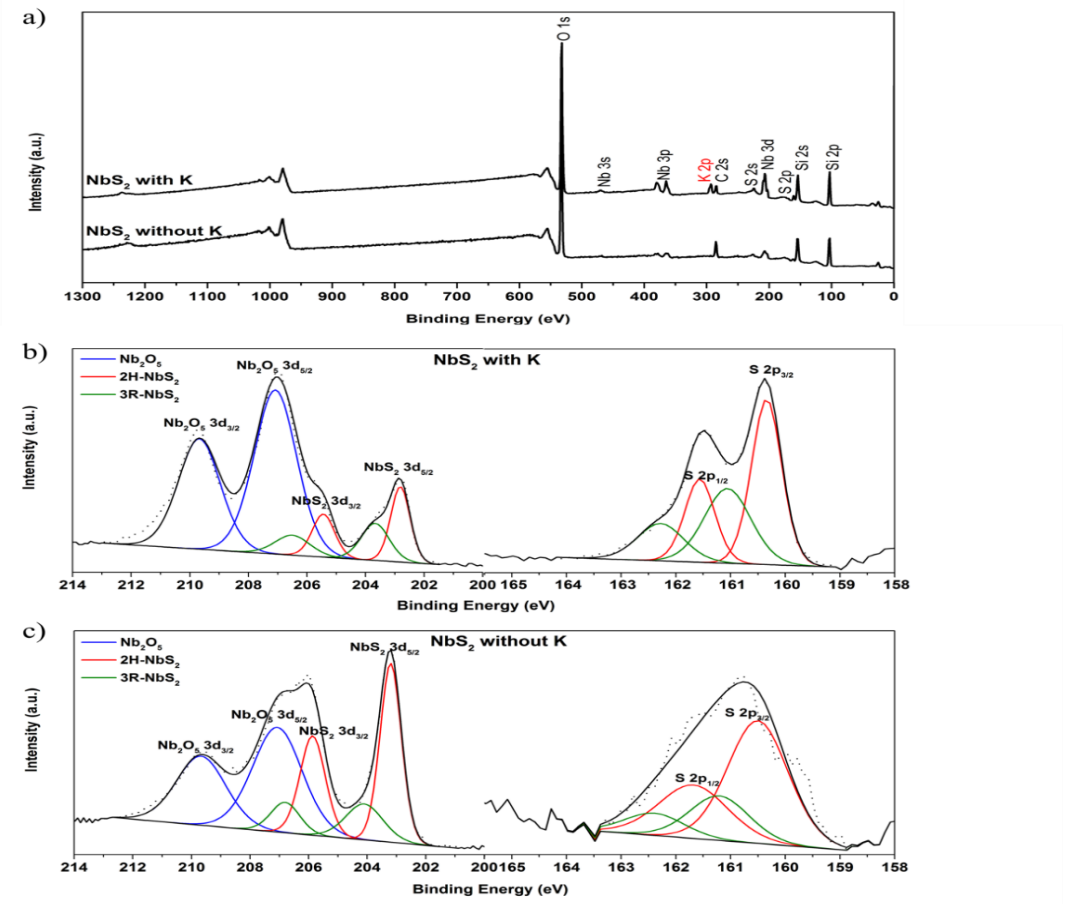

Figure 68 a) XPS survey spectrum of NbS_2 with K and NbS_2 without K. b) XPS analysis of the Nb 3d and S 2p core levels in the NbS_2 with K flakes. c) Nb 3d and S 2pcore levels in the NbS_2 without K flakes. The flakes contain N_2O_5 (blue curve), 2H-NbS_2 (red curve), and 3R-NbS_2 (green curve).

4.5.4.2.4 TEM and HRTEM analysis

The elemental mapping from transmission electron microscopy (TEM) was used to characterize NbS_2 flakes. TEM images of NbS_2 flakes are presented in Figure. The TEM sample was prepared by sonication of NbS_2 samples in ethanol. After transferring the NbS_2 to the TEM grid, Figure 69 shows NbS_2 films folded as multilayers. The thinner and uniform flake area about 3 layers was chosen for the crystal structure characterization (Figure 69b). The high-resolution TEM (HRTEM) image clearly shows visible a hexagonal lattice as shown Figure 69c. The brighter spots are niobium atoms (purple dots) and the dimmer spots are sulfur atoms (yellow dots). Figure 4d shows the electron diffraction patterns of the NbS_2 which corresponds to the [100] crystalline plane of 2H-NbS_2 (Pattern ref. 00-041-0980).

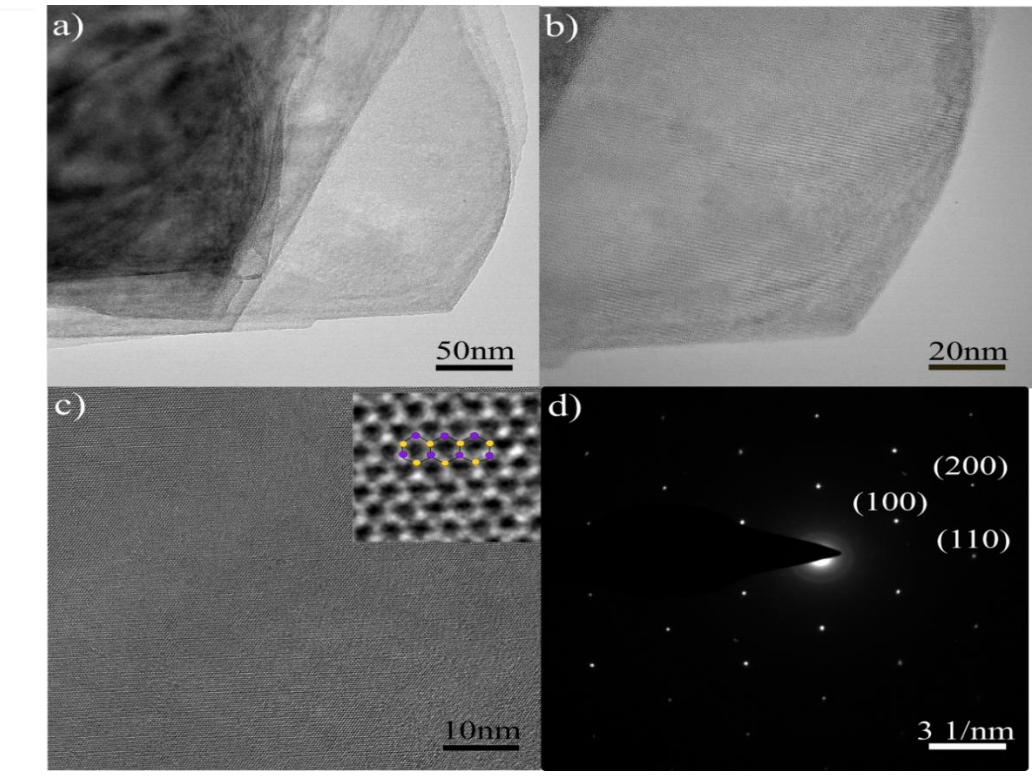

Figure 69 TEM structure and elemental analyzed shows that Nb and Sulfur are on the TEM grid with the structure of top view of 2H-NbS_2 TEM and HRTEM images (a-c) and diffraction pattern from (d) of the NbS_2 flake.

STEM and energy-dispersive X-ray spectroscopy (EDS) measurements were carried out for elemental mapping of NbS_2 with and without K to further investigate the chemical composition. Figure 70 shows that Nb, S, and K were detected in both samples NbS_2 with K flakes, while K was only detected for the flakes grown with KI. The elemental mapping was carried on the transferred NbS_2 flakes and they did not contain any Nb_2O_5 in the flake structure. The atomic ratio of Nb/S is around 1:2 (Table 8). The elemental mappings of Nb, S, and K on the NbS_2 with K flake are shown in Figure 70. The results reveal that during growth process Nb_2O_5 thin film firstly covers on SiO_2 substrate, then NbS_2 flakes grow on Nb_2O_5, which is in good agreement with XPS results.

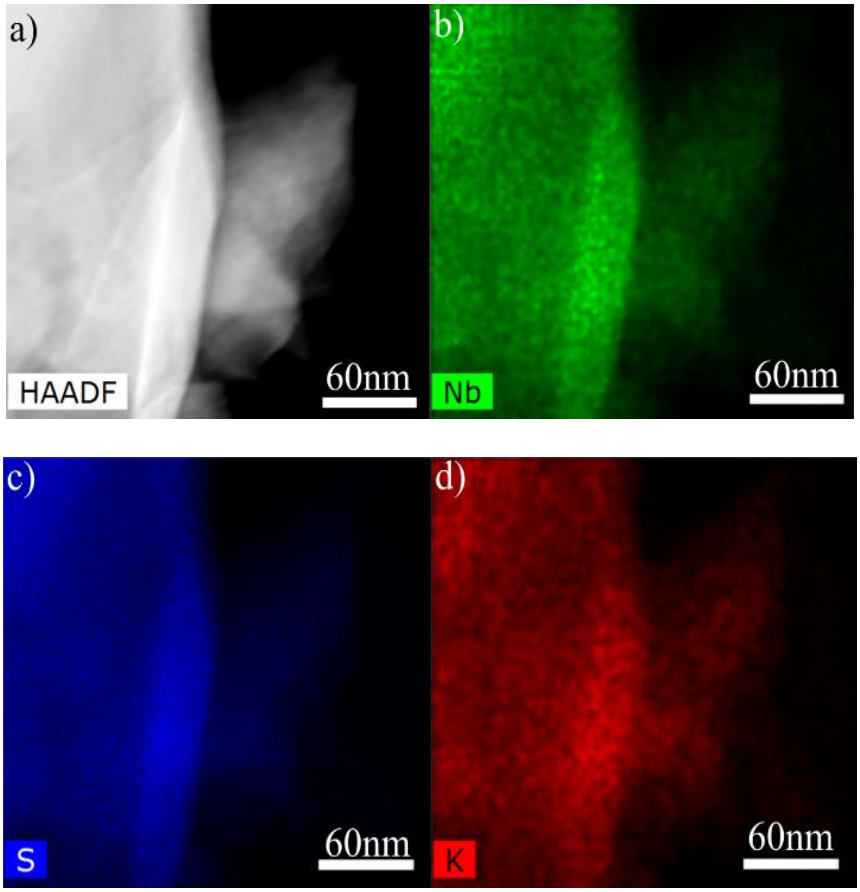

Figure 70 a) STEM/ HAADF EDS elemental mapping of alkali-assisted NbS_2 for each element b) Nb, c) S and d) K

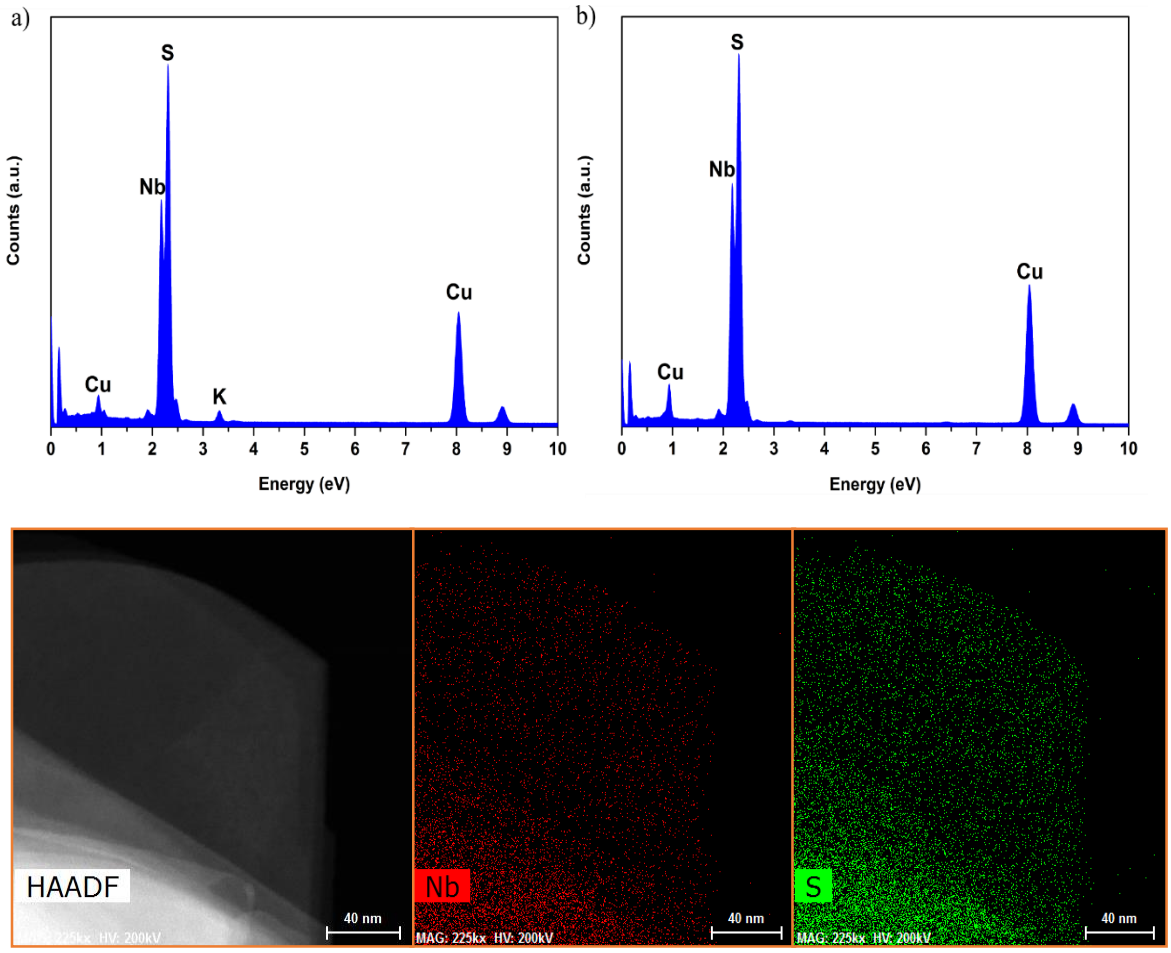

Figure 71 TEM Elemental analysis (a) with and(b) without alkali –assisted flakes exhibits the elemental survey and STEM-EDS element mapping of NbS_2 without any alkali assisted promoter.

4.5.5 Device performances and HER application of CVD NbS_2

Hydrogen is the cleanest fuel and represents one of the most promising energy sources.[170] The electrolysis of water is considered as a well-known principle to produce hydrogen as in a sustainable fashion.[171, 172] The key component in the electrochemical reduction of water is the catalyst for hydrogen evolution reduction (HER). Layered transition-metal dichalcogenide catalysts have been a promising alternative to a platinum catalyst for HER due to their low cost and high intrinsic per-site HER activity.[173-176]

Group-VI TMDs based on molybdenum and tungsten have been studied extensively in various forms for HER applications.[177-181] However, semiconducting TMDs are significantly limited by the density of active sites, which are concentrated only at the edges.[178, 182]Based on the DFT first-principles calculations, group-V MS_2 (V, Nb, or Ta) show improved HER performance due to its metallic behavior and lower energy of hydrogen adsorption.[183, 184] Despite this great potential, group-V TMDs have barely been studied due to difficulties to grow the high quality of MS_2.

To further understand the electrical property of NbS_2, we fabricated devices using electron beam lithography patterning on NbS_2 with and without alkali assisted. CVD grew few layered NbS_2 showed high conductivities over 1000 S/cm for both with and without alkali assisted samples. To demonstrate the HER performance, we have carried out HER test using a microelectrochemical cell set-up developed by our group [185-189]. The HER properties were measured using a three-electrode configuration, with glassy carbon as the counter-electrode, Ag/AgCl electrode as the reference electrode, and one gold pad contacting the NbS_2 as the working electrode. We obtained high current densities due to its metallic nature. The onset potential is around 0.35 V. The Tafel slope is around 150 mV/dec.

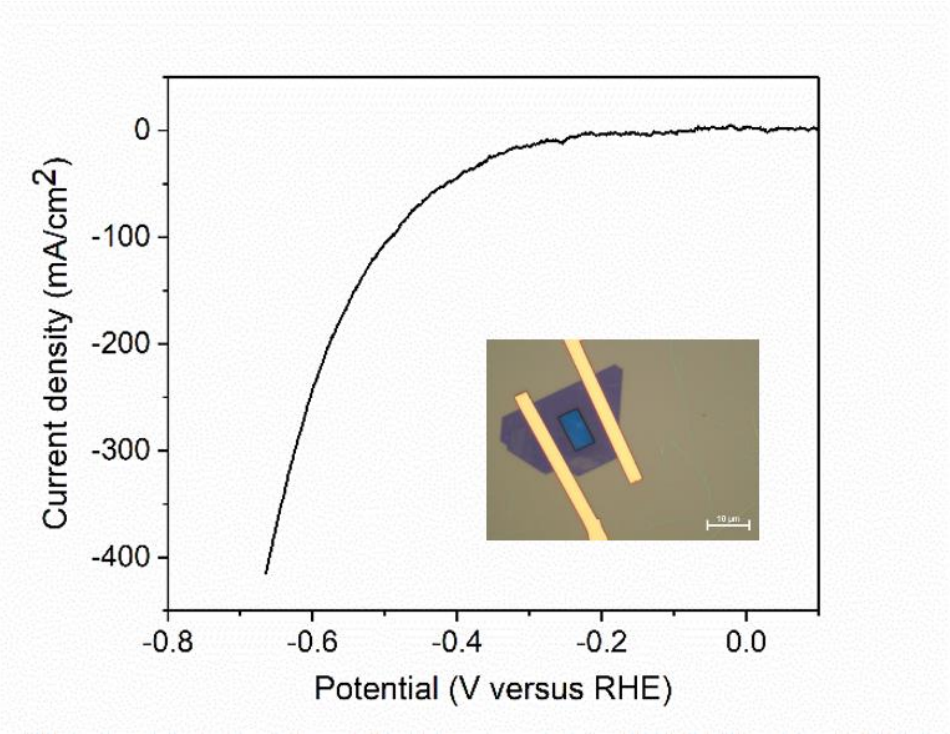

Figure 72 HER application and device performance of CVD NbS_2 flakes on silicon dioxide substrate. The device fabrication was done by electron beam lithography patterning. The conductivity shows over 1000 S/cm for both with and without alkali assisted samples while HER the onset potential is around 0.35 V. The Tafel slope is around 150 mV/dec.

4.5.5.1 Transferring process of different substrate for HER

Further HER application and device performance were also employed on the different substrates to observe HER activity versus substrate effects. Gold coated film and glassy carbon were used due to their metallic behavior. Since HER application requiress conductive substrates for reaction to occur on the substrate surface in terms of observing the catalytic activity, the flakes that were deposited on the silicon dioxide substrate were transferred on glassy carbon with the highly careful transfer process. The following transfer procedures were applied for the flakes on silicon dioxide substrate:

- Coating with PMMA: In order, the successful transfer occurs, the silicon dioxide substrate was coated with PMMA by using spin coating method 2000 rpm with 90 seconds as reported for MoS_2 study [190].
- Baking process: Once the successful coating was completed, the substrates were exposed to a baking process to remove the moisture. Baking was done at 110 C^o for 30 minutes after placing the substrate on glass piece.
- Dissolving process: it has been proving that PMMA can dissolve in acetone solution. The samples were soaked in 50 ml acetone solution to dissolve PMMA completely from the substrate surface. Note that residue of PMMA might cause less performance for HER application or any other transfer process.
- Transferring the flakes: The flakes were suspended in the acetone solution after removing the PMMA. By using a small and clean spatula, the suspended flakes were meticulously transferred on the glassy carbons. On the other hand, it is worth mentioning that the glassy carbon was cleaned and polished prior to the transfer process.
- Annealing: Final step was annealing the substrates to remove any impurity that might come from the previous dissolution of PMMA step. Annealing was done at 300 C^o for 3 hours with the flow rate of 100 sccm by using argon carrier gas. Note that different quartz tune was used for annealing process to avoid any contamination. The glassy carbons were placed and held at the center of the furnace till the room temperature after the annealing process was completed.

The transfer method that was straightforwardly explained earlier was applied to both glassy carbon and gold substrates. The HER performance of each substrate will be demonstrated shortly. However, it is significantly important to show that some characterization techniques needed to be done to prove that the successful transfer occurred on gold and glassy carbon substrates. Especially, Raman spectra were employed on the transferred substrate to demonstrate the successful transfer by analyzing the main peaks as well as SEM and optical microscope to observe the coverage after the transfer.

For HER study, the size of the flakes must be larger than 10 microns in order that the catalytic reaction occurs on the surface. On the other hand, measuring the device performance of NbS_2 requires relatively smaller flake size compare to HER work. A few microns of the flakes have been employed on this work to observe further device performances by either traditional thermal evaporation or electron beam lithography method. After the transfer process, some changes were observed on the flakes. Some of the flakes were destroyed and lost their crystallographic morphology. This is because the long transferring process and some chemical reaction damaged the flakes uniformity. Some holes and truncated triangles were formed after the transfer process. Characterization of these new forms of the flakes was a big challenge to insight the changes in the structure. Before and after transfer, the conditions during the characterizations were held the same to have a better understanding and comparison.

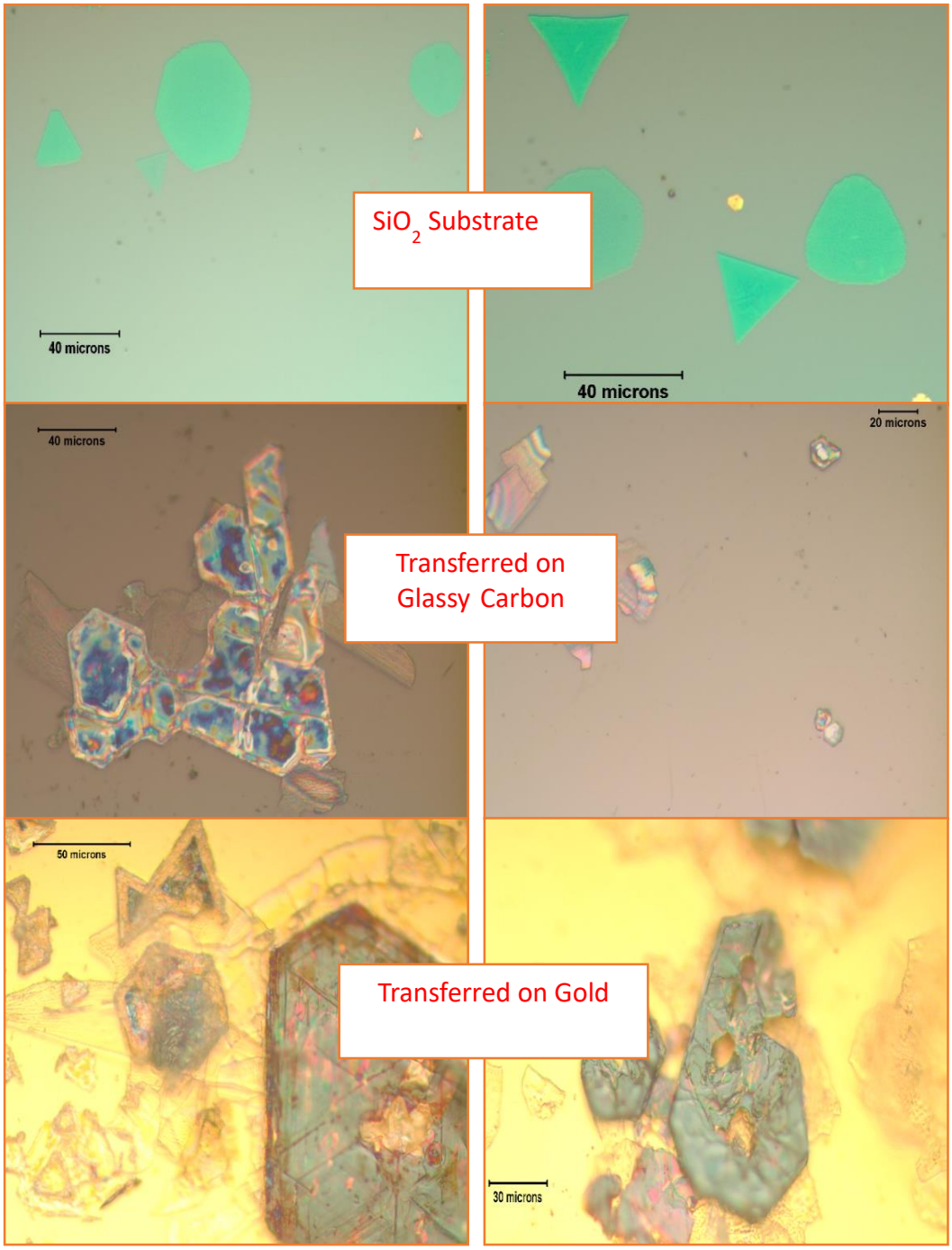

Figure 73CVD grown NbS_2 grown on silicon dioxide was successfully transferred on glassy carbon and gold substrate for HER application. The transferred flakes size was decent enough for HER, on gold substrate relatively larger flakes.

4.5.5.2 Characterizations of the transferred flakes

The Raman spectra are significant and reliable for TMDCS and have been used to differentiate the polytypes of TMDs for decades since it was invented. As an explained previous chapter, there are two main polytypes of NbS_2 that has been considerable studied which are 2H-NbS_2 and 3R--NbS_2. 2H-NbS_2 has four Raman modes which are $E^2_{2g,}$ $E_{1g,}$ $E^1_{1g,}$ $A_{1g,}$ shows 31,260, 304 and 379 cm^{-1} respectively, 3R-NbS_2 has different four Raman modes as E_1, E_2, A_1 and A_2 at 290, 330, 386, 458 cm^{-1}.

After the transferred flakes on glassy carbon, Raman spectra were employed on the substrate from many different regions. As the figure below demonstrates, 2H-NbS_2 peaks were observed dominantly with slight differences. Since the surface roughness of glassy carbon is different than silicon dioxide, there is a slight shift between the main 2H-NbS_2 peaks. The similar Raman spectra result has been obtained from the flakes that were transferred on the gold substrate.

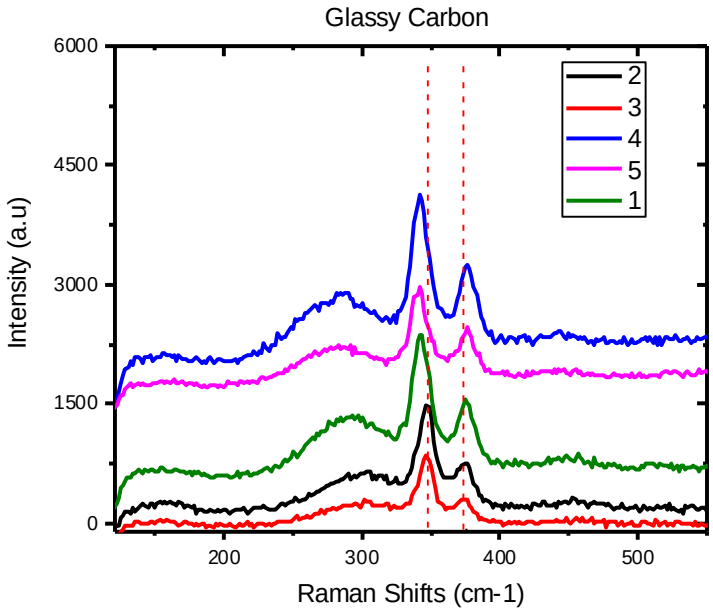

Region	E^1_{2g}	A_{1g}
1	342	376
2	347	375
3	347	375
4	342	377
5	341	376

Figure 74 Raman spectra on glassy carbon after the transferring the flakes from silicon dioxide, the slight shift between the peaks have been observed due to having different surface roughness of the substrates.

For both glassy carbon and gold substrate, similar HER procedure has been applied to measure their performance. 1 ml of H_2SO_4 acidic solution was carefully prepared with 35 ml water in order to have 1 molar of the proton. Cyclic voltammogram (-0.1 ref, 0.7 ref, 5mV/s*2) was employed on the transferred CVD grown NbS_2 flakes. since HER measurement requires slightly larger flakes and coverage density, NbS_2 with alkali assisted flakes were synthesized for this work.

Three-electrode configuration was used for the HER measurement. Glassy carbon as the counter-electrode, Ag/AgCl electrode as the reference electrode, and one gold pad contacting and the NbS_2 as the working electrode were employed to measure the HER performance. The transferred flakes on both gold and glassy carbon represented the similar result by showing that both substrates can be used to for HER application and provide the similar HER activity. The onset potential from transferred on glassy carbon and gold was similar and around 0.30 V while the Tafel slope was around 140 mV/dec.

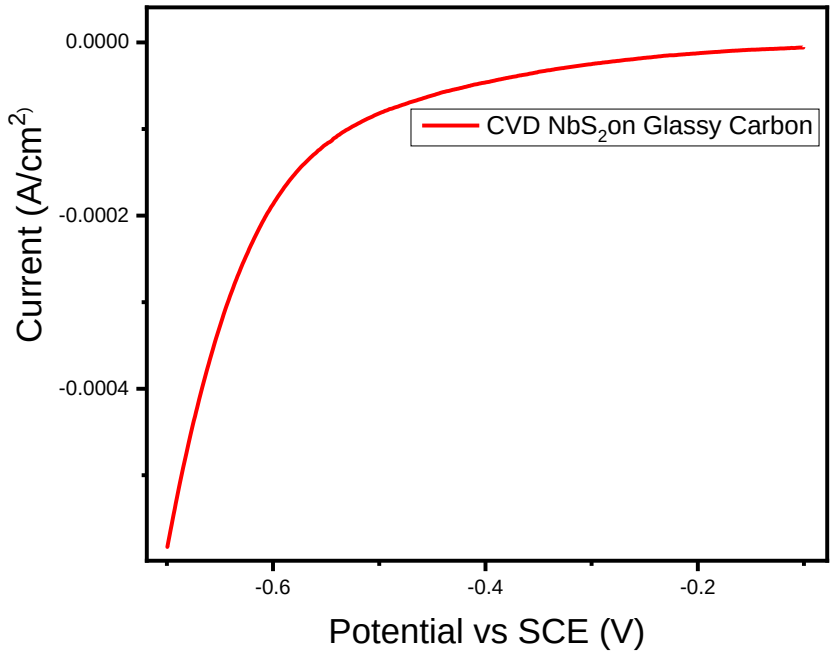

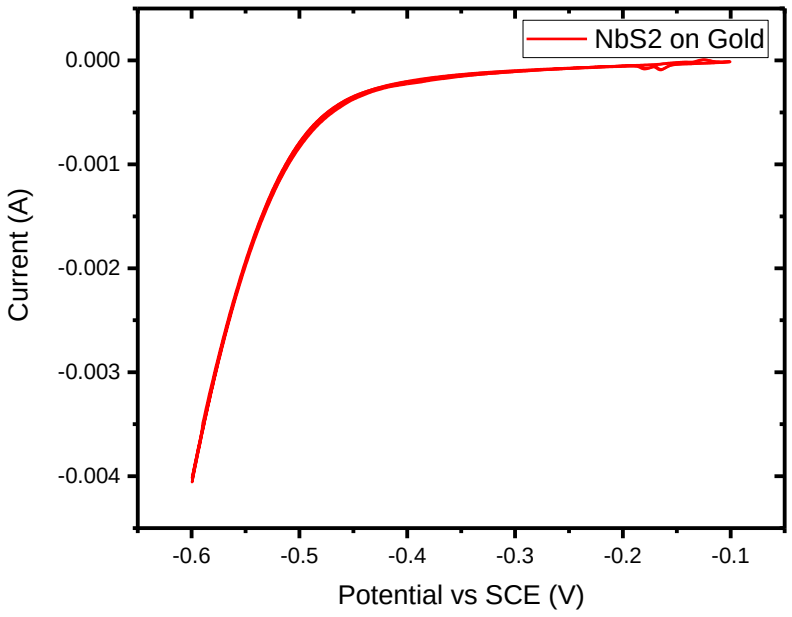

Figure 75 HER activity of CVD NbS_2 transferred on glassy carbon and gold substrate exhibits similar performance at the same experimental conditions. glassy carbon as the counter-electrode, Ag/AgCl electrode as the reference electrode, and one gold pad contacting the NbS_2 as the working electrode.

4.5.5.3 Conductivity measurement of the flakes with a thermal evaporation method

There are many methods to find out conductivity measurements of materials. Thermal evaporation and electron beam lithography are two main methods that have been used in academia and research to reveal materials behavior. Thickness and flake size are important for each method. Electron beam lithography is relatively more sensitive in terms of flake size since from a few hundred nanometers to a few microns' flakes can be easily measured with this method. On the other hand, the thermal evaporation method is more traditional and accessible method and the flake size is needed to be greater than 25 microns for this method to be used. The mash of the pattern is desired a few hundred microns so that the mask and pattern can be successfully covered on the substrate surface.

The alkali-assisted CVD grown NbS_2 leads up to a few hundred microns flake size and that make them desired for thermal evaporation method. There are usually two coating materials used to have maximum and efficient coverage on the surface for thermal evaporation. In this work, titanium and gold were used for contacting prior to conductivity measurement. Titanium was used for an adhesion material and deposited 5-nanometer thickness, on the other hand, gold was deposited 80 nanometers for contacting. Once a successful contacting was done, the conductivity measurement was conducted on two devices. Based on the AFM measurement, the thickness of these two flakes was approximately 2 nm. The resistivity value was 400Ω while the conductivity value was 2500 /Ωcm. The result of these two devices showed the metallic behavior which was a good match to the similar work from the literature[191]. Like electron beam lithography, by using thermal evaporation method, the conductivity value of the flakes represents a good metallic behavior.

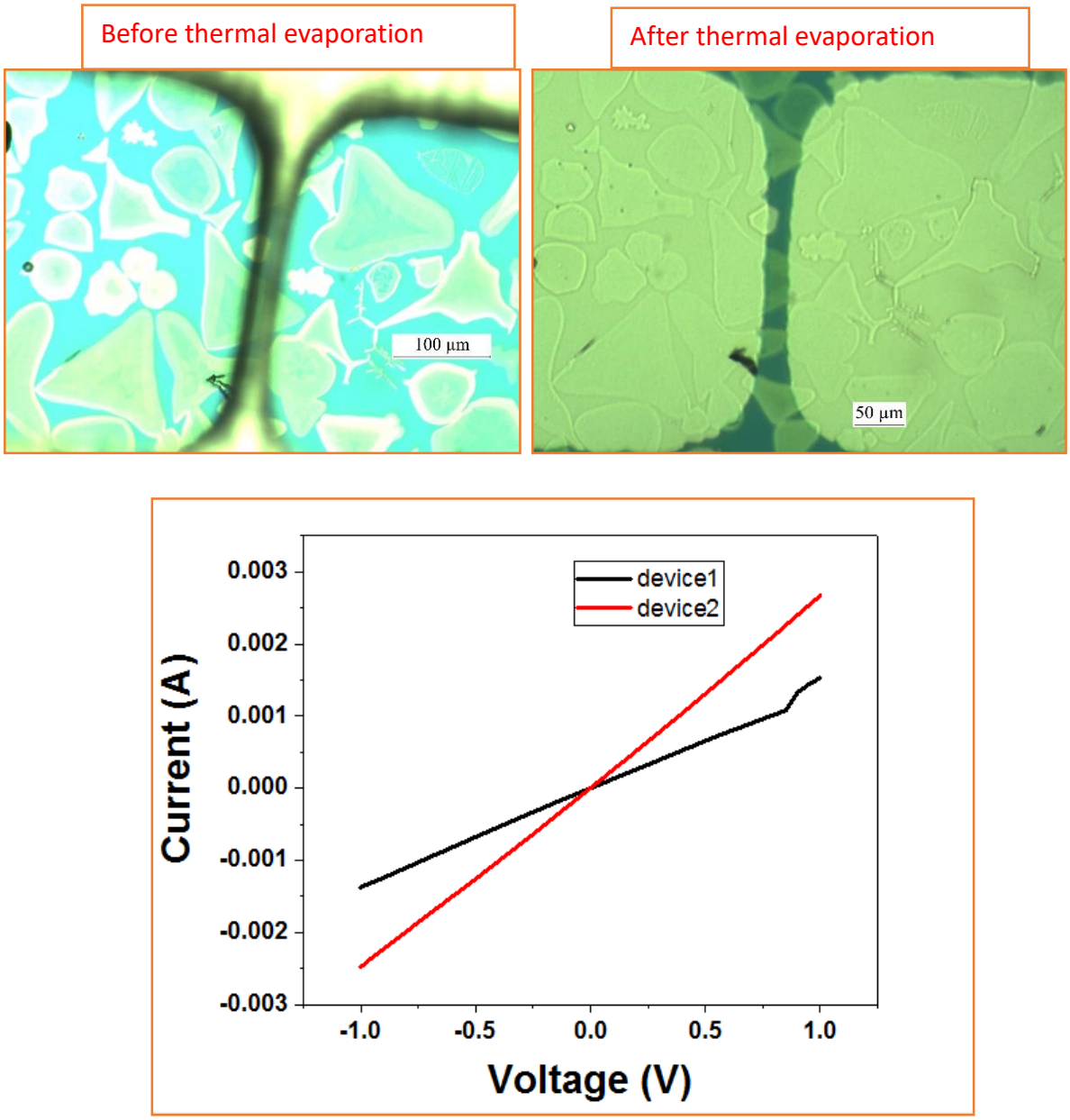

Figure 76 Two devices with alkali-assisted NbS_2 exhibits a high value of conductivity. Titanium was used for adhesion and gold for coating, 5 nm, and 80 nm respectively. The resistivity value was approximately 400Ω while the conductivity value was 2500 /Ωcm for both devices.

CHAPTER 5

5. Discussions and Conclusions

5.1 MoS_2

Two significant members of TMDCS materials were employed in this thesis work. Synthesizing them atomically thin was a big challenge in terms of exploring their layer dependent phenomena. Different experimental set-up was built for each material to optimize their recipe and to have maximum coverage density on the substrate surfaces. To do that, different substrates including sapphire, glassy carbon, gold, doped silicon, quartz were used to discover the optimum substrate for each growth. For the MoS_2 study, Silicon dioxide substrate was favorable to deposit atomically thin films and flakes on the substrate surface while the substrate position was mostly face-up in the quartz tube. The distance between precursors and position of the alumina boat in the quartz tube were well studied to deposit the materials as the desired amount.

A wide range of experimental parameters was well studied to synthesize mono and multilayers of MoS_2 films and flakes. Changing each experimental parameter resulted in a different density of film on the substrate surface. Partial pressure of each reactant exhibited a wide range and effected on the growth with placing them at the different location in the quartz tube. In terms of controlling each reactants' partial pressure, three-zone furnace could be used to achieve more consistent and uniform growth since vaporizing temperature and optimal growth temperatures of each reactant could be controlled even though single zone furnace was used for this work due to the lab condition. For instance, a high relative partial pressure of the Mo source could result in Mo-rich environment by placing it right

under the substrates (assuming that sulfur was not vaporized yet at that reaction temperature).

Once successful deposition was obtained, the further characterization methods were employed on the film and flakes; Optical microscopy, XPS, SEM, Raman spectra, Photoluminescence and AFM. Thanks to all of these characterizations methods and optimizing experimental set-up in the quartz tube, in-depth analysis a better understanding of the kinetics of crystal growth mechanisms of CVD grown MoS_2 were gained. Exploring of methods and parameters to grow CVD MoS_2 taught us significant phenomenon for a successful growth. Optimized crystal growth with reasonable control over resulting nanoscale 2D films was successfully achieved by modifying the growth parameters. A deeper understanding of how each of the parameters influence growth was also well studied for a successful CVD growth.

The conclusion of MoS_2 study provided us many take-home notes. First of all, placing the substrate exactly depends on the applications. For instance, HER application requires the flake size not smaller than 10 microns, on the other hand, a few microns flake size is decent enough for conductivity measurement or transistor systems. Large coverage density and thicker flakes could be obtained by placing the substrate face-down position while face-up- position provides relatively less dense and thinner flakes on the substrate. Although MoS_2 was successfully synthesized on the different substrates, silicon dioxide substrate was the most favorable one for a successful CVD grow in terms of having a wide range of film thickness resulting from single layer to bulk (over 100 nanometers) based on its position in the quartz tube. It is true that most of the MoS_2 studies from the literature do not mention prior cleaning of reaction tube or oxidation procedure for the CVD tube so it

cannot be assumed that there is no residue from previous experiments. Therefore, it is worth mentioning in here that the reaction tube was cleaned prior to each experiment to avoid any contamination from the lab and the previous reaction environment.

5.2 NbS_2

Unlike MoS_2, two different approaches were pursued growing NbS_2 by CVD on SiO_2/Si substrate since the traditional oxide –sulfurization method did not work for NbS_2 CVD growth. The first approach consists in using sulfur (99.5 % from Alfa Aesar) and Nb_2O_5 powders (99.9% from Sigma- Aldrich) as the precursors. However, the flake size and coverage density on the substrate was limited. Alternatively, a mixture of Nb_2O_5 and alkali promoter led to producing a larger flake size. In both approaches, the sulfur powder was located upstream while the substrate and Nb_2O_5 (and mixture with alkali promoter) was located at the center of the furnace. The alkali-assisted promoter allows achieving larger flake size of NbS_2 due to more volatile Nb-rich molecules while less coverage and smaller lateral size of the NbS_2 flakes is synthesized without the alkali-assisted.

Synthesizing NbS_2 was more challenging compared to MoS_2 study due to the fact that CVD NbS_2 growth had more uncontrollable parameters with alkali promoter. Like MoS_2 synthesizing, different substrates were also well studied to explore the optimum substrate. Silicon dioxide substrate was the most favorable one among the sapphire, quartz, glassy carbon, doped silicon substrates in terms of synthesizing larger coverage and thinner flakes. Several alkali promoters from halide group were also used for CVD NbS_2 study to explore the best alkali promoter. KCl, NaCl, KBr, and KI were alkali promoters that were used for the controllable and large area of CVD growth. Any chlorine compound (NaCl or KCl) resulted in etching on the substrate surface. Therefore, KI and KBr were more

preferable for the growth. However, considering layer stability and mass transfer during the reaction, KI gave rise to more controllable CVD growth for NbS_2. Like MoS_2 study, the substrate location and the quartz tube condition were two important parameters influenced on the growth. Silicon substrate was placed at a face-up position during the experiment. The quartz tube was changed and cleaned prior to every experiment to avoid the contamination.

As known, there are many polytypes of TMDCs which are 1T, 2H and 3R, trigonal, hexagonal and rhombohedral crystal structure, respectively. The synthesizing MoS_2 with CVD method provided us 2H crystal structure. However, NbS_2 with the same method showed two important phases together, 2H and 3R from our study. This two-phase appeared together once the film or flake thickness was over 10 nanometers. Having two phases together did not depend on which types of halide group promoter used as well as doing the experiment at different time and temperature. Surprisingly, using different substrates also led us to have these two phases together unlike the expectations of atomic mismatching or twisting the flakes during the growing might cause to grow only one phase.

Further characterization was done by Raman spectroscopy, TEM, EDS, XPS. They have proved that both 2H-NbS_2 and 3R has been synthesized with good uniformity with the different thicknesses. The AFM, SEM were used to characterize the flakes thickness and scale distribution while TEM and EDX were used for elemental mapping and composition. Monolayer and a few layers of other TMD were successfully synthesized to explore their layer-stacking dependency and other physical properties. By using this CVD recipe, several devices were made to calculate conductivity measurement. The result showed that the flakes and films exhibited metallic behavior. HER behavior was also

employed to measure the edge and basal plane activity. The flakes grown on the silicon dioxide substrate were transferred on glassy carbon and gold to see the substrate effect on HER performance.

CHAPTER 6

6. Future Work

TMDCs can be synthesized with many different methods including mechanical exfoliation, chemical exfoliation, physical vapor deposition, and chemical vapor deposition. Different coverage density can be obtained via these methods based on the experimental set-up conditions. However, a controllable monolayer of MoS_2 and NbS_2 still remains a big challenge for the CVD method. For instance, a single layer of MoS_2 shows direct band gap and this feature is desired for many electronic and optoelectronic applications. Even though most of the parameters for a successful growth were controlled in this work for both MoS_2 and NbS_2 work, synthesizing uniform and large area monolayer film will be a difficult step for researchers to overcome. Each parameter for a successful CVD MoS_2 grow was explicitly explained in this thesis, however, applying other parameters (magnetic field, electric field, high-pressure environment or ultra-high vacuum pump) on CVD growth have not been well studied. Reveling the result from these studies will enable us intelligently designed materials for the next generation of miniature electronics.

Once a successful CVD NbS_2 growth is achieved, the mixture of 2H and 3R phase crystal structure is formed in the layer material. This thesis work has proved that 3R phases generally forms on the top of 2H phase once the flake thickness reaches over 10 nanometers. Having this two phases together might not be desired for some applications,

considering that 2H-NbS_2 exhibits metallic behavior while 3R-NbS_2 shows semiconducting resulting unwanted features for potential device performances or HER application. Controlling these two phase formation during the growth is still unexplored. Reveling the reason of what causes this formation will be a significant parameter for NbS_2 future studies.

Phase transformation of MoS_2 was successfully done by many researchers including our group at Rutgers by lithium intercalation via n-butyl lithium of the layered transition metal dichalcogenides. Synthesizing two differentiable phases in thin nanosheets presents unique means of exploring nanoscale features. The electronic behavior considerably changes once 2H MoS_2 is successfully converted to the 1T structure with the reversible process. However, there have been no published studies linking the phase transformation of NbS_2 and its reversible process at the time of writing this thesis. Since NbS_2 has started to gain a great deal of attention by researchers recently, phase transformation of 2H-NbS_2 with lithium intercalation via n-butyl lithium will be promising to see in the future for some electronic applications. Proving that phase transformation also possible for NbS_2 will allow researchers to do the same thing for other TMDCs such as VS_2, TaS_2.

Removing oxygen from the reaction environment has been a big challenge for researchers including me. The oxidation occurs both during the reaction and after, based on the precursors. NbS_2 is very sensitive to air and one of the biggest challenges in this work was how to remove oxygen from the surface. Building experimental set up with the oxygen-free system will be an important thing to consider since having an oxidation layer on the top of the surface will not lead the researchers to extract the correct information.

Therefore, analyzing correct thickness versus the conductivity measurement of NbS_2 study is also significantly important to discover a unique opportunity to advance the electronic, magnetic and optoelectronic fields.

References:

1. Thygesen, F.A.R.a.K.S., *Computational 2D Materials Database: Electronic Structure of Transition-Metal Dichalcogenides and Oxides* The Journal of Physical Chemistry, 2015. **119**: p. 13169−13183.
2. Qing Hua Wang, K.K.-Z., Andras Kis, Jonathan N. Coleman and Michael S. Strano, *Electronics and optoelectronics of two-dimensional transition metal dichalcogenides.* Nature Nanotechnology, 2012. **7**: p. 699-712.
3. Yi-Hsien L, X.-Q.Z., Wenjing Z, Mu-Tung C, Cheng-T, Kai-Di C,Ya-Chu Y, Jacob Tse-W, Chia-Seng C, Lain-J and Tsung-W, J. Am. , Chem. Soc. , 2012.
4. B. Radisavljevic, A.R., J. Brivio, V. Giacometti, and A. Kis, " *"Single-layer MoS_2 transistors.* Nature Nanotechnology, 2011. **vol. 6**: p. pp. 147-150.
5. A. K. Geim and K. S. Novoselov, *"The rise of graphene,.* Nature Materials,, 2007. **vol. 6,**: p. pp. 183-191, .
6. Neto, A.C.G., F.; Peres, N.; Novoselov, K. S.; Geim, A. K. . , *The Electronic Properties of Graphene. Rev. Mod.* Phys, 2009: p. 109-162.
7. Deep Jariwala, V.K.S., Lincoln J. Lauhon, Tobin J. Marks and Mark C. and Hersam, *Emerging Device Applications for Semiconducting Two-Dimensional Transition Metal Dichalcogenides.* ACS Nano, 2014. **8**.
8. Ewels, C. *Idealized structure of a single graphene sheet*. 2018 [cited 2018.
9. Chiu, K.C., et al., *Synthesis and Application of Monolayer Semiconductors (June 2015).* Ieee Journal of Quantum Electronics, 2015. **51**(10).
10. Kitaura, R., et al., *Chemical Vapor Deposition Growth of Graphene and Related Materials.* Journal of the Physical Society of Japan, 2015. **84**(12).
11. Ganorkar, S., et al., *Effect of precursor on growth and morphology of MoS_2 monolayer and multilayer.* Journal of Physics and Chemistry of Solids, 2015. **87**: p. 32-37.
12. Liu, H.F., S.L. Wong, and D.Z. Chi, *CVD Growth of MoS_2-based Two-dimensional Materials.* Chemical Vapor Deposition, 2015. **21**(10-12): p. 241-259.
13. D.Li.R.Kaner., Science 2008. **Vol.320,**: p. 1170.
14. Zhang, X.W., et al., *Vertical Heterostructures of Layered Metal Chalcogenides by van der Waals Epitaxy.* Nano Letters, 2014. **14**(6): p. 3047-3054.
15. Zibiao Li, S.L.W., *Functionalization of 2D transition metal dichalcogenides for biomedical applications.* Elsevier, 2016: p. 1095-1106.
16. Kuc, A., Zibouche, N. & Heine, T., *Influence of quantum confinement on the electronic structure of the transition metal sulfide TS2.* Phys. Rev. B, 2011. **83**: p. 245213 .
17. Xu, H.J., et al., *Nucleation mechanism and morphology evolution of MoS_2 flakes grown by chemical vapor deposition.* Chinese Physics B, 2017. **26**(12).
18. Kim, H., et al., *Synthesis of MoS_2 atomic layers using PECVD*, in *State-of-the-Art Program on Compound Semiconductors*, C. Odwyer, et al., Editors. 2013. p. 47-50.

19. Duan, X., et al., *Two-dimensional transition metal dichalcogenides as atomically thin semiconductors: opportunities and challenges.* Chemical Society Reviews, 2015. **44**(24): p. 8859-8876.
20. Ionescu, R., et al., *Synthesis of Atomically Thin MoS_2 Triangles and Hexagrams and Their Electrical Transport Properties.* Ieee Transactions on Nanotechnology, 2014. **13**(4): p. 749-754.
21. Li, W., et al., *Broadband optical properties of large-area monolayer CVD molybdenum disulfide.* Physical Review B, 2014. **90**(19): p. 195434.
22. Yan, A.M., et al., *Direct Growth of Single- and Few-Layer MoS_2 on h-BN with Preferred Relative Rotation Angles.* Nano Letters, 2015. **15**(10): p. 6324-6331.
23. Zhang, J., et al., *Scalable Growth of High-Quality Polycrystalline MoS_2 Monolayers on SiO2 with Tunable Grain Sizes.* Acs Nano, 2014. **8**(6): p. 6024-6030.
24. Xu, H.T., et al., *Optical identification of MoS_2/graphene heterostructure on SiO2/Si substrate.* Optics Express, 2014. **22**(13): p. 15969-15974.
25. Yanase, T., et al., *Chemical Vapor Deposition of NbS_2 from a Chloride Source with H-2 Flow: Orientation Control of Ultrathin Crystals Directly Grown on SiO2/Si Substrate and Charge Density Wave Transition.* Crystal Growth & Design, 2016. **16**(8): p. 4467-4472.
26. Ling, X., et al., *Role of the Seeding Promoter in MoS_2 Growth by Chemical Vapor Deposition.* Nano Letters, 2014. **14**(2): p. 464-472.
27. Kim, H., et al., *Suppressing Nucleation in Metal–Organic Chemical Vapor Deposition of MoS 2 Monolayers by Alkali Metal Halides*. Vol. 17. 2017.
28. Benavente, E.S.A., M. A.; Mendizabal, F.; Gonzalez, G. Coord., Chem. Rev, 2002. **6,224** p. 87-109.
29. Q. H. Wang, K.K.-z., A. Kis, J. N. Coleman, and M. S. Strano , , *"Electronics and optoelectronics of two-dimensional transition metal dichalcogenides,".* Nature Nanotechnology, 2012. **vol. 7,** : p. pp. 699-712,.
30. Petkov, V.B., S. J. L.; Larson, P.; Mahanti, S. D.; Vogt, T.;Rangan, K. K.; Kanatzidis, M. G. , Phys. Rev. B, 2002, . **65**.
31. Rao, C.N.R.G., J. , *New Directions in Solid StateChemistry.* Cambridge Univeristy Press, 1997.
32. Castellanos-Gomez, A.P., M.; Steele, G. A.; Zant, H. S. J. v. d.; Agraït, N.; Rubio-Bollinger, G., , *Mechanical properties of freely suspended semiconducting graphene-like layers based on MoS_2. .* Nanoscale Research Letters, 2012: p. 233-233.
33. Podzorov, V.G., M. E.; Kloc, C.; Zeis, R.; Bucher, E., , *High-mobility field-effect transistors based on transition metal dichalcogenides.* Applied Physics Letters 2004: p. 3301-3303.
34. Mattheiss, L.F., *Band Structures of Transition-Metal-Dichalcogenide Layer Compounds.* Physical Review B, 1973. **8** p. 3719-3740.
35. Hussain, S., et al., *Controlled synthesis and optical properties of polycrystalline molybdenum disulfide atomic layers grown by chemical vapor deposition.* Journal of Alloys and Compounds, 2015. **653**: p. 369-378.
36. A. Kumar and P. K. Ahluwalia, *"Electronic structure of transition metal*

dichalcogenides monolayers 1H-MX2 (M = Mo, W; X = S, Se, Te) from ab-initio theory: new direct band gap semiconductors,". European Physical Journal B, 2012. **vol. 85,**: p. p. 186,.

37. Splendiani, A.S., L.; Zhang, Y.; Li, T.; Kim, J.; Chim, C.-Y.; Galli, G.; Wang, F., *Emerging Photoluminescence in Monolayer MoS2.* Nano Letters, 2010. **10 (4),** : p. 1271-1275.
38. K. F. Mak, C.L., J. Hone, J. Shan, and T. F. Heinz, " *"Atomically thin MoS_2: A new direct-gap semiconductor,.* Physical Review Letters,, 2010. **vol. 105,**: p. p. 136805,.
39. Yu, Z.G., Y.W. Zhang, and B.I. Yakobson, *An Anomalous Formation Pathway for Dislocation-Sulfur Vacancy Complexes in Polycrystalline Monolayer MoS_2.* Nano Letters, 2015. **15**(10): p. 6855-6861.
40. Yoo, Y.D., Z.P. Degregorio, and J.E. Johns, *Seed Crystal Homogeneity Controls Lateral and Vertical Heteroepitaxy of Monolayer MoS_2 and WS2.* Journal of the American Chemical Society, 2015. **137**(45): p. 14281-14287.
41. Deng, Y., et al., *Black Phosphorus–Monolayer MoS_2 van der Waals Heterojunction p–n Diode.* ACS Nano, 2014. **8**(8): p. 8292-8299.
42. Brec, R.D., P.; Rouxel, J.; and R. Schollhorn, Ed.; , *In Progress in Intercalation Research.* Kluwer Academic Publishers, 1994. **Vol. 17,** : p. pp 177 221.
43. Mulhern, P.J.C., J. Phys, 1989. **67**: p. 1049-1052.
44. Yang, L., et al., *Chloride Molecular Doping Technique on 2D Materials: WS2 and MoS_2.* Nano Letters, 2014. **14**(11): p. 6275-6280.
45. Lemmon, J.P.W., J. H.; Oriakhi, C.; Lerner, M. M. and Electrochim. Acta, 1995. **40,** : p. 2245-2249.
46. A. Castellanos-Gomez, M.B., A. M. Goossens, V. E. Calado, H. S. J. van der and a.G.A.S. Zant, ,, *"Laser-thinning of MoS_2: On demand generation of a singlelayer semiconductor,".* Nano Letters. **vol. 12,** : p. pp. 3187-3192, 2012.
47. Cho, S.B., N. P.; Paglione, J.; Fuhrer, M. S.. , Nano Letters, 2011,. **11,** : p. 1925–1927.
48. Dines, M.B., Mat. Res. Bull.,, 1975,. **10**: p. 287-291.
49. Divigalpitiya, W.M.R.M., S. R.; Frindt, R. F. , Thin Solid Films, 1990: p. 186, 177.
50. Stankovich, S.D., D. A.; Dommett, G. H. B.; Kohlhaas,K. M.; Zimney, E. J.; Stach and A.P. E, R. D.; Nguyen, S. T.; Ruoff, R. S. , , Nature Communications, 2006: p. 442, 282.
51. P. R. Bonneau, R.F.J., and R. B. Kaner, ," , , *"Rapid solid-state synthesis of materials from molybdenum disulphide to refractories.* Nature Communications, 1991. **vol. 349,** : p. pp. 510-512.
52. Balendhran, S., et al., *Two-Dimensional Molybdenum Trioxide and Dichalcogenides.* Advanced Functional Materials, 2013. **23**(32): p. 3952-3970.
53. Chen, J., et al., *Chemical vapor deposition of high‐quality large‐sized MoS_2 crystals on silicon dioxide substrates.* Advanced Science, 2016. **3**(8).
54. Bilgin, I., et al., *Chemical vapor deposition synthesized atomically thin molybdenum disulfide with optoelectronic-grade crystalline quality.* ACS nano, 2015. **9**(9): p. 8822-8832.

55. Yi-Hsien L, X.-Q.Z., Wenjing Z, Mu-Tung C, Cheng-T, Kai-Di C,Ya-Chu Y, Jacob Tse-W, Chia-Seng C, Lain-J and Tsung-W, J. , Am. Chem. Soc. , 2012.
56. Lee, Y.H., et al., *Synthesis of large‐area MoS2 atomic layers with chemical vapor deposition.* Advanced materials, 2012. **24**(17): p. 2320-2325.
57. O'Brien, M., et al., *Plasma assisted synthesis of WS 2 for gas sensing applications.* Chemical Physics Letters, 2014. **615**: p. 6-10.
58. Kim, I.S., et al., *Influence of stoichiometry on the optical and electrical properties of chemical vapor deposition derived MoS_2.* ACS nano, 2014. **8**(10): p. 10551-10558.
59. Liu, Y., et al., *Mesoscale imperfections in MoS_2 atomic layers grown by a vapor transport technique.* Nano letters, 2014. **14**(8): p. 4682-4686.
60. Plechinger, G., et al., *A direct comparison of CVD-grown and exfoliated MoS_2 using optical spectroscopy.* Semiconductor Science and Technology, 2014. **29**(6): p. 064008.
61. Tsai, M.-L., et al., *Monolayer MoS_2 heterojunction solar cells.* ACS nano, 2014. **8**(8): p. 8317-8322.
62. Torrel, S., *CHEMICAL VAPOR DEPOSITION GROWTH OF MOLYBDENUM DISULFIDE AND ITS NANOSCALE TRIBOLOGICAL CORRELATION WITH RAMAN SPECTROSCOPY*, in *Material Science and Engineering* 2017, Rutgers University
63. Dash, J.K., et al., *A Method Toward Fabricating Semiconducting 3R-NbS_2 Ultrathin Films.* The Journal of Physical Chemistry C, 2015. **119**(34): p. 19763-19771.
64. Lv, R., et al., *Transition Metal Dichalcogenides and Beyond: Synthesis, Properties, and Applications of Single- and Few-Layer Nanosheets.* Accounts of Chemical Research, 2015. **48**(1): p. 56-64.
65. Leynaud, O., et al., *Crystal structures and magnetic properties of the two misfit layer compounds: SrGd0.5S1.5 (1.16)NbS_2 and Sr(Fe,Nb)(0.5)S-1.5 (1.13)NbS_2.* Journal of Solid State Chemistry, 2002. **168**(1): p. 41-51.
66. Yang, Z.X., et al., *Electronic structures and transport properties of a MoS_2-NbS_2 nanoribbon lateral heterostructure.* Physical Chemistry Chemical Physics, 2017. **19**(2): p. 1303-1310.
67. Wang, Z.G., et al., *Structure and electronic properties of transition metal dichalcogenide MX2 (M = Mo, W, Nb; X = S, Se) monolayers with grain boundaries.* Materials Chemistry and Physics, 2014. **147**(3): p. 1068-1073.
68. Fisher, W.G. and M.J. Sienko, *Stoichiometry, structure, and physical properties of niobium disulfide.* Inorganic Chemistry, 1980. **19**(1): p. 39-43.
69. Onari, S., et al., *Raman scattering in 3R‐NbS_2.* Solid State Communications, 1979. **31**(8): p. 577-579.
70. Terrones, H. and M. Terrones, *Electronic and vibrational properties of defective transition metal dichalcogenide Haeckelites: new 2D semi-metallic systems.* 2d Materials, 2014. **1**(1).
71. http://pubs.rsc.org/en/content/chapterhtml/2014/bk9781849739542-00001 *Low dimensional transition metal dichalgonide* 2018 [cited 2018.

72. Liu, Z.-L., L.-C. Cai, and X.-L. Zhang, *Novel high pressure structures and superconductivity of niobium disulfide.* Journal of Alloys and Compounds, 2014. **610**: p. 472-477.
73. Zhao, S.H., et al., *Two-dimensional metallic NbS_2: growth, optical identification and transport properties.* 2d Materials, 2016. **3**(2).
74. Liu, Q., et al., *Electronic properties and transistors of the NbS_2-MoS_2-NbS_2 NR heterostructure.* Nanotechnology, 2017. **28**(7).
75. Izawa, K., et al., *A new approach for the preparation, exfoliation, and intercalation properties of niobium layered sulfide material.* Synthesis and Reactivity in Inorganic Metal-Organic and Nano-Metal Chemistry, 2008. **38**(2): p. 181-185.
76. Simchi, H., et al., *Sulfidation of 2D transition metals (Mo, W, Re, Nb, Ta): thermodynamics, processing, and characterization.* Journal of Materials Science, 2017. **52**(17): p. 10127-10139.
77. Güller, F., C. Helman, and A.M. Llois, *Electronic structure and properties of NbS_2 and TiS2 low dimensional structures.* Physica B: Condensed Matter, 2012. **407**(16): p. 3188-3191.
78. Ge, W., et al., *Large-scale synthesis of NbS_2 nanosheets with controlled orientation on graphene by ambient pressure CVD.* Nanoscale, 2013. **5**(13): p. 5773-5778.
79. Nath, M. and C.N.R. Rao, *New metal disulfide nanotubes.* Journal of the American Chemical Society, 2001. **123**(20): p. 4841-4842.
80. Jin, Y.Z., et al., *Large‐Scale Production of NbS_2 Nanowires and Their Performance in Electronic Field Emission.* Angewandte Chemie International Edition, 2004. **43**(42): p. 5670-5674.
81. Martin, M.J., G.H. Qiang, and D.M. Schleich, *NEW LOW-TEMPERATURE SYNTHESIS OF TRANSITION-METAL SULFIDES.* Inorganic Chemistry, 1988. **27**(16): p. 2804-2808.
82. Sihan, Z., et al., *Two-dimensional metallic NbS 2 : growth, optical identification and transport properties.* 2D Materials, 2016. **3**(2): p. 025027.
83. Yanase, T., et al., *Chemical Vapor Deposition of NbS_2 from a Chloride Source with H2 Flow: Orientation Control of Ultrathin Crystals Directly Grown on SiO2/Si Substrate and Charge Density Wave Transition.* Crystal Growth & Design, 2016. **16**(8): p. 4467-4472.
84. Bark, H., et al., *Large-area niobium disulfide thin films as transparent electrodes for devices based on two-dimensional materials.* Nanoscale, 2018. **10**(3): p. 1056-1062.
85. Ge, W., et al., *Large-scale synthesis of NbS 2 nanosheets with controlled orientation on graphene by ambient pressure CVD.* Nanoscale, 2013. **5**(13): p. 5773-5778.
86. Carmalt, C.J., et al., *NbS_2 thin films by atmospheric pressure chemical vapour deposition and the formation of a new 1T polytype.* Thin Solid Films, 2004. **469**: p. 495-499.

87. Ge, W.Y., et al., *Large-scale synthesis of NbS_2 nanosheets with controlled orientation on graphene by ambient pressure CVD.* Nanoscale, 2013. **5**(13): p. 5773-5778.
88. Schuffenhauer, C., R. Popovitz-Biro, and R. Tenne, *Synthesis of NbS_2 nanoparticles with (nested) fullerene-like structure (IF).* Journal of Materials Chemistry, 2002. **12**(5): p. 1587-1591.
89. Liao, Y.H., et al., *Reinvestigation of the electrochemical lithium intercalation in 2H- and 3R-NbS2.* Journal of Power Sources, 2014. **245**: p. 27-32.
90. Jung, Y., Y. Zhou, and J.J. Cha, *Intercalation in two-dimensional transition metal chalcogenides.* Inorganic Chemistry Frontiers, 2016. **3**(4): p. 452-463.
91. Sriram, M.A., K.S. Weil, and P.N. Kumta, *Low-temperature chemical approaches for synthesizing sulfides and nitrides of reactive transition metals.* Applied Organometallic Chemistry, 1997. **11**(2): p. 163-179.
92. Guo, Z., F. Sun, and W. Yuan, *Chemical Intercalations in Layered Transition Metal Chalcogenides: Syntheses, Structures, and Related Properties.* Crystal Growth & Design, 2017. **17**(4): p. 2238-2253.
93. Nakashima, S., et al., *Raman scattering from 2H-NbS2 and intercalated NbS2.* Solid State Communications, 1982. **42**(8): p. 601-604.
94. Liao, Y., et al., *Reinvestigation of the electrochemical lithium intercalation in 2H- and 3R-NbS2.* Journal of Power Sources, 2014. **245**: p. 27-32.
95. Deudon, C., et al., *Quantification of the interlayer charge transfer, via bond valence calculation, in 2D misfit compounds: The case of (Pb(Mn, Nb)(0.5)S-1.5)(1.15)NbS2.* Journal of Solid State Chemistry, 2000. **155**(1): p. 1-8.
96. Mankovsky, S., et al., *Electronic and magnetic properties of 2 H− NbS 2 intercalated by 3 d transition metals.* Physical Review B, 2016. **94**(18): p. 184430.
97. Bonneau, P., J.L. Mansot, and J. Rouxel, *INTERCALATION AND EXFOLIATION OF MISFIT-LAYER COMPOUNDS MNB2S5 (M=PB, SM).* Materials Research Bulletin, 1993. **28**(8): p. 757-766.
98. Goodenough, J.B. and K.-S. Park, *The Li-Ion Rechargeable Battery: A Perspective.* Journal of the American Chemical Society, 2013. **135**(4): p. 1167-1176.
99. Palomares, V., et al., *Na-ion batteries, recent advances and present challenges to become low cost energy storage systems.* Energy & Environmental Science, 2012. **5**(3): p. 5884-5901.
100. Hayashi, K., et al., *Mixed layer phase in the RuS2-NbS_2 system.* Journal of Alloys and Compounds, 2004. **383**(1-2): p. 69-73.
101. Carmalt, C.J., et al., *Chemical vapor deposition of niobium disulfide thin films.* European Journal of Inorganic Chemistry, 2004. **2004**(22): p. 4470-4476.
102. Hamaue, Y. and R. Aoki, *Effects of organic intercalation on lattice vibrations and superconducting properties of 2H-NbS_2.* Journal of the Physical Society of Japan, 1986. **55**(4): p. 1327-1335.
103. Di Salvo, F., et al., *Coexistence of two charge-density waves of different symmetry in 4 H b− Ta Se 2.* Physical Review B, 1976. **14**(4): p. 1543.
104. Geantet, C., et al., *Niobium sulfides as catalysts for hydrotreating reactions.* Catalysis today, 1996. **28**(1-2): p. 23-30.

105. Kumagai, N. and K. Tanno, *Kinetic and structural characteristics of 3R-niobium disulfide as a positive material for secondary lithium batteries.* Electrochimica acta, 1991. **36**(5-6): p. 935-941.
106. Divigalpitiya, W., R. Frindt, and S. Morrison, *Effect of humidity on spread NbS_2 films.* Journal of Physics D: Applied Physics, 1990. **23**(7): p. 966.
107. Peters, E.S., et al., *Aerosol-assisted chemical vapor deposition of NbS_2 and TaS2 thin films from pentakis(dimethylamido)metal complexes and 2-methylpropanethiol.* European Journal of Inorganic Chemistry, 2005(20): p. 4179-4185.
108. Tuschel, D., *Photoluminescence Spectroscopy Using a Raman Spectrometer*. 2016: http://www.spectroscopyonline.com/photoluminescence-spectroscopy-using-raman-spectrometer. p. 14-21.
109. Chang, T., *Raman Spectroscopy and Its Applications*. 2008, https://www.slideshare.net/tzhang1999/Ramanonline Technology, Business.
110. Lee, C., et al., *Anomalous lattice vibrations of single-and few-layer MoS_2.* ACS nano, 2010. **4**(5): p. 2695-2700.
111. Mak, K.F., et al., *Atomically thin MoS 2: a new direct-gap semiconductor.* Physical review letters, 2010. **105**(13): p. 136805.
112. Li, H., et al., *From bulk to monolayer MoS_2: evolution of Raman scattering.* Advanced Functional Materials, 2012. **22**(7): p. 1385-1390.
113. Bertrand, P., *Surface-phonon dispersion of MoS 2.* Physical Review B, 1991. **44**(11): p. 5745.
114. Jeon, J., et al., *Layer-controlled CVD growth of large-area two-dimensional MoS 2 films.* Nanoscale, 2015. **7**(5): p. 1688-1695.
115. McMullan, W.G.I., J. C., , *RAMAN-SCATTERING FROM 2H-NBS_2 AND 3R-NBS_2.* Solid State Communications 1983,. **45**((7),): p. 557-560.
116. Oswald, S., *X‐Ray Photoelectron Spectroscopy in Analysis of Surfaces.* Encyclopedia of Analytical Chemistry, 2013.
117. Magazine, C., *X-Ray Photoelectron Spectroscopy (XPS)*. 2017, ChemViews Magazine: http://www.chemistryviews.org/details/ezine/10463356/X-Ray_Photoelectron_Spectroscopy_XPS.html
118. Barbara L Dutrow, C.M.C., *X-ray Powder Diffraction (XRD)*. 2018, Geochemical Instrumentation and Analysis: https://serc.carleton.edu/research_education/geochemsheets/techniques/XRD.html
119. DISCOVER, X.-R.D.B.D., *X-RAY DIFFRACTION – BRUKER D8 DISCOVER*. 2018, INSTITUTE FOR NUCLEAR AND RADIATION PHYSICS: KU Leuven.
120. Zheng, J., et al., *High yield exfoliation of two-dimensional chalcogenides using sodium naphthalenide.* Nature communications, 2014. **5**: p. 2995.
121. Management, R.a.E., *Scanning Electron Microscope*. 2017, Purdue University https://www.purdue.edu/ehps/rem/laboratory/equipment%20safety/Research%20Equipment/sem.html.

122. Meyer, G. and N.M. Amer, *Novel optical approach to atomic force microscopy.* Applied physics letters, 1988. **53**(12): p. 1045-1047.
123. Zhong, Q., et al., *Fractured polymer/silica fiber surface studied by tapping mode atomic force microscopy.* Surface Science Letters, 1993. **290**(1-2): p. L688-L692.
124. Binnig, G., C.F. Quate, and C. Gerber, *Atomic force microscope.* Physical review letters, 1986. **56**(9): p. 930.
125. Chen, A., *Image reconstruction methods for atomic force microscopy*. 2013, samsi: https://samsiatrtp.wordpress.com/2013/01/28/image-reconstruction-methods-for-atomic-force-microscopy/
126. Edmund, *Understanding Microscopes and Objectives*. 2018, Edmund Optics worlwide https://www.edmundoptics.com/resources/application-notes/microscopy/understanding-microscopes-and-objectives.
127. Nihan Kosku, P. and B. Mehmet, *Investigation of Single-Wall MoS_2 Monolayer Flakes Grown by Chemical Vapor Deposition.* Nano-Micro Letters, 2015. **8**(?).
128. Lanzillo, N.A., et al., *Temperature-dependent phonon shifts in monolayer MoS_2.* Applied Physics Letters, 2013. **103**(9): p. 093102.
129. Diaz, H.C., R. Addou, and M. Batzill, *Interface properties of CVD grown graphene transferred onto $MoS_2(0001)$.* Nanoscale, 2014. **6**(2): p. 1071-1078.
130. Dumcenco, D., et al., *Large-area MoS_2 grown using H2S as the sulphur source.* 2d Materials, 2015. **2**(4).
131. Zhan, Y., et al., *Large‐area vapor‐phase growth and characterization of MoS_2 atomic layers on a SiO2 substrate.* Small, 2012. **8**(7): p. 966-971.
132. Wang, X., et al., *Controlled synthesis of highly crystalline MoS_2 flakes by chemical vapor deposition.* Journal of the American Chemical Society, 2013. **135**(14): p. 5304-5307.
133. Lee, W.Y., T.M. Besmann, and M.W. Stott, *Preparation of MoS 2 thin films by chemical vapor deposition.* Journal of materials research, 1994. **9**(6): p. 1474-1483.
134. Liu, K.-K., et al., *Growth of large-area and highly crystalline MoS_2 thin layers on insulating substrates.* Nano letters, 2012. **12**(3): p. 1538-1544.
135. Van Der Zande, A.M., et al., *Grains and grain boundaries in highly crystalline monolayer molybdenum disulphide.* Nature materials, 2013. **12**(6): p. 554.
136. Najmaei, S., et al., *Vapour phase growth and grain boundary structure of molybdenum disulphide atomic layers.* Nature materials, 2013. **12**(8): p. 754.
137. Wang, S., et al., *Shape evolution of monolayer MoS_2 crystals grown by chemical vapor deposition.* Chemistry of Materials, 2014. **26**(22): p. 6371-6379.
138. Sanna, R., *Structural and morphological characterization of hydrozincite and its interaction with organic molecules*. 2011, Universita'degli Studi di Cagliari.
139. Lee, Y.-H., et al., *Synthesis and transfer of single-layer transition metal disulfides on diverse surfaces.* Nano letters, 2013. **13**(4): p. 1852-1857.
140. Amani, M., et al., *Electrical performance of monolayer MoS_2 field-effect transistors prepared by chemical vapor deposition.* Applied Physics Letters, 2013. **102**(19): p. 193107.

141. Bray, K.R., C.Q. Jiao, and J.N. DeCerbo, *Influence of carrier gas on the nucleation and growth of Nb nanoclusters formed through plasma gas condensation.* Journal of Vacuum Science & Technology B, Nanotechnology and Microelectronics: Materials, Processing, Measurement, and Phenomena, 2014. **32**(3): p. 031805.
142. Kashchiev, D., *Effect of carrier‐gas pressure on nucleation.* The Journal of chemical physics, 1996. **104**(21): p. 8671-8677.
143. Maleki, M. and S.M. Rozati, *Investigation of the Effect of the Substrate Position Relative to the Source on the Optoelectrical and Structural Properties of Pure Nanostructured Tin Oxide by APCVD.* Chemical Vapor Deposition, 2014. **20**(10-11-12): p. 352-355.
144. (MBE), M.b.e., *Behavior of adatoms in the surface deposition process (diffusion until nucleation with other adatoms; deposition on edges)*. 2018, Departmant of Physic: https://www.physik.uni-kl.de/en/hillebrands/research/methods/molecular-beam-epitaxy/.
145. Wu, D., et al., *Effect of Substrate symmetry on the dendrite morphology of MoS 2 Film synthesized by CVD.* Scientific reports, 2017. **7**(1): p. 15166.
146. Zhao, Y., et al., *Large-area synthesis of monolayer MoSe 2 films on SiO 2/Si substrates by atmospheric pressure chemical vapor deposition.* RSC Advances, 2017. **7**(45): p. 27969-27973.
147. Gong, Y., et al., *Vertical and in-plane heterostructures from WS 2/MoS 2 monolayers.* Nature materials, 2014. **13**(12): p. 1135.
148. Sercombe, D., et al., *Optical investigation of the natural electron doping in thin MoS 2 films deposited on dielectric substrates.* Scientific reports, 2013. **3**: p. 3489.
149. Laskar, M., et al., *p-type doping in CVD grown MoS_2 using Nb.* arXiv preprint arXiv:1310.6494, 2013.
150. Laskar, M.R., et al., *p-type doping of MoS_2 thin films using Nb.* Applied Physics Letters, 2014. **104**(9): p. 092104.
151. Xu, E., et al., *p-Type transition-metal doping of large-area MoS 2 thin films grown by chemical vapor deposition.* Nanoscale, 2017. **9**(10): p. 3576-3584.
152. Chae, W.H., et al., *Substrate-induced strain and charge doping in CVD-grown monolayer MoS_2.* Applied Physics Letters, 2017. **111**(14): p. 143106.
153. Suh, J., et al., *Doping against the native propensity of MoS_2: degenerate hole doping by cation substitution.* Nano letters, 2014. **14**(12): p. 6976-6982.
154. Zhang, K., et al., *Manganese doping of monolayer MoS_2: the substrate is critical.* Nano letters, 2015. **15**(10): p. 6586-6591.
155. Nicolosi, V., et al., *Liquid Exfoliation of Layered Materials.* Science, 2013. **340**(6139).
156. Samad, L., et al., *Layer-Controlled Chemical Vapor Deposition Growth of MoS_2 Vertical Heterostructures via van der Waals Epitaxy.* ACS Nano, 2016. **10**(7): p. 7039-7046.
157. Bilgin, I., et al., *Chemical Vapor Deposition Synthesized Atomically Thin Molybdenum Disulfide with Optoelectronic-Grade Crystalline Quality.* Acs Nano, 2015. **9**(9): p. 8822-8832.

158. McMullan, W.G.I., J. C., , *AN INTERPOLYTYPICAL TRANSITION IN NBS_2.* Physica Status Solidi B-Basic Research 1985. **2**: p. 465-469.
159. Onari, S.A., T.; Aoki, R.; Nakamura, S.,, *Raman scattering in 3R ・NbS_2.* Solid State Communications 1979. **8**: p. 577-579.
160. Izawa, K.I., S.; Unal, U.; Yamaguchi, T.; Kang, J. H.; Choy, J. H.; Matsumoto, Y., , *A new approach for the synthesis of layered niobium sulfide and restacking route of NbS_2 nanosheet.* Journal of Solid State Chemistry, 2008. **2**(181): p. 319-324.
161. Yanase, T.W., S.; Weng, M. T.; Wakeshima, M.; Hinatsu, Y.; Nagahama, T.; Shimada, T., *Chemical Vapor Deposition of NbS_2 from a Chloride Source with H-2 Flow: Orientation Control of Ultrathin Crystals Directly Grown on SiO2/Si Substrate and Charge Density Wave Transition.* Crystal Growth & Design, 2016. **8**: p. 4467-4472.
162. Carmalt, C.J.P., E. S.; Parkin, I. P.; Manning, T. D.; Hector, A. L., , *Chemical vapor deposition of niobium disulfide thin films.* European Journal of Inorganic Chemistry, 2004. **22**: p. 4470-4476.
163. McMullan, W.G. and J.C. Irwin, *RAMAN-SCATTERING FROM 2H-NBS_2 AND 3R-NBS_2.* Solid State Communications, 1983. **45**(7): p. 557-560.
164. Berkdemir, A., et al., *Identification of individual and few layers of WS(2) using Raman Spectroscopy.* Scientific Reports, 2013. **3**: p. 1755.
165. Savjani, N., et al., *MoS 2 nanosheet production by the direct exfoliation of molybdenite minerals from several type-localities.* RSC Advances, 2014. **4**(67): p. 35609-35613.
166. Al-Dulaimi, N., et al., *Sequential bottom-up and top-down processing for the synthesis of transition metal dichalcogenide nanosheets: the case of rhenium disulfide (ReS 2).* Chemical Communications, 2016. **52**(50): p. 7878-7881.
167. Kisslinger, K., Lu, T. & Wang, G, *A simple growth method for Nb2O5 films and their optical properties.* RSC Adv, 2015. **5**: p. 36129-36139.
168. Pervov, V.S.M., E. V., *An x-ray photoemission spectroscopy study of interlayer charge transfer in some misfit layer compounds.* J. Phys.: Condens. Matter, 1993. **5**: p. 3817.
169. Dash, J.K., et al., *A Method Toward Fabricating Semiconducting 3R-NbS_2 Ultrathin Films.* Journal of Physical Chemistry C, 2015. **119**(34): p. 19763-19771.
170. Crabtree, G.W.D., M. S.; Buchanan, M. V. , Phys today, 2004. **57**: p. 39-44.
171. Christopher, K.D., R.. Energy Environ. Sci., *A review on exergy comparison of hydrogen production methods from renewable energy sources.* Energy Environ., 2012. **5**: p. 6640–6651
172. Holladay, J.D., Hu, J., King, D. L. &Wang, Y., *An overview of hydrogen production technologies.* Catal. Today, 2009. **139**: p. 244-260.
173. Chhowalla, M., et al., *The chemistry of two-dimensional layered transition metal dichalcogenide nanosheets.* Nat Chem, 2013. **5**(4): p. 263-275.
174. Kibsgaard, J., Chen, Z., Reinecke, B. N. & Jaramillo, T. F. . Nat.Mater. 11, , *Engineering the surface structure ofMoS_2 to preferentially expose active edge sites for electrocatalysis.* Nat Mater, 2012. **11**: p. 963-969.

175. Lu, Q., Yu, Y.,Ma, Q., Chen, B. & Zhang, H. , *2D transition-metal-dichalcogenide-nanosheet-based composites for photocatalytic and electrocatalytic hydrogen evolution reactions.* Adv Mater, 2016. **28**: p. 1917-1933.
176. Zhang, X., Lai, Z., Tan, C. & Zhang,. Angew. , *H. Solution-processed two-dimensional MoS_2 nanosheets: preparation, hybridization, and applications.* Chem. in., 2016. **55**: p. 8816-8838.
177. Voiry, D.e.a.E.c.a.i.s.c.e.W.n.f.h.e., *Enhanced catalytic activity in strained chemically exfoliated WS2 nanosheets for hydrogen evolution.* Nat Mater, 2013. **13**: p. 850-855.
178. Jaramillo, T.F.e.a., *Identification of active edge sites for electrochemicalH2 evolution fromMoS_2 nanocatalysts.* Science, 2007. **317**: p. 100-102.
179. Wu, Z.Z.e.a., *MoS_2 nanosheets: a designed structure with high active site density for the hydrogen evolution reaction.* ACS Catal, 2013. **3**: p. 2101–2107
180. Kappera, R.e.a., *Phase-engineered low-resistance contacts for ultrathin MoS_2 transistors.* Nat. Mater. , 2014. **13**: p. 1–15.
181. Voiry, D.e.a., *The role of electronic coupling between substrate and 2D MoS_2 nanosheets in electrocatalytic production of hydrogen.* Nat Mater, 2016: p. 4660.
182. Kibsgaard, J., Chen, Z., Reinecke, B. N. & Jaramillo, T. F. , , *Engineering the surface structure ofMoS_2 to preferentially expose active edge sites for electrocatalysis.* Nat Mater, 2012. **11**: p. 963-969.
183. Pan, H., *Metal dichalcogenides monolayers: novel catalysts for electrochemical hydrogen production.* Sci.Rep, 2014. **4**: p. 5348.
184. Liu, Y.e.a.N.E., *Self-optimizing , highly surface-active layered metal dichalcogenide catalysts for hydrogen evolution.* Nat. Energy, 2017. **2**(17127): p. 1-7.
185. Voiry, D.e.a.E.c.a.i.s.c.e.W.n.f.h.e., *Enhanced catalytic activity in strained chemically exfoliated WS2 nanosheets for hydrogen evolution.* Nat Mater 2013. **13**: p. 850-855.
186. Voiry, D.e.a., . *The role of electronic coupling between substrate and 2D MoS_2 nanosheets in electrocatalytic production of hydrogen.* Nat Mater 2016: p. 4660.
187. Kappera, R.e.a., *Phase-engineered low-resistance contacts for ultrathin MoS_2 transistors.* Nat. Mater., 2014. **13,**: p. 1–15.
188. Jaramillo, T.F.e.a., , , *Identification of active edge sites for electrochemicalH2 evolution fromMoS_2 nanocatalysts.* Science, 2007. **317**: p. 100-102.
189. Wu, Z.Z.e.a., . , *MoS_2 nanosheets: a designed structure with high active site density for the hydrogen evolution reaction.* ACS Catal, 2013. **3**: p. 2101–2107.
190. Liu, L., et al., *Atomic MoS 2 monolayers synthesized from a metal–organic complex by chemical vapor deposition.* Nanoscale, 2016. **8**(8): p. 4486-4490.
191. Huang, Y., et al., *Transport properties in semiconducting NbS_2 nanoflakes.* Applied Physics Letters, 2014. **105**(9): p. 093106.

Acknowledgment of Previous Publications

This thesis provides significant contributions to some articles which are previously published: ``The role of electronic coupling between substrate and 2D $MoS_2$ nanosheets in electrocatalytic production of hydrogen,- Nature Materials (2016)`` Ultrafast Charge Transfer and Enhanced Absorption in MoS_2–Organic van der Waals Heterojunctions Using Plasmonic Metasurfaces-ACS Nano (2016)``, `` Charge transfer and enhanced absorption in MoS_2-organic heterojunctions using plasmonic metasurfaces- Optical Society of America (2017)``- providing high quality $MoS_2$ flakes for HER and Plasmonic Metasurface applications. Some of which are presently under preparation: ``Metallic few layered of NbS_2 by ambient pressure chemical vapor deposition`` was presented at MRS Fall Conference (2017), under preparation for publication and `` Ultrahigh current density niobium disulfide catalysts for hydrogen evolution, -Nature (2018) (under review at the time of writing this thesis) ``- providing atomically thin film of CVD NbS_2 for HER application.